THESIS

PARALLEL HYDRAULIC PRESSURE ASSIST/WORK CIRCUIT HYBRIDS FOR AUTOMATED SIDE LOADER REFUSE VEHICLES

Submitted by

Nicholas Echter

Department of Mechanical Engineering

In partial fulfillment of the requirements

For the Degree of Master of Science

Colorado State University

Fort Collins, Colorado

Summer 2012

Master's Committee:

Advisor: Thomas Bradley

Guy Babbitt
Peter Young

ABSTRACT

PARALLEL HYDRAULIC PRESSURE ASSIST/WORK CIRCUIT HYBRIDS FOR AUTOMATED SIDE LOADER REFUSE VEHICLES

Hydraulic hybrids have been a subject of study for some time now and the application of these hybrids to refuse vehicles has been thoroughly explored. There is a lesser known subset of these which are known as pressure assist or work circuit hybrids that have unique potential to the field. Work circuit hybrids operate similar to a parallel hydraulic hybrid in that energy is captured and stored during regenerative braking. These hybrids differ in that the energy is then used to operate the hydraulic cylinders that handle and compact the refuse rather than reaccelerating the vehicle. Work circuit hybrids can be applied to many types of vehicles but the refuse vehicle application is the focus of this study. It was known prior to this study that work circuit hybrids are a potential solution to improve the fuel economy of refuse vehicles. However, prior to this study, the design of a work circuit hybrid had not been outlined in the literature. It was the goal of this thesis to answer the following questions. What are the fuel economy and cost characteristics of an optimized work circuit hybrid, and can an advanced hydraulic work circuit design justify further development towards productization?

To answer these questions the study began by exploring, at a high level, the feasibility of work circuit hybrids on refuse vehicles. Then, two automated side loader, 28 cubic yard (21.4 m^3), McNeilus Street Force MA refuse vehicles that operate on residential routes throughout Denver's surrounding areas were instrumented to produce drive cycle and hydraulic duty cycle data. This data was used to understand vehicle operation and to validate a reverse facing dynamic

model of the stock refuse vehicle. A hybrid model was then produces and used in conjunction with a non-linear optimization algorithm to determine the potential benefit of this technology.

This study concluded that a work circuit hybrid providing energy to the arm of a side loader refuse vehicle could achieve a 2.3% reduction in fuel consumption with a 4 year payback period using optimally sized hybrid components. The fuel usage reduction for these hybrids is limited to how well the available energy from regenerative braking is matched with the energy required by the work circuit. For this study, only 16% of the braking energy was utilized due to the selection of vehicle and hydraulic circuit. Work circuit hybrids also enable the use of an idle stop control logic, creating a unique opportunity to combine these two technologies yielding a fuel savings of 21.6% for the same vehicle.

There are still some challenges to overcome before this technology can be truly understood. One such challenge is the fact that these hybrids require control of the torque converter lock up clutch and the transmission shifting strategy to make an engine driven configuration feasible. Implementing idle stop may also have hidden challenges including energy losses and emissions issues. However, it is the conclusion of this study that work circuit hybrids do offer a unique set of desired characteristics that warrant further development for future use in the field.

ACKNOWLEDGEMENTS

I gratefully acknowledge the following individuals,

Jason Allen and Gary Ziegler from Republic Services for their support and patience while the data for this study was collected. The data collected for this research would not have been possible without the expertise and guidance of Jason Allen during the data collection process.

Dave Tscherpel for his insight into how these vehicles operate and for fostering the relationship with Republic Services.

Dr. Thomas Bradley of Colorado State University and Dr. Guy Babbitt of Czero Inc. for their guidance and support, both financially and academically, during this project.

Chris Ohlsen of Czero Inc. for his guidance and support while preparing the measuring equipment for the data logging process. The time that he volunteered was instrumental in the success of this project.

Sheela Backen with CSU Facilities Management, Recycling & Integrated Solid Waste (ISW) for allowing the project to validate the measurement equipment on the CSU recycling vehicle.

Ben Geller for his support and guidance through the nonlinear optimization setup and execution.

And finally, my family, Dave, Anne, Jeff, and Julie Echter, as well as, Marie Ross for their continued support through my engineering curriculum and with this project.

TABLE OF CONTENTS

NOMENCLATURE

Variable	Unit	Definition
$\boldsymbol{a}$	$(m^3/kg)^3 Pa$	BWR constant (see Table 9)
$\boldsymbol{A}$	m^2	Area
$\boldsymbol{A_f}$	m^2	Frontal area of the vehicle
$\boldsymbol{A_0}$	$(m^3/kg)^2 Pa$	BWR constant (see Table 9)
$\boldsymbol{b}$	$(m^3/kg)^2$	BWR constant (see Table 9)
$\boldsymbol{B_0}$	m^3/kg	BWR constant (see Table 9)
$\boldsymbol{c}$	$(m^3/kg)^3 K^2 Pa$	BWR constant (see Table 9)
$\boldsymbol{C_0}$	$(m^3/kg)^2 K^2 Pa$	BWR constant (see Table 9)
$\boldsymbol{C_d}$		Coefficient of drag or discharge
$\boldsymbol{c_f}$	$\frac{J}{kgK}$	Specific heat at constant volume of the elastomeric foam in an accumulator
$\boldsymbol{C_{rr}}$		Coefficient of rolling resistance
$\boldsymbol{c_v}$	$\frac{J}{kgK}$	Specific heat at constant volume
$\boldsymbol{d}$	$\frac{m^3}{rad}$	Displacement
$\boldsymbol{d_m}$	$\frac{m^3}{rad}$	Motor displacement
$\boldsymbol{d_p}$	$\frac{m^3}{rad}$	Pump displacement
$\boldsymbol{e}$		Euler's number
$\boldsymbol{E}$	J	Energy
$\boldsymbol{\dot{E}}$	W	Power
$\boldsymbol{F}$	N	Force
$\boldsymbol{F_t}$	N	Tractive force at the wheels of the vehicle
$\boldsymbol{F_w}$	N	Force of wind drag on the vehicle
$\boldsymbol{F_{rr}}$	N	Force of rolling resistance on the vehicle
$\boldsymbol{g}$	$\frac{m}{s^2}$	Gravitational constant
$\boldsymbol{GR}$		Gear ratio between the pump and the driveshaft
$\boldsymbol{I}$	$kg\, m^2$	Mass moment of inertia
$\boldsymbol{k}$		Adiabatic index
$\boldsymbol{m}$	kg	Mass
$\boldsymbol{m_f}$	kg	Mass of the elastomeric foam in an accumulator
$\boldsymbol{m_g}$	kg	Mass of the nitrogen gas in an accumulator
$\boldsymbol{m_{eq}}$	kg	Equivalent vehicle mass taking into account rotational inertia of engine, transmission, driveline, and wheels
$\boldsymbol{m_v}$	kg	Total mass of the vehicle (including waste)
$\boldsymbol{n}$		Polytropic index

$\boldsymbol{N_1}$	K^3	BWR constant (see Table 9)
$\boldsymbol{N_2}$	K^2	BWR constant (see Table 9)
$\boldsymbol{N_3}$	K	BWR constant (see Table 9)
$\boldsymbol{N_4}$		BWR constant (see Table 9)
$\boldsymbol{N_5}$	K^{-1}	BWR constant (see Table 9)
$\boldsymbol{N_6}$	K^{-2}	BWR constant (see Table 9)
$\boldsymbol{N_7}$	K^{-3}	BWR constant (see Table 9)
$\boldsymbol{N_8}$		BWR constant (see Table 9)
$\boldsymbol{N_9}$	K	BWR constant (see Table 9)
$\boldsymbol{P}$	Pa	Absolute pressure
$\boldsymbol{P_0}$	Pa	Precharge pressure in the accumulator
$\boldsymbol{P_1}$	Pa	Minimum operating pressure in the accumulator
$\boldsymbol{P_2}$	Pa	Maximum operating pressure in the accumulator
$\boldsymbol{P_{acc}}$	Pa	Current pressure in the accumulator
$\boldsymbol{Q}$	$\frac{m^3}{s}$	Volumetric flow rate
$\boldsymbol{R}$	$\frac{m^3 Pa}{kgK}$	Ideal gas constant
$\boldsymbol{RD}$		Rear differential ratio
$\boldsymbol{r_t}$	m	Vehicle tire radius
$\boldsymbol{t}$	s	Time
$\boldsymbol{T}$	K	Temperature
$\boldsymbol{T_{amb}}$	K	Ambient air temperature
$\boldsymbol{v}$	$\frac{m^3}{kg}$	Specific volume
$\boldsymbol{V}$	m^3	Fluid volume
$\boldsymbol{V_0}$	m^3	Accumulator capacity
$\boldsymbol{V_1}$	m^3	Maximum operating volume of gas in the accumulator
$\boldsymbol{V_2}$	m^3	Minimum operating volume of gas in the accumulator
$\boldsymbol{V_{N2B}}$	m^3	Auxiliary nitrogen bottle volume
$\boldsymbol{x}$	m	Linear position
$\boldsymbol{\alpha}$	$(m^3/kg)^3$	BWR constant (see Table 9)
$\boldsymbol{\beta}$	rad	Angle of incline of the road
$\boldsymbol{\gamma}$	$(m^3/kg)^2$	BWR constant (see Table 9)
$\boldsymbol{\varsigma}$	rad	Angle of load port opening on Innas' transformer
$\boldsymbol{\delta}$	rad	Angular position of the Innas' Transformer port plate
$\boldsymbol{\delta_{SS}}$	rad	Steady state angular position of the Innas' Transformer port plate
$\boldsymbol{\zeta}$	s	Thermal time constant of the accumulator
$\boldsymbol{\eta}$		Efficiency
$\boldsymbol{\eta_m}$		Mechanical efficiency
$\boldsymbol{\eta_{mm}}$		Mechanical motor efficiency

$\boldsymbol{\eta_{mp}}$		Mechanical pump efficiency
$\boldsymbol{\eta_{v}}$		Volumetric efficiency
$\boldsymbol{\eta_{vm}}$		Volumetric motor efficiency
$\boldsymbol{\eta_{vp}}$		Volumetric pump efficiency
$\boldsymbol{\theta}$	rad	Angle of swash plate or bent axis
$\boldsymbol{\xi}$	rad	Angle of accumulator port opening on Innas' transformer
$\boldsymbol{\rho}$	$\frac{kg}{m^3}$	Fluid density
$\boldsymbol{\sigma}$		Correction factor for accumulator pressure working range
$\boldsymbol{\tau}$	Nm	Torque
$\boldsymbol{\tau_m}$	Nm	Motor torque
$\boldsymbol{\tau_p}$	Nm	Pump torque
$\boldsymbol{\varphi}$	rad	Angle of vent port opening on Innas' transformer
$\boldsymbol{\omega}$	$\frac{rad}{s}$	Rotational speed
$\boldsymbol{\omega_p}$	$\frac{rad}{s}$	Rotational speed of the pump

INTRODUCTION

The solid waste industry is an integral and critically important part of our society. The United States Environmental Protection Agency (EPA) reported in 2009 that Americans produced about 243 million tons (220 million metric tons) of trash and 82 million tons (74 million metric tons) of recycled and composted material over the year. That equates to 4.39 pounds (1.99 kg) per person per day, 1.46 pounds (0.66 kg) of which were recycled or composted [1]. Operating in the background of our day to day life, this industry is one of the most fundamental and important in keeping our society running smoothly. In order to keep this large infrastructure working, nearly 136,000 refuse collection vehicles run each day in the United States collecting trash and recyclables [2]. The industry provides jobs for 300,000 people and the net revenues approach US$50 billion dollars per year [3]. Companies have spent a tremendous amount of money to build up and maintain this infrastructure of trucks, collection bins, routes, and collection and disposal technology. Yet the refuse vehicle is among the five least fuel-efficient single body vehicles with an average fuel economy of 5.1 mpg (46.1 L/100km) according to Argonne National Laboratory [4]. This fuel economy value is on the high end of published values for refuse vehicles with another paper reporting values as low as 2.1 mpg (112.0 L/100km) [5]. These trucks are also tremendous emissions producers, generating 42 $MtCO_2e$ per year. This is almost six times the emissions of a large family sport utility vehicle per kilometer driven [5]. Despite the introduction of stricter emissions laws and the trend of increasing fuel prices, the refuse vehicle's poor fuel economy has not improved much over the last thirty years. This is because of two factors that are present in the industry. The first reason for poor fuel economy is due to the harsh nature of the drive cycle. Each truck makes between 8

and 1,200 stops every day to collect solid waste and the average speed on route is less than 15 mph (24.1 kph). The large number of quick accelerations and decelerations drives the fuel economy down and the vehicle maintenance costs up. The other reason that fuel economy in these trucks is so poor is due to the lack of time in the national spotlight. As of 2003, 82% of the refuse collection vehicles on the road were owned and operated by private companies. Other publicly funded fleets, such as transit buses, feel more political pressure to show fuel economy improvements [6].

Even though the fuel economy has not improved much, there have been significant changes in the vehicles used in a refuse fleet. It used to be that a fleet owner could operate with only rear and front loaded trucks. Fleets today include these vehicles along with other specialty trucks such as: roll-off trucks, grapple trucks, pneumatic collection trucks, and recycling trucks; however, there are typically fewer of these vehicles in the fleet. The last vehicle that has become common in waste collection fleets is the automated side loader which has been developed to increase the efficiency of collection. Each of these vehicles has different crew requirements and collection capabilities. The rear loaders typically have one driver and one to two loaders. Waste is collected by hand and deposited into the hopper at the back of the truck. A hydraulic sweeper then compresses the garbage in the hopper at a density of 10 to 15 pounds per cubic foot (160 to 240 kg/m^3) at the curbside. Once the hopper is filled, the main compaction cylinder compresses the waste into the body of the truck at 20 to 25 pounds per cubic foot (320 to 400 kg/m^3). The compaction allows the rear loaders to collect between 11 and 31 cubic yards (8.4 to 23.7 m^3) of trash, depending on the size of the truck, at 550 to 650 pounds of waste per cubic yard (326 to 385 kg/m^3). Some rear loaders are equipped with hydraulic “tippers” that lift heavy cans into the hopper once the operator has carried it to the truck. For front loaders, typically only a driver is

needed and hydraulic forks, similar to those of a fork lift, are used to pick up dumpsters and deposit the solid waste into a hopper behind the cab of the truck. These vehicles are able to compress the garbage to similar densities of the rear loader, however; the bodies are generally bigger with capacities of 30 to 40 cubic yards (23 to 31 m^3). The automated side loaders only require a driver which controls a hydraulic arm that can extend out, grab the can, and lift and tip the can into the hopper. These vehicles typically have a smaller capacity at 6 to 28 cubic yards (5 to 21 m^3) [7]. Despite the lower capacity, these vehicles make more stops, require a smaller crew, and load the garbage quicker and safer than the equivalent rear loader [8]. With typical shifts lasting 8-10 hours, the automated side loader reduces the difficult job of manually loading the cans into the trucks. Automated side loaders seem to have a clear advantage over rear loaders; so the question arises, why don't fleets only use automated front and side loading trucks? The answer to that question stems from the nature of the routes in a typical city. Some streets and allies are simple to tight to safely operate a hydraulic arm around cars, buildings, and pedestrians. Therefore, a smaller rear loader with a crew that manually loads the solid waste is really the only way to collect in these situations [8]. Another reason comes from a need to satisfy customers. In many cities, like the cities surrounding Denver, there is more than one collection company competing for business. Because of the competition, companies are forced to pick up bags of waste and large items that automated loaders are not equipped to handle in order to keep customers. Depending on the how frequently this occurs on route affects the fleet owner's decision to use an automated truck. There are also smaller refuse fleets that cannot afford the new and more expensive automated side loaders. Therefore, these companies run a more traditional fleet of rear and front loaders only. Some of the companies that choose to invest in the automated trucks also opt to provide standardized bins to their customers in order to further

streamline the process. But, as mentioned before, this doesn't guarantee that the customers will put or be able to fit all items in the provided bins. Because of all of these factors, the fleet owner must weigh out what vehicle and crew to use for each route based on how rural the route is, whether the route is commercial or residential, the quantity of solid waste for collection, the types of containers the route encompasses, and whether there is a high occurrence of items that must be hand loaded.

In addition to the changes in fleet vehicles, in the past decade there has been an increased interest in improving the performance characteristics of these vehicles. Some of the areas of focus have been,

1. Speeding up the collection process
2. Reducing potential safety hazards
3. Reducing operational costs
4. Reducing the noise that the trucks produce

Speeding Up the Collection Process

Refuse collection companies have come up with a number of ways to speed up the collection of solid waste. One such way is determining the optimal collection routes to maximize the operators time on route. There are several published works that describe methods for how to choose these optimal routes. One series of papers developed a model to estimate route collection time based on route and collection characteristics [9–11]. The time required to collect waste is also directly related to the cost of collection. A paper by Rhoma et. all [12], describes a municipal solid waste logistic model to estimate the total costs per ton of waste and to examine

the effect of different scenarios, like different service options and different types of vehicles. There was also a derived probability model that can be used to estimate vehicle and labor requirements for municipal solid waste collection systems [13,14]. It is debated whether collection rate can also be closely related to fuel usage. One study showed that refuse vehicles can save between 1 and 21.5 liters of fuel per day by driving optimal routes [15]. A recent study used GPS tracking and statistical analysis to understand the refuse vehicle drive cycle and they argue that deviation from optimal routes may not be as important as delays at landfills for time and fuel usage [16]. Another way to speed up collection, as discussed earlier, is to use as many automated trucks as possible. The tradeoffs for that decision are complex and were explored earlier. There are also other options available from truck manufacturers that speed up the collection process that will be discussed later.

Reducing Potential Safety Hazards

By reducing potential safety issues, these companies are able to reduce the amount of workman's compensation they have to pay as well as the amount of money spent on property damage reimbursement and truck maintenance. In order provide a safe method of collection, the trucks are outfitted with dozens of sensors, a rear view camera, and fire extinguishers. Automated side loaders offer added benefit by removing the need for operators to manually carry the waste to the vehicle. This greatly reduces the physical strain on the collection crew. In addition, most companies have numerous safety protocols in effect that help to reduce the risks associated with operating these large vehicles.

Reducing Operational Costs

Like any other company, refuse collection companies are always looking for ways to reduce the cost of operation which allows the company to offer cheaper services and generate increase profits. Most refuse haulers recognize that investing in new technologies often allows for reductions in maintenance, labor, and fuel costs. This section will summarize many of the technologies that have been developed. Keep in mind that refuse vehicles are typically built by two separate companies, the first producing the chassis of the vehicle and the second builds and mounts the body on the chassis. There are design changes that can be implemented on both the body and the chassis that can reduce operational costs.

Vehicle Improvements

Argonne National Laboratory has explored the improvements that can be gained from reducing aerodynamic drag and rolling resistance on heavy duty vehicles and they conclude that refuse vehicles do not follow a driving schedule that allows reduced aerodynamic drag to make much of a difference. The average speed of the vehicle is too slow to produce significant drag forces especially when compared to on-highway type trucks. Decreasing rolling resistance is predicted to only make a very slight gain in fuel economy. They do determine that using higher efficiency transmissions and engines could improve the fuel economy by 2 to 10%. Reduced or alternative auxiliary load power is also considered but the paper does not specifically predict improvements for refuse vehicles [17]. Beyond simply improving the engine efficiency, some papers consider the possibility of using different fuels all together [2,6,17,18]. The fuels considered include natural gas, methane, biofuel, and hydrogen. There have been a few test refuse trucks that have run on methane and biofuel but natural gas is the only alternative that has

been extensively implemented. One drawback that has been mentioned about using natural gas is that the same size engine produces less torque than before but the cleaner combustion and reduced emissions seems to outweigh this disadvantage [19].

Another way that the refuse haulers have tried to reduce costs is by reducing maintenance. There are a number of methods for reducing the amount of time and money it takes to perform maintenance on these vehicles. One such method that has become popular with the industry is the use of the Telma Frictionless Brake System. These units are installed in the driveline of the vehicle and act as an electromagnetic retarder when energized. Telma claims that their system can extend the life of most brakes from 3 to 10 times [20]. Most of the larger companies have these units installed on the majority of their trucks.

Refuse Body Improvements

The manufacturers that produce the refuse bodies focus heavily on reducing operational costs because it directly correlates to how well the company can sell the vehicles. These companies advertise choices in control valves, body durability, controls on both sides of the vehicle, drop frames for easy entry, different body sizes, various compaction capabilities, and tag axles for increased load carrying capacity. All of these options are intended to improve the efficiency of collection and reduce maintenance issues. Most of these options are focused on reducing operation time and vehicle maintenance to reduce costs. There are also options that are offered that focus on the reduction of fuel consumption. It is reported that approximately 40 percent of the total fuel consumed while the vehicle is in collection mode is used to generate hydraulic power [3]. To understand why this is, one must understand the way that the auxiliary work circuit functions. The traditional hydraulic layout consists of a series of open center valves powered by an engine driven pump as shown in Figure 1. The hydraulic pump is directly

connected to the harmonic balancer of the engine and follows the same speed profile as the engine. Typically the pumps that are used for this open center configuration are fixed displacement pumps. This means that any time the engine is running, the pump is pumping fluid. If no cylinder is actuated then the fluid flows through the center of the valves and back to the reservoir [21]. Although this is done with no load pressure, the restriction in the circuit itself generates losses. Another consequence of using this type of hydraulic control is that the speed of the cylinder actuation is directly coupled to the engine speed. Therefore, the operator revs up the engine at every stop to speed up the cylinder actuation. There are a couple of simple options available to reduce the losses in these open center circuits. Newer trucks offer load at idle systems in which the desired speed of cylinder actuation is achieved at engine idle speed thus reducing the fuel needed to pump fluid. The main drawback of this technology is that it requires the use of larger pumps. There are also special valves available on the pumps that reduce the flow losses while the hydraulic system is not needed. There are two general types of these valves, dry valves and unloader valves, which are similar in operation. Both types restrict the amount of fluid that is sent to the open center valves and reroute the flow directly back to the reservoir. Dry valves restrict the flow to the inlet of the pump and only allow enough flow to lubricate the pump. The flow that is allowed for lubrication is rerouted back to the reservoir in the traditional manor. Unloader valves block the flow of oil at the outlet of the pump and redirect the flow to the reservoir. Both systems are activated manually by the operator when the hydraulics are not needed and offer some improvements in system efficiency. Muncie, a company that manufactures pumps and both types of these valve has published several pieces of literature describing this and other pump technology [22–24]. The drawback of these systems is

that they only provide savings when the hydraulic system is not in use which is less than 30% of the time.

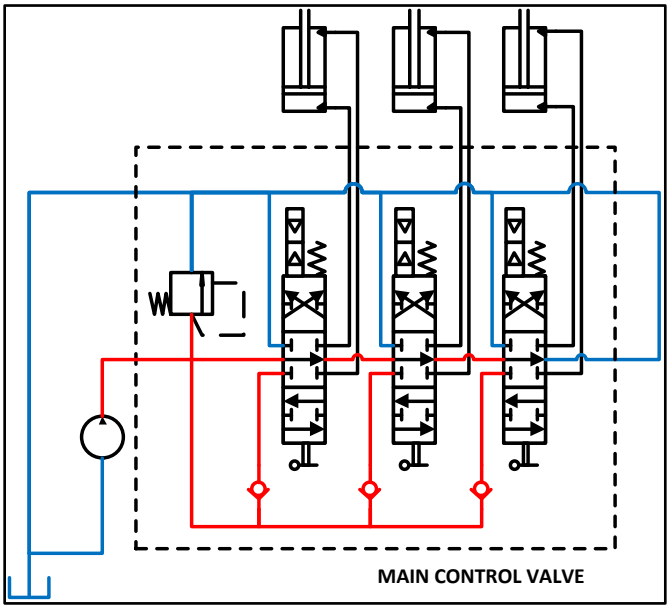

Figure 1: Open Center Flow Control with a Fixed Displacement Pump

Another more sophisticated flow control system has been introduced into some of the new vehicles known as load sensing control strategy. An example of this type of system is shown in Figure 2. This type of system uses a variable displacement pump and load sensing circuitry to dynamically adjust the flow rate of the pump to provide only what is needed. The load sensing circuit is typically a group of shuttle valves that ensure that the pump is controlled for the largest pressure load. Let's say for example that the operator wants to operate the first cylinder at half speed. The first variable orifice in Figure 2 is opened to 50%. Ignoring the pressure compensator for now, the flow from the pump would build up pressure upstream of the variable orifice thus creating a flow through the orifice proportional to the pressure drop across it. However, as the actuator moves, the external load on the actuator may increase. The increased load then increases the pressure downstream of the adjustable orifice and the flow through the orifice would

normally decrease. In the load sensing circuit, the cylinder pressure is fed back to the pump which causes the displacement to increase, thus compensating for the pressure rise. The pressure compensator comes into play when there is more than one actuator being used at once. As discussed before, the load sensing system always compensates the pump displacement for the highest load pressure. Therefore, if the second actuator requires less pressure than the first to perform its task, the second actuator speed would vary as the pump displacement changes without some other type of regulation. Figure 3 shows how a pressure compensating valve moves to create the desired restriction to hold the flow rate to the second actuator constant. There are also electrohydraulic configurations of this type of control that have added benefits [25,26].

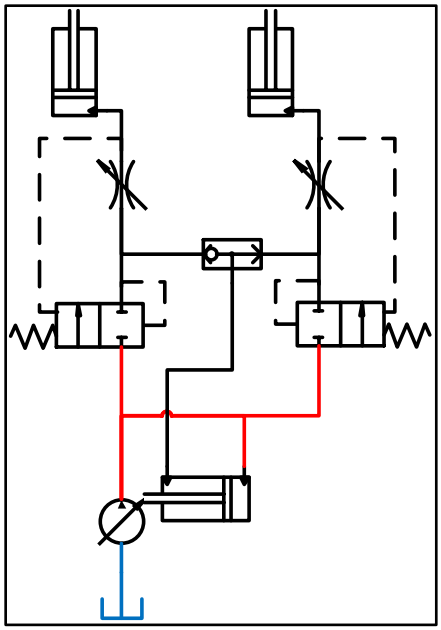

Figure 2: Simplified load sensing circuit

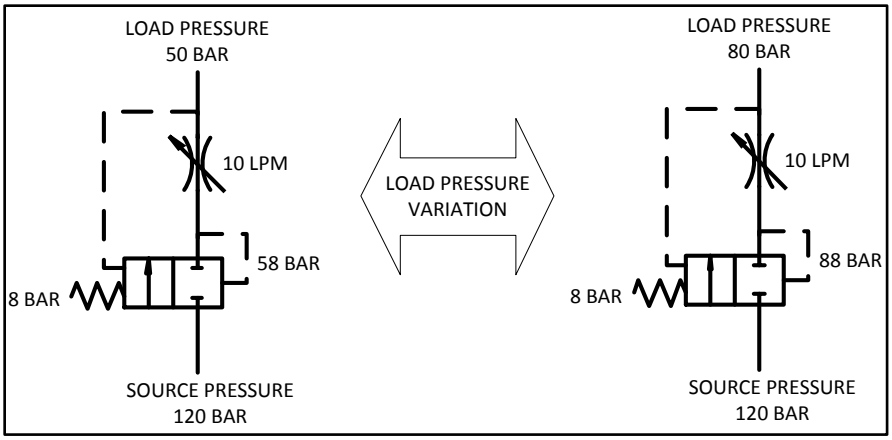

Figure 3: Pressure Compensation

The load sensing type of control is much more efficient than the traditional open center control but there are still some metering losses, especially when more than one actuator is being used at the same time. The Southwest Research Institute has explored yet another type of control that they call Regenerative Hydraulic Circuit. This system incorporates a variable displacement pump and multiple variable displacement motors in order to remove the metering losses created from more than one actuator being used. In addition, this system incorporates an energy storage devise to capture energy while decelerating or lowering a mass instead of dissipated the energy through an orifice [27]. This type of system does not make as much sense for refuse vehicles because of the added weight, additional cost of components, and the fact that the actuators typically have much higher loads while raising than while lowering. The last type of control that has been suggested uses a hydraulic transformer. A hydraulic transformer is a device that transforms high pressure and low flow into low pressure and high flow or vice versa. Innas, a company that has developed a hydraulic transformer, combines this technology with what they call the Common Pressure Rail (CPR). The CPR is essentially a rail that has fluid supplied by a variable displacement pump and the pressure is held steady with a hydraulic accumulator. Flow is provided to each cylinder by a hydraulic transformer [28–34]. This technology offers some

unique advantages but the technology is still new and has not been fully developed. The hydraulic transformer has also been suggested in a digital linear version [35].

Despite the various different types of control methods, the fact that these vehicles have high hydraulic power demands in order to collect waste is consistent. The actual power required to perform these functions will be discussed later; however, it is clear that control methods alone may not yield the optimal solution for reducing the required power for collecting refuse.

Hybrid Technologies

It is interesting that despite the tremendous amount of money that is poured into optimizing these trucks, that the industry has been so slow to enter the hybrid marketplace. This is due to a number of likely reasons. The first being, until recently the refuse companies have been more concerned with vehicle reliability than saving fuel. While saving fuel does reduce operational costs for the company, the effects of a truck out of service are much worse. Like many service based companies that people use on a day to day basis, the solid waste handling companies are often characterized by their failures rather than their successes. People don't notice when things operate smoothly and behind the scenes but they do notice if their trash cans are not emptied on their trash pick-up day. Another likely reason is that many of the technologies that have been developed for passenger vehicles are difficult to implement in a vehicle with this high of a power requirement. None the less, there has been a significant amount of research done on hybridizing refuse vehicles that will be discussed.

A hybrid vehicle is defined as a vehicle that is powered by more than one source of power. The two simplest and most common configurations are the series and parallel configurations. The series configuration arranges the sources of power in series such that only

the final power source is able to provide direct power to the vehicle. This type of configuration is easily controlled and offers slightly higher fuel economy gains than parallel configurations but it requires larger components and is very different from the traditional drivetrain. In a parallel configuration, all power sources can directly power the vehicle. This allows for easy integration into existing systems, and the ability to downsize the primary power source at the cost of a more complex control scheme. There is also a configuration that combines the characteristics of both systems known as a torque split or power split. The torque split hybrid offers the highest opportunity for fuel economy improvements but is also more complex to implement and control and requires more components. These hybrid configurations are well known and will not be discussed further. The options for hybridization that have been explored for refuse vehicles are electric hybrid drives and hydraulic hybrid drives. Hydraulic hybrids are similar to electric hybrids in function but use a hydraulic pump/motor rather than an electric motor to transfer power to and from the energy storage devise. In addition, a high pressure hydraulic accumulator is used as the energy storage device rather than a battery. Both types have their own set of tradeoffs; one of which is the balance of power density versus energy density. Batteries have the ability to store large amounts of energy but are limited in how much current can flow in and out of the battery. This makes electric hybrids very energy dense and lack power density. Accumulators on the other hand, are able to provide fluid at incredible high flow rates but the pressure quickly drops. This is similar to a capacitor in an electric circuit. Therefore, hydraulic systems have high power density but low energy density. In heavy vehicles, significantly more power is needed to accelerate the vehicles which in turn, means there is considerably more power during deceleration as well. This fact gives a distinct advantage for using hydraulic hybrid technologies for heavy vehicle applications [36]. There is another advantage for using hydraulic

hybrid technology in heavy vehicles. In most fleet vehicles, the auxiliary circuit, or work circuit as it will be referred to in this document, is a hydraulic circuit that actuates the arms, forks, compaction cylinders and other equipment on the vehicle. Because this circuit in typically hydraulic, it allows for the possibility to break the hydraulic parallel hybrid drive into parallel torque assist and parallel pressure assist hybrids. The parallel torque assist is a traditional parallel hybrid where regenerative braking is used to capture the vehicles energy while stopping and then the stored energy reaccelerates the vehicle. A parallel pressure assist, or work circuit hybrid, captures the vehicles braking energy and uses the stored energy to power the work circuit. This type of hybrid may offer specific advantages depending on the application.

For the most part, production of hybrid units for refuse vehicles has been on test vehicles only. The big players in the hybrid refuse vehicle market at this time are Eaton Corporation, Bosch Rexroth, and Parker Hannifin. Each of these companies offers years of experience in hydraulics and extensive product lines. Eaton Corporation has developed the Hydraulic Launch Assist (HLA) which is a parallel torque assist system. According to the company, refuse vehicles can expect between 17-28% fuel economy improvements and reduced emissions of NOx, particulates, and CO_2 of up to 20% [37]. The technology, which was developed at EPA's National Vehicle and Fuel Emissions Laboratory (NVFEL) in Ann Arbor, Michigan, is being tested in UPS delivery trucks [38]. In addition, 11 refuse vehicles in Houston, Texas and 1 refuse vehicle in Denver, Colorado have been fitted with the HLA as part of a Houston Advanced Research Center (HARC) grant [39]. As of 2011, Spokane, Washington is also working to purchase four HLA garbage trucks to help offset the nearly 440,000 gallons (1.67 million liters) of diesel used last year for Spokane's waste and recycling collection. The HLA trucks are reported to cost about US$343,000 as compared to the traditional vehicles at about US$325,000

[40]. Bosch Rexroth has built the Hydrostatic Regenerative Braking (HRB) parallel hydraulic torque assist hybrid and claims fuel savings of up to 25% for refuse vehicles. The company also offers a hydraulic series hybrid for vehicles using hydrostatic transmissions [41]. Bosch is working with the New York City Department of Sanitation to validate the technology on Compressed Natural Gas (CNG)/Hydraulic Hybrid trucks. As mentioned earlier, a reported fallback of CGN vehicles is reduced torque capabilities. The HRB system is quoted to be able to make up for this loss in torque which creates a unique opportunity for two new technologies to integrate together [19]. Parker Hannifin has dabbled in several different hybrid designs, the most recent being the RunWise Advanced Series Hybrid Drive system which is reported to have 30-50% fuel economy savings depending on route density and operating conditions. The RunWise system is a series configuration incorporating a three speed gearbox to allow the vehicle to operate in a large speed range [42]. In a partnership with Autocar, Parker has delivered eleven refuse trucks to three south Florida municipalities including Hialeah, Miami-Dade County, and the City of Miami. While testing these vehicles, it was reported that the vehicles used 42% less fuel, reduced carbon emissions by 38 tons (34.5 metric tons) along routes with frequent stops and increased brake life by up to 8 times [43]. Parker has also developed the Stored Energy Management System (SEMS) which is a hydraulic parallel pressure assist, or work circuit hybrid, for snow plow trucks [44]. This technology is also available for refuse vehicles where the compacting and packing cylinders are powered by the regenerative braking system. The information on this system is very limited although it sounds as if the system may be using a technology similar to a hydraulic transformer [45]. A few others have also built prototype hybrid systems for refuse vehicles including Czero, a Colorado based company that has developed a hydraulic parallel torque assist system [46], Norcal Waste Systems, Inc., which has tested a

hybrid natural gas/electric system [6], and BAE Systems which has developed both electric series and electric parallel hybrid drives [47].

Beyond the companies that have created working prototypes of hybrid systems for refuse vehicles, there has been a tremendous amount of theoretical research on the subject. The Center for Automotive Research at Ohio State University in conjunction with the National Renewable Energy Laboratory (NREL) and Oshkosh Truck Corporation published a paper on modeling and optimizing refuse series hybrid electric drives [48]. Bosch engineers discuss the modeling of the HRB system in an SAE paper [49]. In addition, the two most common configurations for a torque split HHV, input coupled and output coupled, have been examined [50]. Other publications talk about the control of hydraulic hybrid systems. Fuzzy logic controls for a parallel HHV have been suggested by some [51–53] and others have suggested using dynamic programming [54]. Yet another control strategy suggested was Nonlinear Programming by Quadratic Lagrangian [55]. Optimal sizing of components for HHV's has also been explored and a genetic algorithm applied [56,57]. Yet another paper explores the frequency response characteristics of critical structural components using FEA to reduce the weight of a hydraulic drive system [58]. Other publications of interest regarding hybrids for heavy vehicles can be found in [59,60].

Reducing Refuse Vehicle Noise

The final change that the refuse collection companies have been aiming to improve on is the noise produced by these vehicles. Because refuse vehicles work long hours and drive in residential areas, there are many times when the noise of a collection vehicle loading garbage can be a nuisance to the customers. The problem is caused by the fact that the vehicle comes to a stop

with squeaky brakes, many drivers rev up the engine to speed up the hydraulic cylinders, bins full of wastes are poured into a metal hopper, and then the vehicle is rapidly accelerated towards the next stop. There are a few ways that this noise is reduced in current vehicles. First, the Telma frictionless brakes are much quieter that the traditional friction brakes. Also, the new CNG vehicles are reported to be much quieter than diesel engines [2]. The pack at idle work circuits also offer reduced noise. In addition to these common solutions, hybrids also offer the opportunity to reduce noise. Regenerative braking is quieter than friction brakes and hybrids that use the stored energy to reaccelerate the vehicle produce a quieter means to get the vehicle back up to speed. Work circuit hybrids and alternative auxiliary controls allow for operation of the hydraulics with reduced noise. One caveat however, there can be new noise introduced from the use of a hydraulic hybrid due to vibrations in the system. This issue can be addressed in many ways, one of which is mounting the hybrid unit on dampened mounts [61].

Work Circuit Hybrids

There are many publications, technologies, and products that exist with the intent to improve the performance of refuse vehicles; however, there is a relatively small amount of research that has been done on work circuit hybrids. There are only two groups that have done extensive work on these pressure assist hybrid systems. The first being the Transportation Development Centre of Transport Canada. A detailed report was generated by Piotr Drozdz with vePower Technologies in collaboration with the Centre for Electric Vehicle Experimentation in Québec (CEVEQ) discussing the feasibility of hybrid technology with regards to refuse vehicles. Parallel and series electric hybrid drives as well as parallel pressure assist, parallel torque assist, and series hydraulic hybrid drives were evaluated. The report concluded that the work circuit

hybrid was the most promising technology. The study used Équipement Labrie's test data collected on a typical residential route in Saint-Nicolas, Quebec for an Autocar side loader truck. The report showed that fuel consumption could be reduced by 19% by the hydraulic pressure assist system which was the highest reduction achieved by any of the configurations. After evaluating energy efficiency performance, emissions, noise, implementation, maintenance, weight, system cost, and development effort, the hydraulic pressure assist scored the highest out of the systems. Although this report laid out solid ground work for the development of work circuit hybrids, the report only examined one work circuit hybrid architecture. The architecture evaluated in the study has a hydraulic motor located post transmission in the drivetrain and an engine driven hydraulic pump to operate the hydraulics [3]. The second group that has explored work circuit hybrids is Parker Hannifin. As discussed earlier, they have developed the Parker's Stored Energy Management System (SEMS) but almost no information in publically available on the project. It is unknown exactly how the system is configured but from what little information is available, it appears that a technology similar to a hydraulic transformer is being implemented. There has been no published work to determine the optimal configuration for work circuit hybrid refuse vehicles and how the optimized system's benefits compare with the other available technologies.

Refuse Vehicle Drive Cycle

In order to accurately predict the improvements that any hybrid technology might have in a vehicle, the drive cycle characteristics must be understood. The first characteristic of interest is how much time a refuse vehicle spends in different categories of driving. A refuse drive cycle can be divided into: driving to and from the route, driving on route, idling on route, and unloading. Other information of interest includes the velocity profile and the hydraulic power

profile. Drozdz reported that driving to and from the route consumed 20% of vehicle operation time, on route collection consumed 76% of the time, and unloading took the last 4% of the time. The study also provides a comparison between three refuse drive cycles which is summarized in Table 1. The St. Nicholas drive cycle is based on operating data collected in 2003 in Saint-Nicolas, Quebec, by Équipement Labrie and an example can be seen in Figure 4 [3]. The U.S. Department of Energy's Advanced Heavy Hybrid Propulsion System (AHHPS) project funded the National Renewable Energy Laboratory (NREL) in conjunction with Oshkosh Truck Company and the Center for Advanced Research at Ohio State University to produce a refuse vehicle drive cycle. The team integrated sensors into a 2003 Autocar chassis with a McNeilus side loader body. The vehicle was driven in five cities that represented the harshest of drive cycles and the data was then used to produce statistically derived drive cycles [62]. One of the drive cycles that was constructed from this data can be seen in Figure 5 [63].

Table 1: Comparison of Refuse Vehicle Drive Cycles

	St. Nicholas Drive Cycle	**NYC Drive Cycle**	**ARC Drive Cycle**
Type of Vehicle	Automated Side Loader	Rear Loader	Automated Side Loader
Maximum Speed (km/hr)	25	20	23
Time per Stop (s)	4-24 (Ave < 10)	16-40	16
Compaction Time (s)	6-8	30 (w/ 30 extra every 3rd)	
Acceleration to 20 km/hr (s)	4-5	6	5
Stops per Hour	144	90	
Hydraulic Power per Stop	25kW for 7s (starting 2-3s prior to stop) and 42kW for 5s		

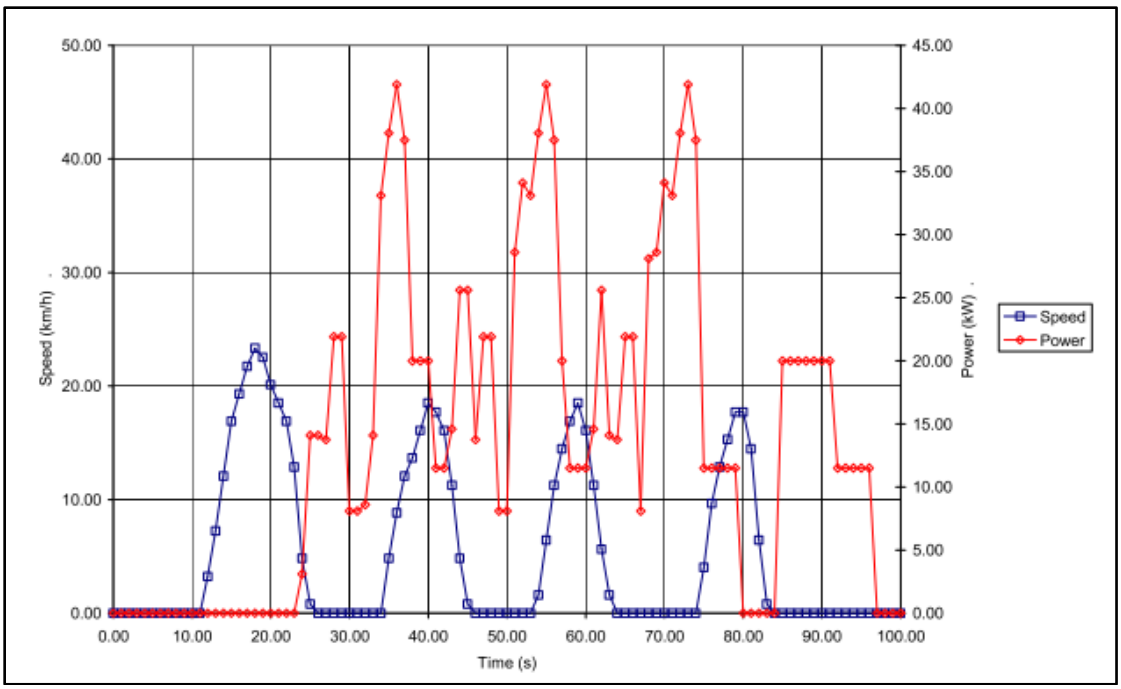

Figure 4: Part of the St. Nicholas Refuse Vehicle Drive Cycle

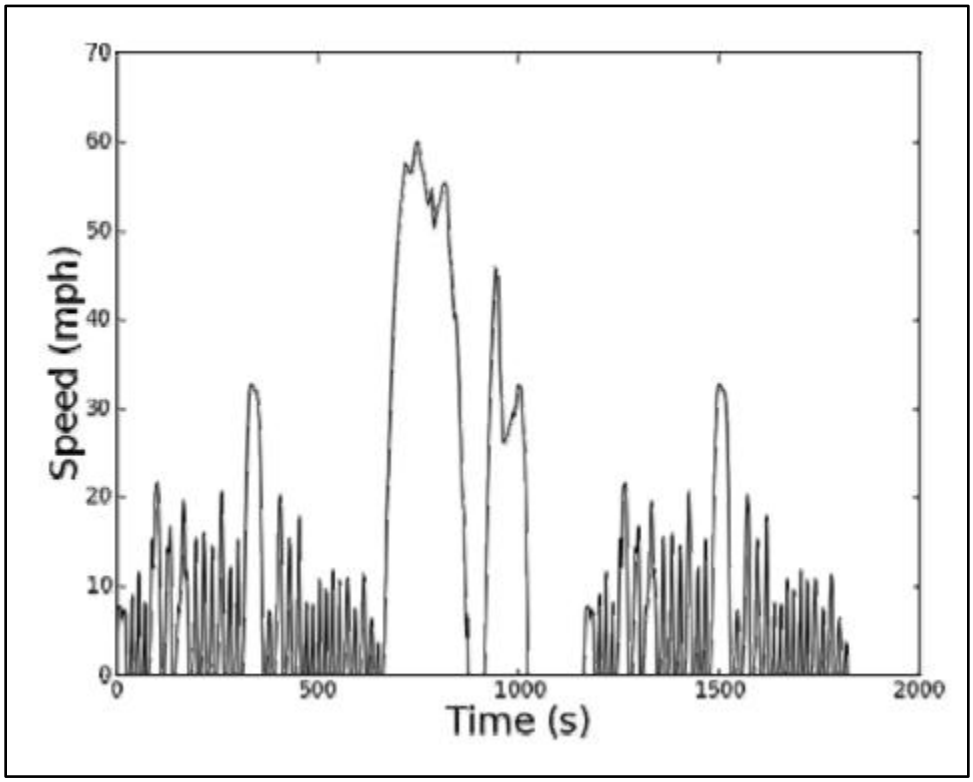

Figure 5: DOE, NREL, Oshkosh, and Ohio State University refuse vehicle Drive Cycle

Other groups have also worked to understand the statistics of the duty cycle that a refuse vehicle might follow. One group collected GPS data on fleets of refuse vehicles. From this data the time required per house was reported to be 28-46 seconds for a co-collection vehicle [16]. A later paper reported that 6.7-8.7 seconds was required per house for a regular garbage collector and 3.4-10.9% of the fuel was used during idle on route while 64.7-78.3% of the fuel was used while driving on route depending on the density of collection points [15]. Another study collected GPS data on 5 vehicles for 13 months and concluded that the vehicle idled for 52% of the drive cycle and consumed 16% of the fuel during this time. They also reported that the average fuel consumption during idle was 3.1 L/hr and 0.9 km/L for driving [5]. A rear loader in New York City was monitored for 12 months and had an average of 21.7 km/hr with 51.4% of the time spent idling and 18.1% of the time with the hydraulics engaged. The vehicle averaged 0.55 km/L during the study [64]. There is also a study that derives physically based metrics of drive cycles in order to help in the characterization of those drive cycles [65].

RESEARCH QUESTIONS AND THESIS OVERVIEW

Based on this state of the field, the central research question posed by this thesis is formulated as follows:

> *Hydraulic work circuits in refuse vehicles are a candidate for hydraulic system hybridization, but the detailed design of these systems has not been investigated. What are the fuel economy and cost characteristics of an optimized work circuit hybrid, and can an advanced hydraulic work circuit design justify further development towards productization?*

This research question is answered through the following procedure (corresponding to the next 4 chapters of this thesis),

1. Explore the feasibility of refuse vehicle work circuit hybrids and develop the tools and methods required to size and analyze the hybrid components.
2. Produce and present data on what a Denver based automated side loader drive cycle looks like and the hydraulic demands associated with that cycle.
3. Develop a detailed model of the best candidate work circuit hydraulic hybrid architecture.
4. Optimize the architecture to determine component sizes to produce the highest fuel economy gains.

A conclusion section summarizes the results from these studies and provides a discussion of the answer to the research questions along with recommendations for future work.

CHAPTER 1: WORK CIRCUIT HYBRID FEASIBILITY

Recall that a work circuit hybrid is similar to other hybrids in its ability to capture braking energy and store that energy for later use. The work circuit hybrid differs from other hybrids in that it uses the stored energy to power the auxiliary components of the vehicle. On a refuse vehicle, the auxiliary circuit is used to control the hydraulic cylinders that load, sweep, compact, and dump the collected waste. These cylinders have flow, pressure, and power requirements in order to achieve their tasks. To understand whether work circuit hybrid make sense to explore further, three fundamental characteristics must be evaluated. These characteristics include:

1. How much braking energy is available for regeneration?
2. How much energy does the work circuit require?
3. How is energy transferred and stored in the hybrid unit and what are the effects of the method used?

The focus of this feasibility study is to rapidly evaluate different trucks and energy transfer and storage methods. Many simplifying assumptions will be made to create a quick first order understanding of whether this research should continue and in what areas. While examining the above questions it will be useful to functionally decompose the system to understand what the tradeoffs are for each component.

Braking Energy

The only drive cycle that was available at the start of this study was the drive cycle shown in Figure 5. Using this refuse drive cycle, the energy available for regeneration can be calculated and later compared to the required hydraulic energy to see if there is enough to operate the work circuit. Starting with fundamental two dimensional vehicle dynamics equations, the energy available for regeneration can be calculated. The force balance at the wheels can be written as follows,

$$F_t - F_w - F_{rr} - m_v g sin\alpha = m_{eq}\ddot{x}$$

Where,

$$F_t = Tractive\ Force$$

$$F_w = Drag\ Force = \frac{1}{2}\rho\dot{x}^2 A_f C_d$$

$$F_{rr} = Rolling\ Resistance = m_v g C_{rr}$$

For this analysis the road can be assumed level and paved since this is typical for a refuse vehicle. The energy used over the drive cycle will be,

$$E = \int \dot{E}\, dt = \int F_t \dot{x}\, dt = \int \left(m_{eq}\ddot{x} + \frac{1}{2}\rho\dot{x}^2 A_f C_d + m_v g C_{rr}\right)\dot{x}\, dt$$

If the power is positive, then the energy must be provided by the engine. When the power becomes negative, then the energy is available for regeneration. The values used for this analysis are summarized in Table 2.

Table 2: Values Used for Analysis

Variable	Unit	Value	Definition
m_v	kg	9,000-27,000	Total mass of the vehicle (range depends on vehicle size and amount of waste)
m_{eq}	kg	m_v + 300 kg	Equivalent mass taking into account rotational inertia of engine, transmission, driveline, and wheels
g	$\frac{m}{s^2}$	9.81	Gravitational constant
α	rad	0	Angle of incline of the road
ρ	$\frac{kg}{m^3}$	1.29	Density of air
A_f	m^2	7.5 (FL) 5.6 (RL) 7.3 (SL)	Frontal area of the vehicle (averaged from published data) FL-front loader, RL-rear loader, SL-side loader
C_d		0.4	Coefficient of drag (estimate)
C_{rr}		0.013	Coefficient of rolling resistance (for pavement)

Using Matlab software, the velocity profile was differentiated using an approximate numerical derivative method and the two vectors were fed into a Simulink model. The model then calculates the energy used and available for regeneration. The simulation outputs are plotted in Figure 6. A refuse drive cycle is unique because the vast majority of the energy that is put into the vehicle is energy to accelerate and decelerate it. Because there is very little time spent at a constant speed, almost all of the energy provided to the vehicle by the engine can be regenerated in the ideal case. Notice how the energy available for regeneration almost lies right on top of the energy required for the first portion of the drive cycle where the vehicle is doing frequent stops and starts. The difference comes in the middle of the drive cycle where the vehicle leaves the route to transfer the waste to the land fill. Once back on route, the energies match closely again. This analysis was done for the three types of trucks with the minimum and maximum weights expected. The results are summarized in Table 3. The available energy for regeneration excluding the highway portion and divided by the number of stops is calculated for the ideal case. In general, variation in frontal area, rotational mass, and coefficient of drag variation only

affect the results by less than 6%. It is interesting to note the drastic difference between a truck that is empty and a truck that is full. A loaded vehicle needs approximately 2.5 times the amount of energy input in order to follow the cycle. The increase in mass also causes a shift in the percentage of energy lost to wind drag which allows about 13% more energy recovery. This fact will be important to consider when sizing the components of the hybrid.

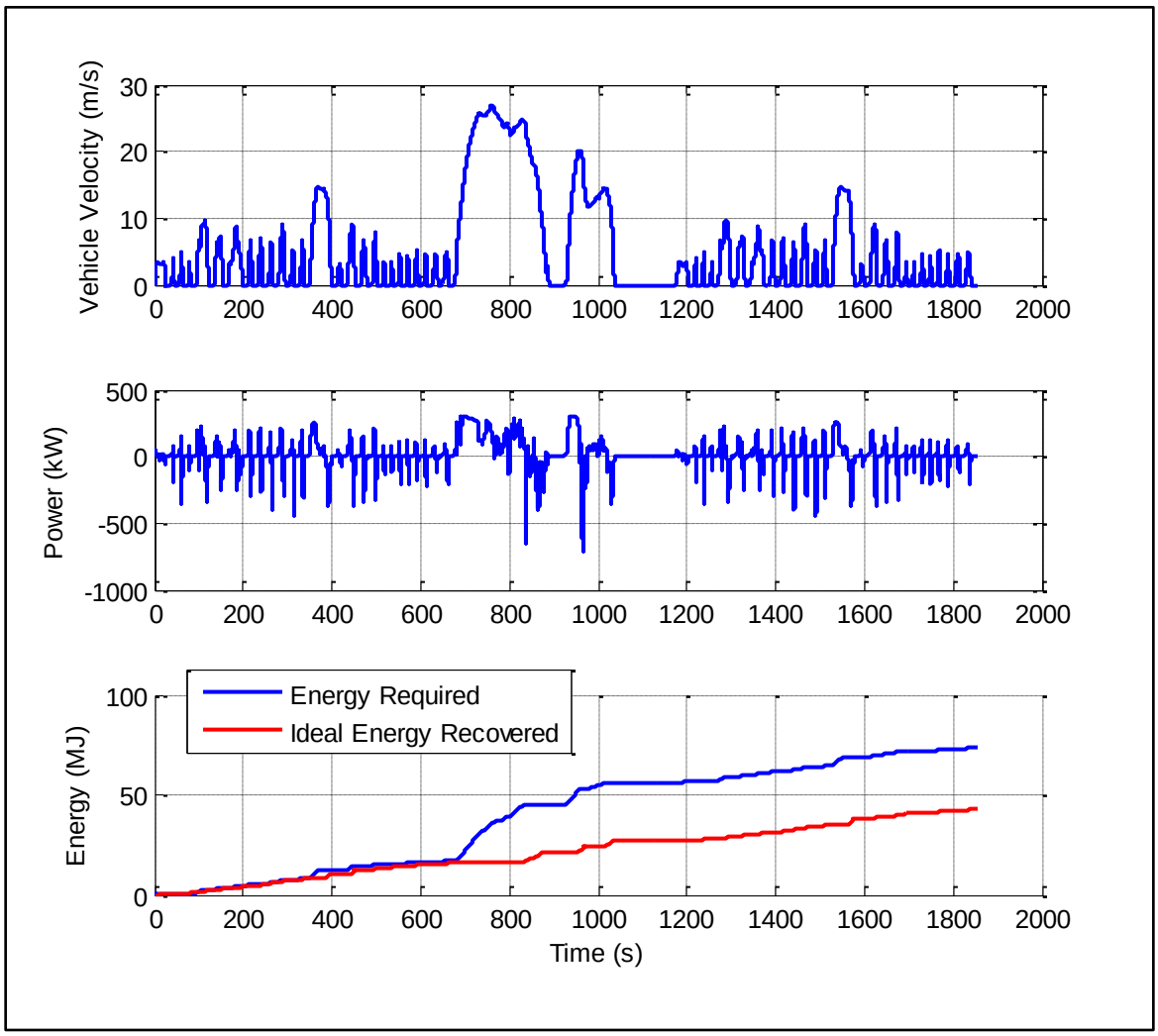

Figure 6: Energy Analysis of the DOE, NREL, Oshkosh, and Ohio State University refuse vehicle Drive Cycle

Table 3: Summary of Energy Analysis for the DOE, NREL, Oshkosh, and Ohio State University refuse vehicle Drive Cycle

Truck Weight (kg)	Truck Type	Required Energy (MJ)	Energy Available for Regeneration (MJ)	Energy per Stop on Route (MJ/stop)	Overall % Energy Available for Regeneration
9000	Rear Loader	28.3	14.1	0.207	49.8
	Side Loader	30.8	13.7	0.206	44.6
	Front Loader	31.1	13.7	0.206	44.1
27000	Rear Loader	70.9	43.4	0.614	61.2
	Side Loader	73.3	42.9	0.613	58.5
	Front Loader	73.5	42.9	0.612	58.3

Required Hydraulic Energy

A similar method for the hydraulic power duty cycle could be used to determine the energy needed by the work circuit. However, because the hydraulic power cycle was unavailable at the time of this feasibility study, some assumptions were made in order to make a first pass approximation. In order to do this, a few characteristics about the vehicles have to be known. The information provided by refuse body manufacturers can vary significantly in level of detail. Some manufacturers publish more than others and the published information is not the same between manufacturers. Information was compiled from EZ Pack, McNeilus, New Way, and Labrie which owns Wittke and Leach in order to generate enough data [66–69]. Front, rear, and side loaders were examined for basic body information. A summary of this information is shown in Table 4. The published information on average cylinder sizes has been compiled for each type of vehicle and can be seen in Table 5 through Table 7. A few things should be noted about the compiled information. Values seen in the tables that have an asterisk (*) next to them are values calculated from small data sets. Therefore, these values have a much higher uncertainty than the others. Also, pack, body lift, and ejector cylinders are typically multi-stage or telescoping

cylinders and the full dimensions are often unavailable causing the numbers with a double asterisk (**) to also be uncertain. An average value for each type of telescoping cylinder is provided by Muncie [22] and was used with the dimension given by the body manufacturers to generate the data in the table. Finally, it is important to note that only one cylinder is needed for some operations and two for others. An 'N/A' in the second cylinder column indicates that only one cylinder is typically used.

Table 4: Basic Refuse Body Statistics for Front, Rear, and Side Loader Vehicles (From Survey of Manufacturers)

		Rear Loader	Front Loader	Side Loader
Hopper Size (m^3)	Min.	0.8	7.6	
	Max.	2.8	9.2	
	Ave.	2.2	8.4	1.1*
Body Size (m^3)	Min.	4.6	18	4.6
	Max.	25	34	37
	Ave.	15	28	23
Max Operating Pressure (bar)	Min.	124	155	124
	Max.	190	190	207
	Ave.	156	174	171
Pump Displacement (cc/rev)	Min.	56	133	54
	Max.	133	136	170
	Ave.	96	135	100*
Reservoir Volume (l)	Min.	83	178	91
	Max.	265	265	322
	Ave.	178	208	201

Table 5: Average Cylinder Volumes for Front Loader Refuse Vehicles (From Survey of Manufacturers)

Front Loader	Piston Side	Rod Side	1 Cylinder	2 Cylinders
Arm Cylinder Volume (l)	11.9	8.9	20.8	41.6
Fork Cylinder Volume (l)	3.1	2.2	5.3	10.6
Tailgate Cylinder Volume (l)	3.6	2.1	5.7	11.4
Pack/Ejector Cylinder Volume (l)	56.6**	43.9**	100.5**	200.9**

Table 6: Average Cylinder Volumes for Rear Loader Refuse Vehicles (From Survey of Manufacturers)

Rear Loader	Piston Side	Rod Side	1 Cylinder	2 Cylinders
Slide/Pack Cylinder Volume (l)	9.8	4.3	14.1	28.2
Sweep Cylinder Volume (l)	5.5	2.4	7.9	15.8
Tailgate Cylinder Volume (l)	4.5	1.3	5.9	11.8
Ejector Cylinder Volume (l)	35.7**	9.3**	45.0**	N/A

Table 7: Average Cylinder Volumes for Side Loader Refuse Vehicles (From Survey of Manufacturers)

Side Loader	Piston Side	Rod Side	1 Cylinder	2 Cylinders
Grabber Cylinder Volume (l)	0.23	0.15	0.42	N/A
Reach Cylinder Volume (l)	2.9	1.9	4.8	N/A
Lift Cylinder Volume (l)	2.1	1.5	3.6	N/A
Swing Cylinder Volume (l)	0.72	0.45	1.2	N/A
Tailgate Cylinder Volume (l)	3.0	1.8	4.8	9.6
Pack Cylinder Volume (l)	11.0	5.8	16.7	33.5
Body Lift Cylinder Volume (l)	54.2**	46.7**	100.8**	201.7**

With these values, an approximation of the hydraulic energy requirements can be made using the fact that the energy absorbed into the fluid will be,

$$E = \int QP\, dt$$

Where Q is the volumetric flow rate of the pump and P is the pressure at the pump outlet. The worst case scenario would be if the pump had to operate at its maximum pressure at all times. Any pressure below this value will require less energy input. It will be assumed that the pressure

is at the system maximum for now to book end the problem. By making this assumption, the energy integral becomes,

$$E = P_{max} \int Q \, dt = P_{max} V_{displaced}$$

Where $V_{displaced}$ is the volume of fluid displaced over the loading cycle. The analysis was done based on a single stop and assumes that the work circuit hybrid will only operate the loading functions of the vehicle. The compacting and ejection of the waste is assumed to be done using the standard method because these operations require a lot more fluid. Rear loaders often pack and sweep the garbage is a single operation; therefore, both a pack and sweep cycle and just the sweep cycle were evaluated. Assuming that the cylinders move from fully retracted to fully extended and back again, the volume of fluid needed and the corresponding energy is shown in Table 8.

Table 8: Refuse Vehicle Work Circuit Flow and Energy Requirements for Loading Operation

	Front Loader Lift Operation (Arm and Fork Cylinders)	**Rear Loader Pack and Sweep Operation**	**Rear Loader Sweep Operation**	**Side Loader Lift Operation (Grabber, Reach, Lift, Swing Cylinders)**
Displaced Volume (l)	50.3	43.9	15.9	9.8
Maximum Operating Pressure (bar)	190	190	190	207
Energy Needed (MJ)	0.990	0.832	0.301	0.187

These results, although calculated as the worst case, have an important conclusion. It is know from the braking energy analysis that the refuse vehicle drive cycle will allow for 206-614 kJ of energy to be stored ideally. The analysis of the work circuit shows that 187-990 kJ are

required to operate the work circuit. Granted, the required work circuit energy will decrease with more accurate numbers but the energy that is actually stored and supplied to the work circuit with decrease as well due to the inefficiencies of the hybrid system. The work circuit hybrid will have the advantage of being able to control the flow of oil much more precisely than the original system. This is because the circuits currently are designed to have the pump running all the time with large amounts of energy being dissipated through the open center valves. With all these considerations and the fact that these numbers should scale equally for each type of truck, it is clear that the side loader is the type of vehicle that offers the most promising characteristics for work circuit hybridization.

Hybrid Energy Storage

The components that make up the work circuit hybrid can be functionally decomposed into components that achieve energy storage and energy transfer. The function of energy storage in hydraulics is accomplished using an accumulator. Recall that, in a liquid or gas, energy can be stored in the form of pressure or heat. Accumulators store energy in the pressure form. Hydraulic fluid is highly incompressible, which is a desirable characteristic for lifting heavy loads with a cylinder. Yet, it would be extremely difficult to control the energy stored in the accumulator through the compression of the hydraulic oil. A very small leak in the system would dramatically affect the pressure and pressure spikes would also be a continuous problem. Not to mention that the actual amount of energy stored in the compression of hydraulic oil is much lower than energy stored in a gas. A 40 liter accumulator at 350 bar that stores the energy in oil pressure may be able to store 14 kJ while an equivalent accumulator filled with gas will be able to store about 400 kJ. An accumulator uses hydraulic oil in order to interface with the rest of the hydraulic system

but the energy is stored by compression of a gas that shares the volume of the accumulator, creating two chambers. If there was no barrier between the hydraulic oil and the gas, the gas at high pressure would rapidly entrain in the oil to an amount determined by Henry's Law and would cause issues in other components. In addition, it would be extremely difficult to precharge the gas to a desired pressure. This fact leads to the creation of two separate chambers in the accumulator that can change size and share a common volume. There are three common ways to separate the gas and the oil: a rubber bladder, a rubber diaphragm, or a piston. The advantages and disadvantages of each type are nicely described by Damen Technical Agencies (DTA) [70]. To summarize, bladder accumulators offer a good range of sizes, fast response to pressure variation, and provides high power output. Diaphragm accumulators offer slightly higher gas compression ratios than the bladder type but are limited in volume. Diaphragms also can have a bigger issue with the gas permeating through the diaphragm. Piston accumulators offer the highest gas compression ratios as well as the highest flow rates and volumes. But, the piston accumulators are heavier, have higher friction from the piston seals which leads to slower reaction times, and cleaner oil is required to keep the piston seals running smoothly. For mobile applications that use the accumulator as an energy storage device, the bladder accumulator is utilized most often. The bladder accumulator will be used in this study because of the weight and response advantages as well as the need to store a large amount of fluid. In addition, the oil cleanliness in a refuse truck work circuit is generally not ideal for the piston type of accumulator. Nitrogen is typically the gas used in hydraulic accumulators because it is chemically inert, non-flammable, and abundant.

The work circuit hybrid will be limited in the amount of fluid and energy that it can store based on the size and configuration of the accumulator. Using a model of a bladder accumulator,

we can understand how much energy can be stored before the limitations of pressure and volume are reached. Modeling bladder accumulators can be done several ways with varying degrees of accuracy. For this study, the accumulator will be modeled both using a simple isentropic model and using a more advanced model that takes into account the thermal properties of gas compression. The isentropic model is accurate enough to make a first pass at the best accumulator size, precharge, and configuration. The equation for polytropic gas compression is,

$$PV^n = P_0{V_0}^n = P_1{V_1}^n = P_2{V_2}^n$$

Where P_o, V_0 are the initial or precharge pressure and the initial gas volume respectively and P_2, V_2 are the maximum pressure and corresponding minimum volume of the gas after compression occurs. P_1, V_1 are the minimum pressure and maximum volume allowed during the cycle and these will be discussed later. The actual gas compression should lie somewhere between isothermal where $n = 1$ and adiabatic where $n = k = 1.4$ (for nitrogen) depending on the rate of gas compression and the accumulator design. The energy in the accumulator can be derived using,

$$dE = -PdV$$

The negative sign represents the fact that energy increases as volume decreases. Taking the derivative of PV^n yields,

$$V^n dP + nPV^{n-1}dV = 0$$

$$dV = -\frac{V}{nP}dP$$

Knowing that,

$$V = \left(\frac{P_0}{P}\right)^{\frac{1}{n}} V_0$$

Substituting,

$$dV = -\frac{{P_0}^{1/n} V_0}{n P^{(n+1)/n}}\, dP$$

$$E = \frac{V_0 {P_0}^{1/n}}{n} \int_{P_0}^{P^2} P^{-1/n} dP = \frac{V_0 {P_0}^{1/n}}{n-1} \left({P_2}^{(n-1)/n} - {P_0}^{(n-1)/n}\right)$$

This equation helps to understand the fundamental nature of an accumulator's ability to store energy. Keep in mind that P_2 is restricted by the physical strength of the accumulator and V_0 is the empty volume of the accumulator. Therefore, it is desirable to choose a P_0 such that the maximum energy storage is achieved given the physical restrictions of the accumulator. Notice that the equation is zero for two cases, when $P_0 = 0$ and when $P_0 = P_2$. There is also a maximum that can be found by calculating when,

$$\frac{dE}{dP_0} = 0$$

Yielding,

$$E_{max} = \frac{V_0 P_2}{n^{n/(n-1)}}$$

This occurs when,

$$P_0 = \frac{P_2}{n^{n/(n-1)}} = 0.308 P_2 \quad for\ n = 1.4$$

A similar derivation can be done for the isothermal (n=1) case yielding,

$$E = V_0 P_0 \ln\left(\frac{P_2}{P_0}\right)$$

And,

$$E_{max} = \frac{V_0 P_2}{e}$$

When,

$$P_0 = \frac{P_2}{e} = 0.368 P_2$$

The full derivations can be seen in [71]. The strong relation between precharge and energy storage can be seen clearly by plotting the gas compression on a P-V diagram. Recall that energy is represented in the P-V diagram as the area under the curve. Figure 7 shows a side by side comparison of the P-V curve for three identical accumulators with different precharge pressures. By way of example, each accumulator starts with 75 liters of nitrogen at the precharge pressure and then the nitrogen is compressed adiabatically until the maximum pressure is reached. The volume of hydraulic oil that flows into the accumulator is limited by the maximum pressure of 350 bar, which is a typical maximum pressure rating for this type of accumulator. With a low precharge pressure, as seen in the left case, the largest volume of fluid is accepted because the gas can be compressed more before reaching the maximum pressure. The drawback is that the energy stored in the accumulator is relatively low because the pressure is low for the majority of the gas compression. For the case on the right, the precharge is so high that very little fluid is allowed in to the accumulator before the maximum pressure is reached. The energy is low in this case because although the pressure is high, the change in gas volume is relatively low.

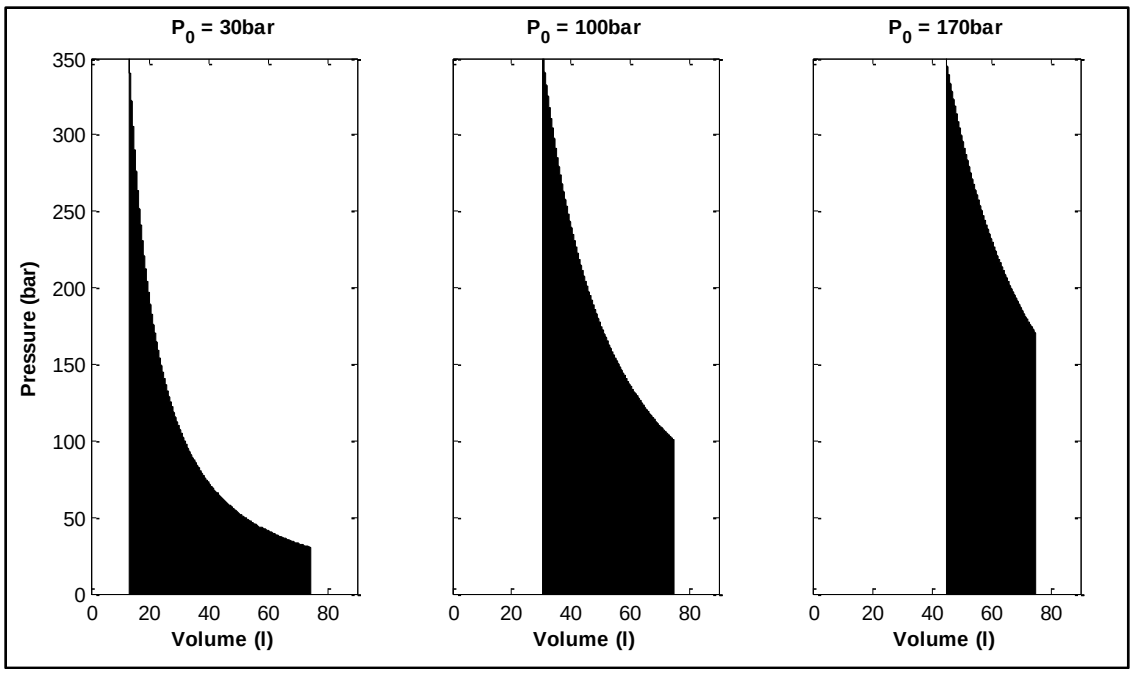

Figure 7: Adiabatic Gas Compression of a Nitrogen Filled Bladder Accumulator at Three Different Precharge Pressures

This phenomenon leads designers to pick a precharge and accumulator size that balances good energy storage with desired fluid storage. For work circuit hybrids, both characteristics are equally important. As mentioned previously, it is desired to set the accumulator precharge at the value that leads to the highest energy storage and then adjust the amount of fluid stored by changing the accumulator size. Figure 8 shows the energy and volume that can be stored while maintaining the derived relationship for ideal precharge pressure. Notice how the energy storage capacity is a function of the maximum pressure of the accumulator and the accumulator size while the volume of oil stored in the accumulator ($V_0 - V_2$) is only dependent on accumulator size. This is because of the fixed ratio between P_0 and P_2. This can be shown by recalling,

$$P_0{}^{1/n} V_0 = P_2{}^{1/n} V_2$$

We define the maximum oil volume as,

$$\Delta V = V_0 - V_2 \xrightarrow{yields} V_2 = V_0 - \Delta V$$

Substituting,

$$P_0{}^{1/n} V_0 = P_2{}^{1/n} (V_0 - \Delta V)$$

Rearranging and simplifying,

$$\Delta V = V_0 \left[1 - \left(\frac{P_0}{P_2} \right)^{\frac{1}{n}} \right]$$

Using the relationship derived earlier for maximum energy storage in the accumulator, $P_0 = 0.308 P_2$ for $n = 1.4$, the equation simplifies to,

$$\Delta V = 0.569 V_0$$

This equation applies for adiabatic nitrogen compression.

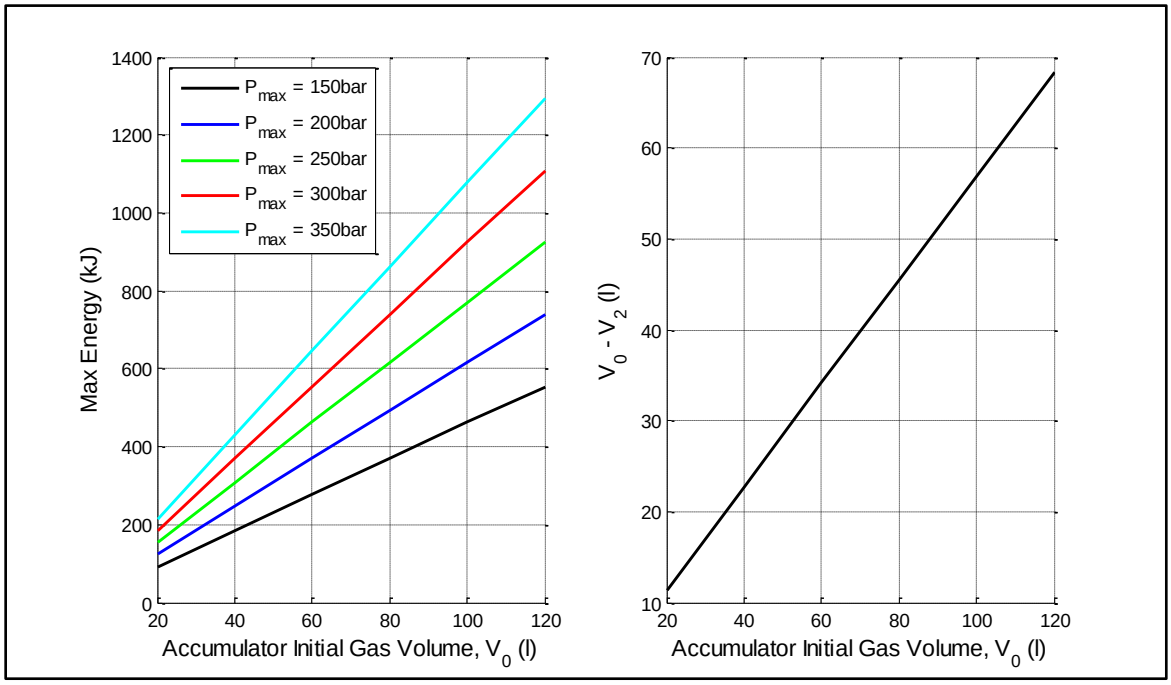

Figure 8: Accumulator Maximum Energy and Oil Volume Stored when $P_0 = 0.308\ P_2$ for Adiabatic Gas Compression

By using the relationships shown in Figure 8, an accumulator can be sized for both energy and volume storage. This is true for ideal adiabatic compression; therefore, the actual storage capacity will be reduced. There are two corrections that can be applied to these relationships to better size the accumulator. The two corrections are for thermal losses and for the fact that accumulators should not be emptied all the way to the precharge pressure. There is also the possibility to add an auxiliary nitrogen bottle which is connected to the nitrogen filled bladder of the accumulator. This effectively increases the volume of nitrogen gas.

Correction for Accumulator Working Range

The bladder in an accumulator can wear out prematurely if some basic precautions are not followed. The accumulator has an opening in one end to allow oil to enter/exit and this port is often quite large. If the accumulator is precharged and has no oil in it then the bladder will fill the full volume of the accumulator and has the possibility of extruding out of the oil port. To prevent this, bladder accumulators are equipped with a bladder extrusion poppet valve. These valves are often similar to a normally open, spring loaded check valve in operation and only close off the port when the bladder begins to push on it. Therefore, these valves do not affect the normal operational characteristics of the accumulator when the volume of the gas is less than the volume of the accumulator with the exception of a minor drop across the valve. The problem is created when the accumulator is fully emptied during use. When the extrusion poppet closes suddenly as the accumulator reaches an empty state it creates a dead headed situation for all the other circuit components. This can cause numerous system problems that are severe enough that it is important the accumulator never reaches this state. Most accumulator manufacturers recommend that the pressure in the accumulator should not drop below P_1 where P_1 is defined as, $P_1\sigma = P_0$ and $0.7 \leq \sigma \leq 0.9$. Obviously, by imposing this constraint, the energy and fluid

storage capacities of the accumulator are decreased. However, most of these losses can be eliminated by recalculating the optimal value for the accumulator precharge like the previous analysis but using the new pressure range. The relationships are as follows,

$$E_{max} = \frac{V_1 P_2}{n^{n/(n-1)}} = \frac{V_0 P_2 \sigma^{1/n}}{n^{n/(n-1)}}$$

This occurs when,

$$P_0 = \frac{P_2 \sigma}{n^{n/(n-1)}} = 0.308 P_2 \sigma \quad for\ n = 1.4$$

Using this relationship, the volume capacity becomes,

$$\Delta V = V_0 \left[\sigma^{1/n} - \left(\frac{P_0}{P_2} \right)^{1/n} \right] = 0.569 V_0 \sigma^{0.714} \quad for\ P_0 = 0.308 P_2 \sigma\ and\ n = 1.4$$

Unfortunately, there is still some loss because a smaller portion of the accumulator volume is utilized. Those losses can be calculated as follows,

$$\%E_{lost} = \%\Delta V_{lost} = \left(1 - \sigma^{1/n}\right) * 100$$

Figure 9 shows how this reduced working range affects the storage characteristics. It is clearly desirable to be as close to the upper boundary in the range to preserve as much storage capacity as possible. The actual lower pressure limit chosen for an application is dependent on how quickly the system can be controlled.

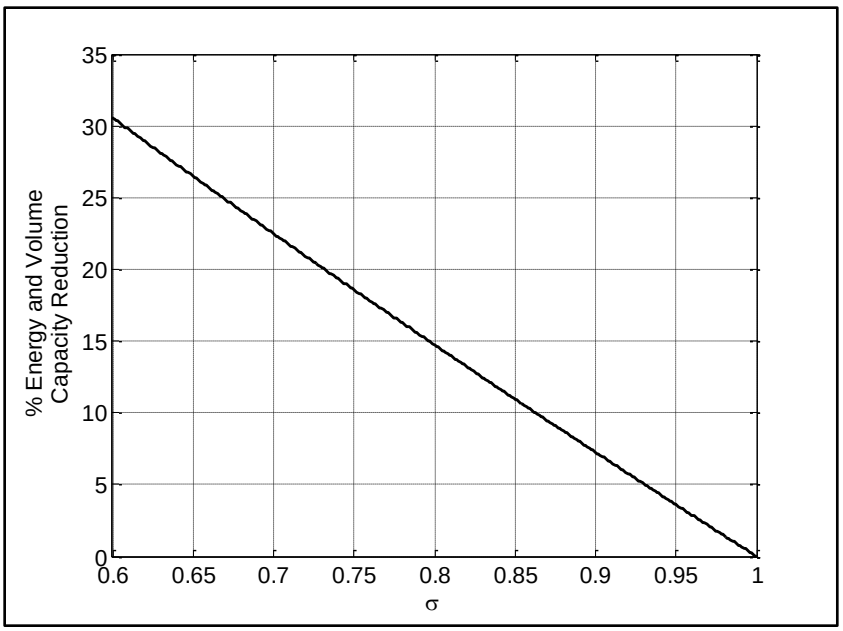

Figure 9: Effect of Reduced Working Range on Energy and Fluid Storage Capacities

Using an Auxiliary Gas Bottle

As mentioned, it is possible to connect the bladder of the accumulator to a second bottle that only has nitrogen. By doing this, it can increase the storage capacity of the accumulator with a much cheaper, less complex, and lighter gas bottle. The important thing to know about adding this auxiliary bottle is that it creates the possibility of compressing all of the gas out of the accumulator before the maximum pressure is reached. This will cause the same problem that the bladder extrusion poppet protects against, only it will occur in the gas port instead. In order to avoid this problem, we must restrict the size of the gas bottle to assure the max pressure is reached within the volume of the accumulator. To do this, the basic polytropic equation is revisited,

$$P_0{}^{1/n}V_0 = P_2{}^{1/n}V_2$$

Redefining the volume to account for the auxiliary bottle,

$$V_0 = V_0 + V_{N2B}$$

$$V_2 = V_2 + V_{N2B}$$

Substituting,

$$P_0{}^{1/n}(V_0 + V_{N2B}) = P_2{}^{1/n}(V_2 + V_{N2B})$$

Solving for V_{N2B},

$$V_{N2B} = \frac{V_2 P_2{}^{1/n} - V_0 P_0{}^{1/n}}{P_0{}^{1/n} - P_2{}^{1/n}}$$

Recall that for maximum energy storage,

$$P_0 = \frac{P_2 \sigma}{n^{n/(n-1)}}$$

Which when substituted in yields,

$$V_{N2B} = \frac{V_2 n^{1/(n-1)} - V_0 \sigma^{1/n}}{\sigma^{1/n} - n^{1/(n-1)}}$$

The critical auxiliary tank volume where the maximum pressure in the accumulator is reacted at the same time that the gas volume is exactly zero $(V_2 = 0)$ yields,

$$V_{N2B} \leq V_0 \frac{\sigma^{1/n}}{n^{1/(n-1)} - \sigma^{1/n}}$$

Therefore, as long as the auxiliary nitrogen bottle is smaller than this critical value, there will be no issues. The accumulator and the nitrogen bottle total volume can be used as an equivalent accumulator volume for the rules already developed. The percentage of energy and volume storage gained by adding the auxiliary tank is equal to the percentage of initial gas volume

increase. This can be a substantial amount especially considering how simple and inexpensive the change is.

Correction for Thermal Losses

Although the adiabatic equation is helpful to understand relative sizing, it does not take into account thermal losses and deviation of the gas from an ideal gas which can be quite high in these systems. Many accumulator manufacturers offer correction factors to help their customers size the accumulator for these differences but ultimately they do not offer a good set of equations to model the overall dynamics of the accumulator cycling. In order to model these accumulators more accurately, the Benedict-Webb-Rubin (BWR) equations are applied [72,73]. The BWR equations are derived from both fundamental thermodynamics as well as though empirical data sets. They essentially boil down into one differential equation and two algebraic equations that relate pressure, temperature, and specific volume. The BWR equations are as follows,

$$\frac{dT}{dt} = \frac{T_{amb} - T}{\zeta} - \frac{1}{c_v}\left[\frac{RT}{v}\left(1 + \frac{b}{v^2}\right) + \frac{1}{v^2}\left(B_o RT + \frac{2C_o}{T^2}\right) - \frac{2c}{v^3 T^2}\left(1 + \frac{\gamma}{v^2}\right)e^{\frac{-\gamma}{v^2}}\right]\frac{dv}{dt}$$

$$P = \frac{RT}{v} + \frac{B_o RT - A_o - \frac{C_o}{T^2}}{v^2} + \frac{bRT - a}{v^3} + \frac{a\alpha}{v^6} + \frac{c\left(1 + \frac{\gamma}{v^2}\right)e^{-\frac{\gamma}{v^2}}}{v^3 T^2}$$

$$c_v = \left[\frac{N_1}{T^3} + \frac{N_2}{T^2} + \frac{N_3}{T} + (N_4 - 1) + N_5 T + N_6 T^2 + N_7 T^3 + N_8\left(\frac{N_9}{T}\right)^2 \frac{e^{\frac{N_9}{T}}}{\left(e^{\frac{N_9}{T}} - 1\right)^2}\right] R$$

$$+ \frac{6}{T^3}\left(\frac{C_o}{v} - \frac{c}{\gamma}\right) + \frac{3c}{T^3}\left(\frac{2}{\gamma} + \frac{1}{v^2}\right)e^{-\frac{\gamma}{v^2}}$$

The terms of the BWR equations are described in Table 9. These equations are based on the idea that the rate of heat exchange between the accumulator and the environment can be modeled

using a thermodynamic time constant, ζ. This thermodynamic time constant defines how quickly the temperature of the gas will change given the temperature difference between the gas and the ambient air. The technical definition of the thermal time constant is the time required for the gas temperature to drop by 63.2% at constant volume after a rapid compression process [74]. The value for the time constant varies with accumulator orientation and the specific cycle that is being used although an average overall range of values has been experimentally obtained and is reported to be between 13.1 and 16 seconds for an un-insulated accumulator [72]. This correlates well to a paper by Pourmovahed and Otis where they have provided an empirical curve fit for several accumulator sizes [75]. Although the exact time constant should be experimentally obtained for each application, the equations are fairly insensitive to the values of this constant. This type of model is substantially easier to implement than a full model for heat transfer and the thermal time constant is easy to measure with relatively good accuracy in a physical system. However, there have been full finite element models developed to describe the thermodynamics of the system even more accurately [76].

An example of what the accumulator cycle looks like with this model compared to the adiabatic and isothermal models is shown in Figure 10. The accumulator started without any oil in it and the nitrogen is at ambient temperature. Oil is pumped in compressing the nitrogen to 350 bar. The compression of the gas very closely matches the adiabatic model which is expected because the compression happens quickly. Then a 10 second wait period occurs. During this time, heat is transferred out of the accumulator to the environment. This causes the temperature and pressure to drop in the accumulator. Once the flow is reversed, the pressure is allowed to drop to $P_1 = P_0/0.9$ and held for another 10 seconds. The temperature of the nitrogen at this point is actually lower than the ambient temperature and heat is transferred into the gas. The

energy transferred in causes the pressure to rise before the cycle starts over. After the first three cycles the equilibrium is reached and all subsequent cycles are the same. The thermal losses from the accumulator are a strong function of the time delay between charging and discharging. This can greatly reduce the overall efficiency of the accumulator. Figure 11 shows this variation between three cases. All cases were cycled until equilibrium was reached and then the energy and hysteresis were captured.

Table 9: Definition of BWR Coefficients

Variable	Valuable	Units
A_0	136.0436	$(m^3/kg)^2 Pa$
B_0	1.454397E-3	m^3/kg
C_0	1040558	$(m^3/kg)^2 K^2 Pa$
a	1.156984E-1	$(m^3/kg)^3 Pa$
b	2.966165E-6	$(m^3/kg)^2$
c	3357.338	$(m^3/kg)^3 K^2 Pa$
R	296.7923	$m^3 Pa/kgK$
α	5.786149E-9	$(m^3/kg)^3$
γ	6.753738E-6	$(m^3/kg)^2$
N_1	-735.210	K^3
N_2	34.224	K^2
N_3	-0.557648	K
N_4	3.5040	
N_5	-1.7339E-5	K^{-1}
N_6	1.7465E-8	K^{-2}
N_7	-3.5689E-12	K^{-3}
N_8	1.0054	
N_9	3353.4061	K

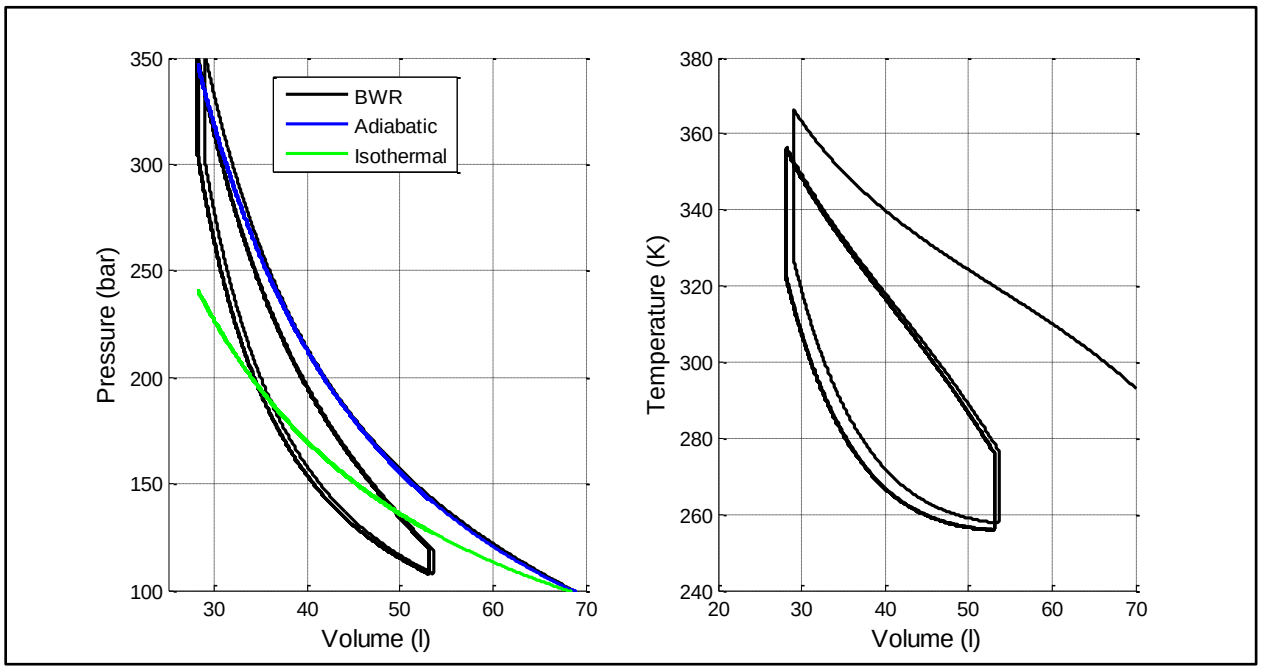

Figure 10: Comparison of Adiabatic, Isothermal, and BWR Bladder Accumulator Models

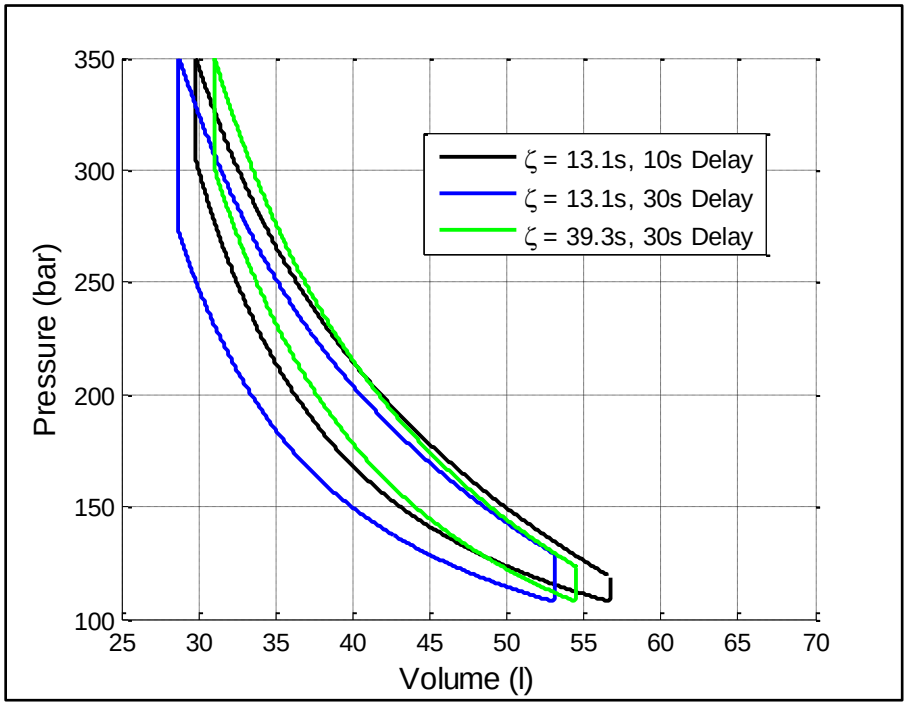

Figure 11: Thermal Losses of a Bladder Accumulator

Table 10: Bladder Accumulator Energy Storage for Three Cases

	ζ = 13.1s, 10s Delay	**ζ = 13.1s, 30s Delay**	**ζ = 39.3s, 30s Delay**
Energy Input (kJ)	545.7	510.7	482.2
Energy Released (kJ)	446.8	386.1	405.8
Thermal Energy Lost (kJ)	98.9	124.6	76.4
Accumulator Efficiency	82%	76%	84%

The delay time between pressurizing and depressurizing the accumulator has a direct effect on the energy storage capacity because the thermal change during the delay reduces the allowable volume change before the pressure limits are reached. It is interesting to note that increasing the thermal time constant also reduces the energy storage capacity although it drastically improves the efficiency. This is due to the fact that not as much energy is being used to change the temperature of the gas which changes the shape of the P-V curve. Increasing the thermal time constant of an accumulator can be achieved by adding elastomeric foam to the accumulator. The foam captures the gas within the pockets of the material and isolates the gas from the accumulator walls. In addition, the foam has a specific heat such that the gas compression causes almost no temperature rise. This process can be modeled by changing the differential BWR equation to,

$$\left[1+\frac{m_f c_f}{m_g c_v}\right]\frac{dT}{dt}=\frac{T_{amb}-T}{\zeta}$$

$$-\frac{1}{c_v}\left[\frac{RT}{v}\left(1+\frac{b}{v^2}\right)+\frac{1}{v^2}\left(B_o RT+\frac{2C_o}{T^2}\right)-\frac{2c}{v^3T^2}\left(1+\frac{\gamma}{v^2}\right)e^{\frac{-\gamma}{v^2}}\right]\frac{dv}{dt}$$

Where m_f and c_f are the mass and the specific heat of the foam respectively and m_g is the mass of the gas. Experimentally, this has been shown to create an almost perfect isothermal

compression while holding the efficiency of the accumulator at or above 95%. The thermal time constant with foam is on the order of several minutes [73,74]. Using elastomeric foam has been shown to hold up well over long term cycling as well. Pourmovahed showed that no chemical changes occurred to the foam after 36,000 cycles and only slight compression set occurs which reduces the efficiency by about 3% [77].

By using the BWR equations, the accumulator can be modeled with all of the previously described characteristics such as reduced working range, use of auxiliary nitrogen bottles, and now, thermal losses. This model will be carried forward into the models of the work circuit hybrid. For the purposes of understanding the feasibility of work circuit hybrids, it is suggested from this study that the accumulator should be sized roughly 10-30% oversized to account for the thermal losses and real gas dynamics that will occur in the accumulator. Hydac's correction tables seem to be even more conservative with a recommended increase of approximately 50% in accumulator size [78]. It is also recommended that some form of thermal insulation is used in conjunction with the hydraulic accumulator to reduce the thermal losses.

Hybrid Energy Transfer

The techniques developed to understand the energy storage of work circuit hybrids will be used to size the accumulator. But first the losses and capabilities of the energy transfer must be evaluated. The energy can be transferred throughout the system in a number of ways, each with its own losses and tradeoffs. These circuit architectures must be developed and quickly explored in order to decide which setup will yield the best results. The performance of the method in which power is provided to the work circuit can be measured knowing only the pressure and flow rate requirements of the auxiliary hydraulic system. Therefore, for simplicity,

the work circuit load can be thought of as a pressure drop over a variable orifice. By making this simplification, the complex dynamics of the auxiliary hydraulic system can be ignored for now. The feasibility study is meant for design space exploration which means that using book ended values will be sufficient to come to a conclusion about which designs are favored over others. While exploring the different architectures, it is more important to understand the robustness of each architecture against variations in the system than it is to optimize the architecture. The system can be generally represented as shown in Figure 12.

A hydraulic pump will be used to convert the rotational energy of the vehicle into a source of flow. This flow will fill the accumulator generating pressure and in turn, the pressure will provide the effort to move the cylinders, or in the simplified system, the effort to drive flow though the variable orifice. This pump may be the original engine driven pump or a secondary pump that can be located and sized appropriately to achieve the best performance. The sizing and location options for the hybrid pump will be explored separately from the rest of the circuit. The pump combined with the accumulator make up the regenerative braking portion of the system. There will also be a devise that controls the power flow out of the accumulator to the work circuit. This device can be manifested in several ways and will be examined second. It will be important that there is always a method of providing power to the work circuit. Therefore, it will be a requirement of each architecture that if the accumulator pressure is too low to provide the required power to the work circuit, a backup method for providing power will be available which can include using the original engine driven pumping method.

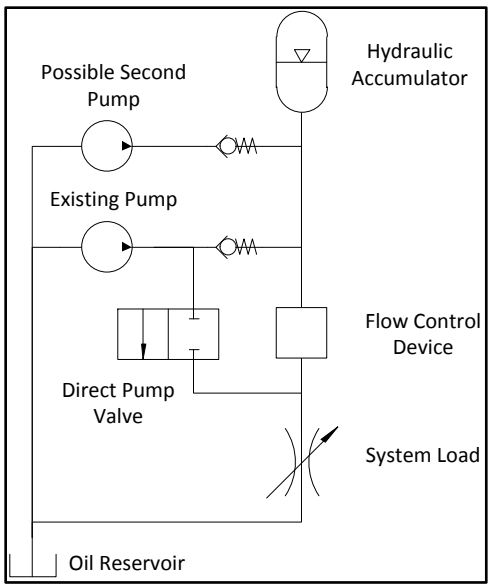

Figure 12: Simplified Work Circuit Hybrid Model

Energy Transfer to the Accumulator

Energy can be transferred to the accumulator in two ways. The first method utilizes the original pump location as shown in Figure 13 on the left side. Recall that most refuse trucks have an engine driven pump with no gearing or clutch. Here, either the stock pump, or a different pump, can be used in conjunction with a directional valve to achieve both regenerative capabilities and direct work circuit flow. There are challenges caused from using the pump in the stock position to accomplish regenerative braking. First, in order to capture the energy of the vehicle, the pump has to be able to utilize the momentum of the vehicle to generate the torque for pumping fluid. In a traditional hybrid, this is very straight forward because the pump is mechanically coupled to the road. In the case of an engine driven pump in a vehicle that utilizes an automatic transmission, the pump is no longer directly coupled to the road because of the torque converter that allows the vehicle to stop while the engine is running without completely disengaging the engine from the vehicle. The vast majority of refuse vehicles use an automatic

Allison transmission. To better understand the torque carrying capacity of a torque converter, recall that a torque converter is a specialized fluid coupling with three elements: the pump, the turbine, and the stator. The pump, not to be confused with the hybrid pump, is the housing of the torque converter connected to the engine and contains ribs or blades on one side to direct fluid tangentially in the direction of engine rotation. The turbine is a disc within the housing that also contains ribs and is mechanically connected to the inlet of the transmission. With these two parts alone a fluid coupling is created. If the pump is rotated in the direction of the engine then the paddles begin rotating the fluid in the housing. The rotating fluid has momentum that applies a force to the turbine blades causing the turbine to begin rotating in the same direction. This fluid coupling has a lag between the input speed and the output speed and the torque transferred between the two is limited by the fluids ability to transmit the shear load imparted by the blades. The final element of the torque converter is the stator. The stator is a smaller disc with specially designed blades and is connected to a one way clutch. This stator is designed such that when the pump is going faster than the turbine, the one way clutch is locked and the stator acts to redirect the fluid to create a torque multiplication between the pump and the turbine. The magnitude of the torque multiplication depends on how much of a speed differential there is between the two elements. If the speeds become close to the same, the torque multiplication goes to one. Now here is where the problem lies. If the speed of the turbine becomes faster than the speed of the pump, the one way clutch releases and the stator free wheels with the fluid flow which makes the torque converter look like a simple fluid coupling again. This occurs when the vehicle is slowing down which is the condition when the work circuit hybrid will need to store energy. With the losses inherent in a fluid coupling and without the stator providing torque multiplication, the torque converter will not provide the needed torque transfer to achieve regenerative braking. A

way around this would be to utilize the lockup clutch on the torque converter that allows the pump and turbine to be locked together mechanically. This option is often available in new transmissions for higher speeds but the controls are set to release at a minimum speed because if the clutch is not released in time, the engine will stall out as the vehicle comes to a stop. It is possible that the signal to lock the torque converter may be altered to achieve lock-up at lower speeds but there are inherent risks associated in doing this.

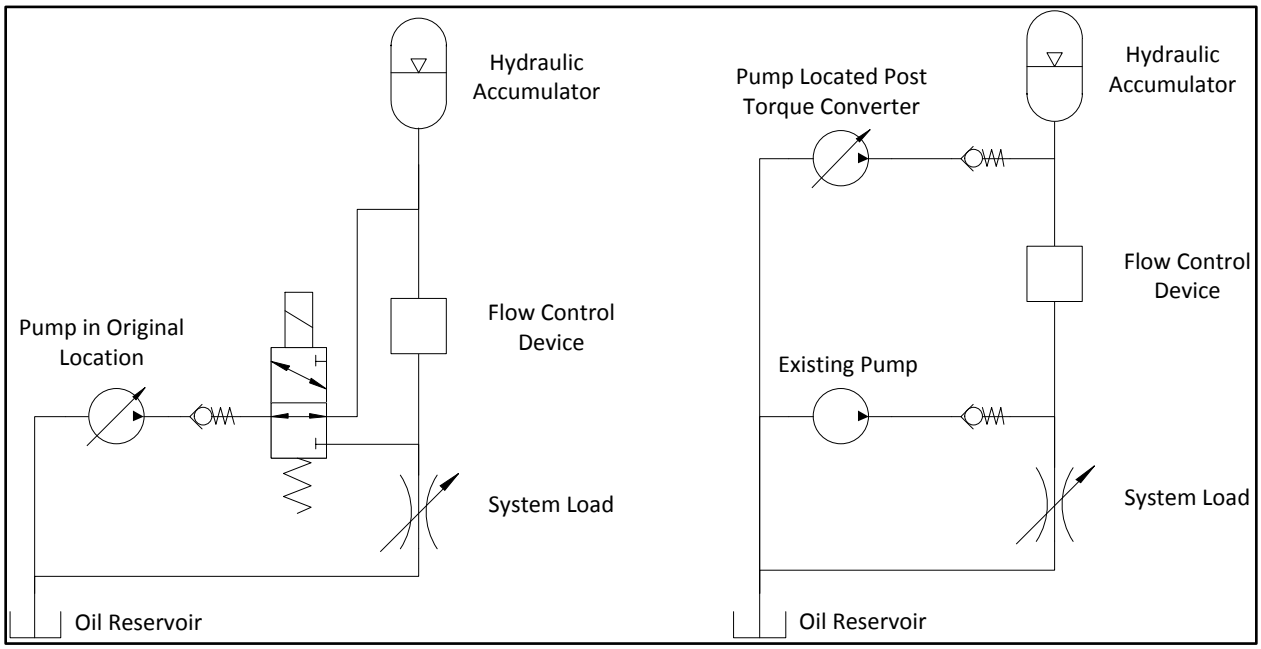

Figure 13: Left – Regeneration Achieved by a Variable Displacement Engine Driven Pump, Right – Regeneration Achieved by a Variable Displacement Pump Located Post Torque Converter

The second implication of needing to transfer energy backwards through the transmission is that the current transmission gear ratio at the time of regeneration will affect the torque of the pump. Typically, a transmission controller does not shift down until there is a positive torque command large enough to warrant it. Therefore, each time the vehicle slows down, the shifting logic can be requesting different gears and therefore, the resistive torque will be different. This will affect the performance of the hybrid energy transfer as well as the rate of hybrid

deceleration. Allison does offer an option called engine brake enable which is designed to downshift the transmission when engine braking is commanded and the torque converter lockup clutch is applied. This option or something similar would have to be utilized with a modified lockup signal to effectively brake using the regenerative braking system. Even with this system, the transmission will likely never shift below second gear because of engine speed limitations. While using the original pump location is convenient for minimizing part count, the difficulties in hybrid control may make this an undesirable solution.

The other method of transferring energy from the vehicle to the accumulator is to use a pump located after the torque converter of the vehicle as seen in Figure 13 on the right side. This method is identical to a traditional hydraulic hybrid where the pump requires a fixed gear and a clutch between the drivetrain and the pump. The problem with this configuration is that when the vehicle is stopped, there is no means of providing additional flow to the work circuit in the case that the accumulator is empty. To maintain the ability of running the work circuit if the accumulator is out of fluid and the vehicle is stopped, the original engine driven pump needs to be in the circuit in addition to the new pump. The pump in the standard position will not be needed the majority of the time and will only add losses to the system. Because of this potential failure mode, the system is heavier, requires more components, and is more expensive than the other method. However, the advantage, as discussed before, is that the gear ratio is known and there are no losses through the torque converter. In both methods it is desirable to have the regenerative pump be able to ramp up the torque using variable displacement. This will allow for a smoother transition to braking and prevent pumping losses during the portion of the drive cycle where the hybrid is not used.

A summary of the tradeoffs for both methods are shown in Table 11. Clearly, using the pump located in the engine driven position is better when compared with the post torque converter method in all categories except control strategy.

Table 11: Tradeoffs for Methods of Transferring Energy from the Vehicle to the Accumulator

	Engine Driven Pump	**Pump Post Torque Converter**
Added Cost	Variable Displacement Pump, Valves	Variable Displacement Pump, Valves, Gear Box with Clutch
Part Count	3-4 New Components	5 New Components
Added Weight	Almost none	~140 kg
Control Strategy	Requires torque converter lockup and transmission gearing control	Simple, typical hydraulic hybrid strategy

Now that the two configurations have been discussed, the required pump size can be evaluated for the two layouts. The pump size will be based on the amount of torque required to stop the vehicle and then the available oil volume from a single deceleration event will be calculated based on the pump size. The stock pump is sized such that it can provide the oil flow and pressure necessary to run the work circuit. It will be important to maintain this functionality while sizing the pump for the hybrid application; however, the requirements for regenerative braking are more demanding in both flow rate and pressure. Using the pump for hybrid operation will require the pump to run at variable speeds corresponding to the engine or vehicle speed during a deceleration event. In addition, the pump will need to provide a flow rate that is large enough to store the required fluid at the high accumulator pressure. The minimum accumulator pressure needs to be higher than the pressure required to operate the work circuit which means that the accumulator pressure will be much higher when full. It has already been established that the energy available for regeneration is only marginally larger than needed at best so it will be

important to pump the fluid as efficiently as possible. For first pass pump sizing, some assumptions are made to understand the relationships between pump displacement, vehicle deceleration rate, and volume of fluid pumped. First, the accumulator is assumed to operate between 100 and 350 bar which means the average will be somewhere around 225 bar. It is also assumed that the pump is operated at max displacement at all times which should be accurate enough because the time to ramp up to full displacement will be relatively short. The deceleration of the vehicle will be assumed constant for now and will represent the average deceleration rate calculated from the Ohio State University drive cycle which is 0.855m/s^2. Finally, it will be assumed that the pump is sized such that all braking torque can be provided by the pump. In reality, this would be the optimal case because all of the vehicle's energy would be utilized for pumping energy. Unfortunately, this may not be possible. With these assumptions, the pump displacement can be described by recalling,

$$\tau_p = \frac{P_{acc} d_p}{\eta_m}$$

Where τ_p is the torque produced by the pump, P_{acc} is the accumulator pressure, d_p is the pump displacement, and η_m is the mechanical efficiency of the pump. The pump torque can be related to the vehicle acceleration as follows,

$$-\frac{\tau_p \, GR \;\; RD}{r_t} - F_w - F_{rr} = m_v \ddot{x} = m_v \ddot{x}_{ave}$$

Where GR is the gear ratio between the pump and the driveshaft, RD is the rear differential ratio, and r_t is the tire radius. Combining and solving for the pump displacement,

$$d_p = -\frac{\eta_m r_t (m_v \ddot{x}_{ave} + F_w + F_{rr})}{P_{acc} \; GR \;\; RD}$$

Using this equation, the required pump displacement for decelerating the vehicle can be calculated for different gear ratios. The results are shown in Table 12. As expected the pump size increases as the gear ratio is reduced and as the mass of the vehicle increases. To understand how large the pump would have to be in the engine driven configuration, the gear ratios from a common refuse vehicle transmission were used. One additional gear ratio was also calculated to represent what the other configuration may be able to achieve with greater design freedom. If the transmission can be controlled so that it is always in second or first gear while decelerating, then using an engine driven pump will be possible using reasonable sized pumps. However, if the transmission is in a gear higher than second and possibly some cases while in second, the vehicle will not decelerate quickly enough without the use of a very large pump and another form of braking. If another form of braking is coupled with the pump to slow the vehicle, it will reduce the amount of energy and oil volume that is stored. For the other configuration, the pump size can be smaller because the gear ratio will be independent from the predetermined transmission ratios.

Table 12: Pump Displacement (cc/rev)

Vehicle Mass (kg)	**Gear Ratio (From Allison 3000 Series)**				
	4th 1	**3rd 1.41**	**2nd 1.86**	**1st 3.49**	**Other 5**
9000	170	120	91	49	34
27000	517	366	278	148	103

The volume displaced by the pump during this deceleration can be calculated using,

$$V_{disp} = \int Q dt = \int_0^{t_{stop}} \eta_v \omega_p d_p dt$$

Where Q is the volumetric flow rate of the pump, t_{stop} is the time that is required for the vehicle to come to a stop, ω_p is the pump speed, and η_v is the volumetric efficiency of the pump. It is also known that,

$$\omega_p = \frac{\dot{x}\ GR\ RD}{r_t}$$

Combining and integrating with the assumption that the vehicle decelerates at a constant rate,

$$V_{disp} = \frac{\dot{x_o}^2 d_p GR\ RD\ \eta_v}{2 r_t \ddot{x}_{ave}}$$

Substituting in the equation for displacement,

$$V_{disp} = \frac{\dot{x_o}^2 \eta_v \eta_m (m_v \ddot{x}_{ave} + F_w + F_{rr})}{2 \ddot{x}_{ave} P_{acc}}$$

Using this simplified analysis, an average starting velocity of 7m/s, and assuming the pump is chosen to provide the full braking torque, the volume displaced comes out between 9 and 28 liters depending on the vehicle mass. It seems odd to relate the volume displaced to the vehicle mass instead of the pump displacement but recall that it is assumed that the pump is sized to be able to provide the full braking torque. In other words, the heavier the vehicle, the bigger the pump which corresponds to a higher volume of oil pumped. Comparing this range to the required amount of fluid, which was calculated at about 10 liters for a side loader, it appears that storing the required amount of oil is possible but may be difficult for some instances. With this information it is now possible to size the accumulator.

Initial Accumulator Sizing

Now that the accumulator models have been developed and the options for energy transfer to the accumulator have been evaluated, these tools can be used to determine roughly how large of an accumulator is needed and what the desired precharge will need to be in order to store the required amount of energy and fluid volume. To give the best chance of operating the work circuit, the side loader was chosen as discussed earlier. Recall that in addition to the 10 liters of volume, the side loader requires approximately 186kJ of energy to operate. Concentrating of the energy storage first and assuming 15% thermal losses in the accumulator, 15% lost in the energy transfer out of the accumulator, and a 7% correction for using a good working range, the accumulator can be sized as follows,

$$E_{acc} = \frac{E_{req}}{0.85 * 0.85 * 0.93} = 277kJ$$

The minimum pressure that the accumulator will supply fluid from will be the limiting factor because without adequate pressure, the cylinder lifting capacity will be affected. Therefore, the accumulator maximum pressure must be maintained as high as possible in order to provide this 277kJ of energy. Given that the maximum working pressure for these work circuits is around 210 bar, the system will likely operate around 105 bar. In order to keep the minimum accumulator pressure above this, the accumulator will need to operate at 350 bar max. Therefore, the accumulator needs to be at least a 30 liters capacity as seen in Figure 8. The fluid volume must also be enough to produce a full stroke in the hydraulic cylinders which was determined to be 10 liters of oil. The pump will provide between 9-28 liters of oil so it is desirable to size the accumulator to hold as much of this oil as possible. Assuming that the volumetric efficiency of the fluid transfer out of the accumulator is 95%, the thermal efficiency is 85%, and the reduced

working range correction generates 7% reduction in storage volume, the accumulator must be sized as follows,

$$V_{acc} = \frac{V_{req}}{0.569 * 0.95 * 0.93 * 0.85} = 24\ to\ 66\ liters$$

Looking at both the energy storage and oil volume capacities of the accumulator, an initial accumulator volume should be about 40 liters. This size should provide the required energy and volume storage needed as well as capture most of the oil displaced by the pump. This is a reasonable size for commercially available accumulator.

Energy Transfer from the Accumulator to the Work Circuit

The hybrid system as it stands now is capable of capturing and storing energy in a high pressure hydraulic accumulator. The work circuit is also in place which allows the operator to direct the fluid to the desired cylinder. The final piece of the system that has to be examined to round out the first pass analysis of work circuit hybrids is the method in which energy is transferred to the work circuit from the energy storage devise. Recall that the accumulator pressure will decrease as the oil volume is reduced. Therefore, it is necessary for the starting pressure of the accumulator to be higher than the desired work circuit operating pressure in order to use the full volume of fluid in the accumulator to operate the cylinders. This will require a devise that controls the pressure and flow to the work circuit from this high pressure source. As discussed in the energy storage section, the accumulator maximum pressure can be adjusted as long as the precharge is also adjusted. Depending on the flow control devise chosen, the accumulator sizing and pressures can be tweaked to get better performance.

Adjustable Orifice Valve

This is the simplest of all the flow control devices. A simple variable orifice flow control valve can be used to control the flow to the system. We can calculate the flow through the orifice using the basic orifice equation,

$$Q = C_d A \sqrt{\frac{2(P_{acc} - P_{load})}{\rho}}$$

By solving this equation for $C_d A$ the desired flow can be used to find the correct setting in the valve. The valve is only limited by the minimum and maximum flow area and this is reflected in the valves ability to provide the desired flow with the given accumulator pressure. It is worth noting that the efficiency of the orifice flow control valve is,

$$\eta = \frac{\dot{E}_{out}}{\dot{E}_{in}} = \frac{P_{load} Q}{P_{acc} Q} = \frac{P_{load}}{P_{acc}}$$

This shows that the more pressure we have stored in the accumulator, the less efficient we are at releasing it. This type of loss is often referred to as a throttling loss. Controlling the system in this fashion is simple, inexpensive, and easy to implement and control. The drawback is that the efficiency is extremely poor.

Hydraulic Transformer

A hydraulic transformer is a device that converts high pressure and low flow to low pressure and high flow or vice versa. This device can be created in multiple ways as discussed briefly in the introduction. For this research, two hydraulic transformers will be evaluated. The first is built as a reverse hydrostat where a motor is hydraulically driven by the accumulator. The output shaft of the motor is connected to the input shaft of a pump. The pump hydraulically powers the work

circuit. In order to get variable transformations, either the pump or the motor must be variable displacement. A diagram of the implementation of this system is shown in Figure 14. The other hydraulic transformer that will be evaluated here is the Inna's Transformer technology which is covered next. For the reverse hydrostat transformer, the following relationships for this system hold,

$$\tau_m = P_{acc} d_m \eta_{mm}$$

$$\tau_p \eta_{mp} = P_{out} d_p$$

$$T_m - T_p = I \frac{d\omega}{dt}$$

$$Q_{acc} \eta_{vm} = d_m \omega_m$$

$$Q_{des} = d_p \omega_p \eta_{vp}$$

$$\omega_p = \omega_m = \omega$$

Combining these equations, the system becomes,

$$P_{acc} d_m \eta_{mm} - \frac{P_{out} d_p}{\eta_{mp}} = I \frac{d\omega}{dt}$$

$$\frac{Q_{acc} \eta_{vm}}{d_m} = \frac{Q_{des}}{d_p \eta_{vp}}$$

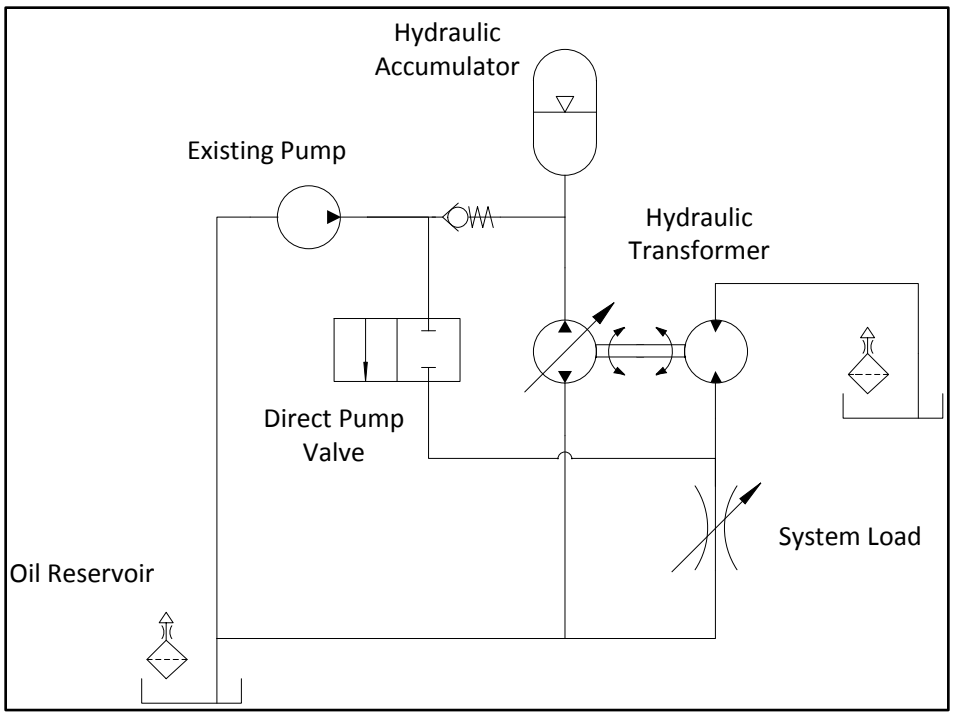

Figure 14: Work Circuit Hybrid with Reverse Hydrostat Transformer Flow Control

This system offers some distinct advantages over the variable orifice control. First, the power that is available at the work load is theoretically equal to the input power. This is the fundamental difference between the hydraulic transformer and the adjustable orifice control. The adjustable orifice dissipates the excess energy through throttling losses while the hydraulic transformer converts the energy into another form. In actuality, the transformer efficiency is reduced by friction and flow losses but the hydraulic transformer is more efficient because it fundamentally starts that way. The second note that can be made is that because the power has to be the same at the inlet and outlet minus efficiency losses, the flow rate out of the accumulator can be substantially lower than the flow rate to the work circuit when the accumulator pressure is high. This is extremely beneficial because it means that having high pressure in the accumulator will reduce the rate of pressure drop. This is exactly opposite of the variable orifice where the efficiency drops with higher pressure. On the contrary, the hydraulic transformer is clearly more

complex and more expensive. There are some potential ways to simplify and/or reduce cost for the transformer including making only the accumulator side variable displacement. It is necessary to have variable displacement on the accumulator side because it allows for a consistent way to stop the flow from the accumulator. The pressure on the work load side only exists when fluid is provided to the circuit by the transformer and therefore, a fixed displacement unit will work in this location. Another method of cost reduction would be to use a gear or vane unit instead of a piston unit on either side. However, hydraulic gear and vane units are difficult to find with operating pressures above about 200 bar.

It is also important to consider the controllability of this circuit. If this type of system is to be implemented in a work circuit hybrid, it will be necessary for the transformer to be stable under all circumstances, especially because over speeding a hydraulic pump or motor will rapidly decrease the life of the unit, or worse, the unit may be damaged and stop working. In actuality, it may be extremely difficult to control the acceleration rate of the transformer because the inertia of the unit is so small. If the pressure varies as a function of the flow rate, large variations in the resistive torque will occur and this torque is required to control the acceleration. To get around this problem, an adjustable orifice can be placed downstream of the transformer which allows for the regulation of pressure on the outlet. This causes an additional inefficiency by creating a pressure drop in the line. However, this pressure drop is substantially lower than the pressure drop without the transformer so the overall efficiency should remain higher. For now it will be assumed that the hydraulic transformer is controllable under all circumstances. Further development and understanding of the control requirements will be left for future work.

Innas' Hydraulic Transformer

As discussed previously, Innas has come up with a unique solution for creating a hydraulic transformer. They have taken a regular swash plate or bent axis hydraulic piston pump design and modified the port plate to have three ports. In addition, the port plate can rotate with respect to the top dead center (TDC) of the pump. The drive shaft is not necessary for this application and is removed. A mock up diagram of the rotating group and the custom port plate is shown in Figure 15. To understand how this works, imagine that the cylinder block that contains the pistons and the pistons themselves rotate with the slipper plate that the pistons are attached to. The swash plate at the end maintains the angle shown so that as the pistons rotate, they also translate in and out of the cylinder. Now imagine if the load and vent pressures are zero and the position of the port plate relative to TDC is located as shown. This position results in the torque on the rotating group being balanced. The accumulator pressure pushes on each side of top dead center equally and no rotational torque occurs. If the angular position of the port plate is moved, then the accumulator pressure will act with a bias in one direction of rotation and the transformer will accelerate. If the load and/or vent pressure is nonzero, then a new position for the port plate would be required to maintain steady state torque balance between the pistons on either side. This is represented in Figure 16 as δ_{SS}. The actual angle of port plate rotation past the steady state point is indicated as δ. The port openings on the plate encompass a certain angle of the plate and these will be used in calculated the amount of torque provided by each port.

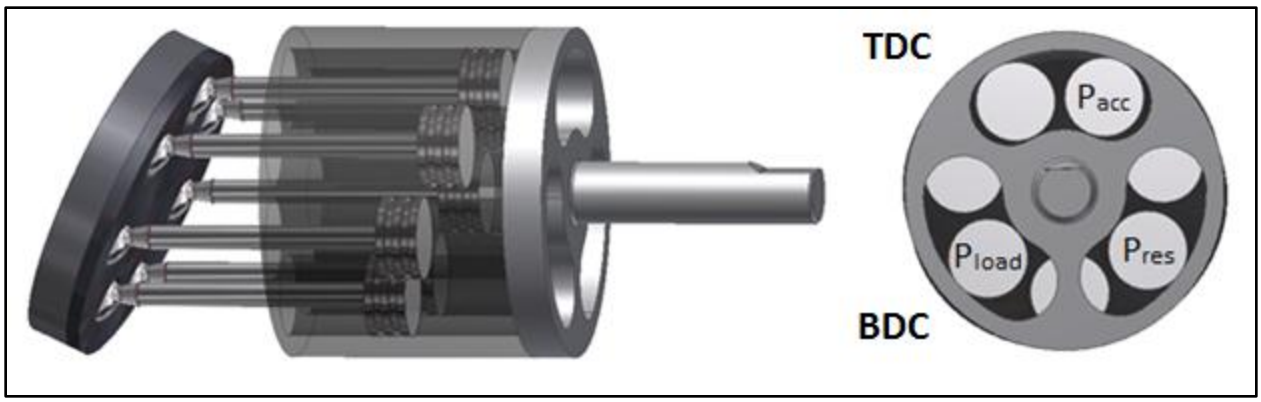

Figure 15: Innas' Hydraulic Transformer Mock Up

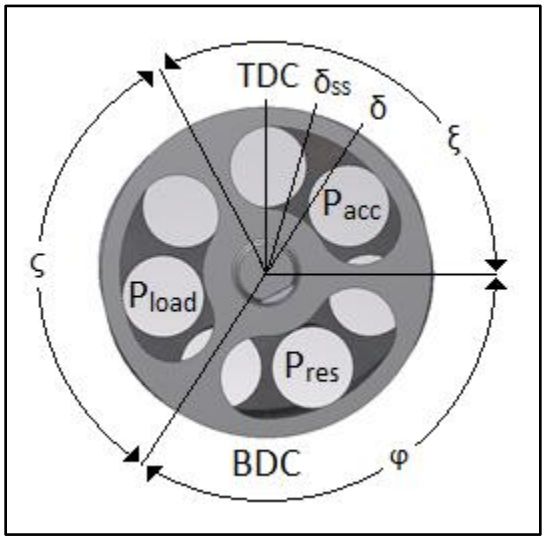

Figure 16: Innas' Hydraulic Transformer Notation

The amount of torque applied to the rotating group by each port can be calculated using,

$$\tau = Pd\sin(\delta)\sin\left(\frac{Port\ Opening\ Angle}{2}\right)$$

Therefore, the sum of the torques on the center axis can be represented as follows,

$$\left[P_{acc}\sin(\delta)\sin\left(\frac{\xi}{2}\right) + P_{load}\sin\left(\delta - \frac{\xi}{2} - \frac{\varsigma}{2}\right)\sin\left(\frac{\varsigma}{2}\right) + P_{res}\sin\left(\delta + \frac{\xi}{2} + \frac{\varphi}{2}\right)\sin\left(\frac{\varphi}{2}\right)\right]d$$

$$= I_t\frac{d\omega}{dt}$$

Where ξ, ς, and φ are the angles encompassed by the port openings which do not have to be equal. For this analysis it will be assumed that $\xi = \varsigma = \varphi = 120°$ however which results in,

$$\left[P_{acc}\sin(\delta) + P_{load}\sin\left(\delta - \frac{2\pi}{3}\right) + P_{res}\sin\left(\delta + \frac{2\pi}{3}\right)\right]\frac{\sqrt{3}}{2}d = I_t\frac{d\omega}{dt}$$

We can find the flow rates using,

$$Q = -\omega d\sin(\delta)\sin\left(\frac{Port\ Opening\ Angle}{2}\right)$$

Therefore,

$$Q_{acc} = -\frac{\sqrt{3}}{2}\omega d\sin(\delta)$$

$$Q_{load} = -\frac{\sqrt{3}}{2}\omega d\sin\left(\delta - \frac{2\pi}{3}\right)$$

$$Q_{res} = -\frac{\sqrt{3}}{2}\omega d\sin\left(\delta + \frac{2\pi}{3}\right)$$

These are the dynamic equations for the system and a schematic of the system using the Innas' schematic symbol for their transformer is shown in Figure 17.

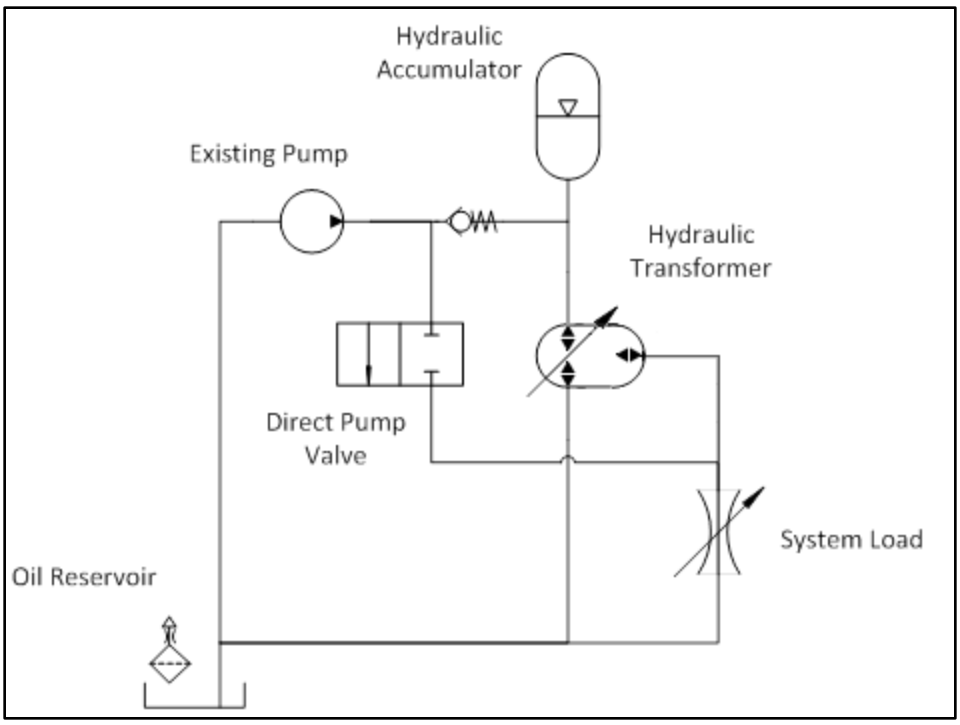

Figure 17: Work Circuit Hybrid with the Innas' Transformer Flow Control

Note that this devise suffers from the same controllability issue as the reverse hydrostatic transformer because the inertia is small and the work circuit inlet pressure may still vary with transformer flow rate. Again, the controllability problem will be ignored for now. This devise offers further advantages from the reverse hydrostatic transformer by combining the pump and motor into one devise. It also yields higher efficiencies because only one rotating group is needed as well as the improvements gained by using Innas' Floating Cup Principle [79]. The drawbacks of the devise besides the possible controls issue include that this technology is not yet fully developed and commercially available. In addition, pressure spikes and cavitation are a problem because the port transitions occur at points where the piston has velocity instead of at TDC and BDC.

Work Circuit Hybrid Architecture Comparison and Selection

This chapter was meant to take the idea of a work circuit hybrid and develop it into a set of physical components that can be evaluated in order to understand the benefit of this technology. The system has been functionally decomposed into the fundamental components required to make a work circuit hybrid. This section is meant to summarize the predicted performance of each component and to select the most promising architecture for further exploration. The chapter was broken down into braking energy, required hydraulic energy, hybrid energy storage, hybrid energy transfer to the accumulator, and hybrid energy transfer to the work circuit. In the braking energy analysis it was determined that the typical refuse vehicle must dissipate 206-614 kJ of energy per stop depending on the weight and dimensions of the vehicle. This will also vary based on the average speed that the vehicle is stopping from. Because only the Ohio State University drive cycle was available for this portion, there is some uncertainty in this number. In the required hydraulic energy analysis, side loaders required the least amount of energy and fluid volume to run the work circuit at 187 kJ and 10 liters respectively. Therefore, the side loader was chosen as the most promising candidate for hybridization. In addition, it was determined that if the hybrid efficiency is high, there is a good likelihood that the work circuit hybrid will be able to provide all of the work circuit energy for the majority of the stops.

The hybrid energy storage section developed a method for sizing a bladder accumulator for a mobile application. It was shown that for adiabatic compression of the bladder, the maximum energy storage is achieved when the precharge is 0.308σ of the maximum working pressure. Holding the pressures to this ratio, it was also determined that the oil storage capacity

of the accumulator is $0.569\sigma^{0.714}$ of the initial gas volume for the ideal case. Then correction factors were developed for thermal losses. Finally, the options of using elastomeric foam and auxiliary nitrogen bottles to enhance the performance of the accumulator were explored. The elastomeric foam yields a much higher thermodynamic efficiency from the un-insulated case and the auxiliary nitrogen bottle increases the oil capacity of the accumulator economically and with better weight properties. It is important to remember that the auxiliary bottle should never be more than a calculated percentage of the accumulator volume to prevent the bladder from being damaged near the maximum pressure limit. The next section analyzed the method of transferring energy to the accumulator with two candidate configurations. The first configuration used an engine driven pump to deliver the fluid while the second used a post torque converter pump. It was determined that the engine driven pump is better for simplicity, part count, and weight reasons. However, it will be necessary to control the torque converter lockup clutch and the transmission shifting strategy to make this configuration work well. It will be assumed that the ability to control the transmission as desired is available as this seems to be accepted by the industry. Therefore, with the engine driven configuration, the pump and accumulator were sized using this first pass analysis and the recommended are a 150 cc/rev pump and a 40 liter accumulator. Using the post transmission pump requires an additional gear box but the pump size can be reduced to about 100 cc/rev. The last component examined was the method of transferring energy from the accumulator to the work circuit. The main problem here is that the accumulator pressure will be higher than the desired pressure at the inlet of the work circuit which, if not controlled, will results in unsafe cylinder velocities. Three methods of flow control were examined, an adjustable orifice, a traditional hydraulic transformer, and the Innas' hydraulic transformer. The adjustable orifice is simple but creates significant throttling losses

that greatly decrease the potential of this technology. The traditional transformer is heavy, complex, and because it used two hydraulic units, the efficiency is still not very promising. The Innas' transformer is clearly the best candidate for success; however, the controllability of the unit needs to be looked at in further detail.

With these details worked out, it is clear that the work circuit hybrid is a feasible and promising new technology. To fully understand the potential of these hybrids, more detail about the operating conditions of refuse vehicles must be known. In addition, a dynamic model must be developed to determine the optimal sizes of the components. These items will be explored in the following chapters.

CHAPTER 2: DRIVE CYCLE CHARACTERIZATION

Chapter 1 was meant to address the feasibility of work circuit hybrids and to roughly understand the component sizes and configurations needed to achieve the desired functionality. This is a necessary step in the process; however, the more important question about what value this technology offers has yet to be answered. In order to predict what benefit this technology might produce, a more accurate set of operating conditions is needed. Since there has been relatively little data collected on refuse vehicle drive cycles, there is still a high uncertainty about how these vehicles are driven. There are only three available drive cycles for refuse vehicles, one of which is for rear loaders, the other two for side loaders. Out of the two for side loaders only one contains hydraulic power demands. In addition, only one of the three drive cycles has data that is publically available. Therefore, in order to further understand and validate the work that has already been done, data was collected on two Denver based refuse vehicles. To be more specific, these vehicles are used in the smaller cities surrounding Denver itself. Both vehicles used for the study were 28 cubic yard (21.4 m^3) McNeilus Street Force MA refuse trucks that operate on residential routes throughout Denver's surrounding areas. These vehicles were made available by Republic Services which is currently the second largest waste collection company in the US. Data was collected though two sources; the first being the vehicle's J1939 CAN bus which provides information about the vehicle's engine, transmission, and chassis. The second source, which was only operational for the second vehicle, is a pressure transducer that is located on the outlet of the work circuit pump. This pressure signal is fed to a CANverter unit that converts the analog signal into CAN messages. Both the vehicle's CAN messages and the CANverter CAN messages are recorded in a Kvaser Memorator Pro data logger. The logger

automatically synchronizes both channels of data and has enough capacity to collect about 30-40 hours of data before running out of memory. This allows the logger to be placed on the vehicle for a full shift or multiple shifts before interfacing with a computer. The data is then converted to Matlab vectors in engineering units with the conversions provided by the SAE J1939 standard protocol [80,81]. Using this setup, the signals in Table 13 were collected and analyzed. In addition to the data collected by the data logger, Republic Services provided additional information about the vehicles which is summarized in Table 14.

Both vehicles were driven on various residential recycling routes in Denver. Data was collected for a total of 14 days between the two vehicles for shifts lasting around 11 hours. The data logger automatically powers up when the vehicle's ignition is keyed on and all available data is collected. The data is broken down and analyzed using two methods. The first method looks at all driving and idling conditions including when the truck is warming up, driving on the highway, at the land fill, and on route. This method is used to generate overall maps of how the engine and transmission function. A fuel rate map can be populated by interpolating specific values out of an extensive array of data. In addition to generating component maps, the first method is useful to examine how much fuel and time is used overall at different operating conditions. The second method looks only at the data produced while on-route. This method is important in generating the statistics needed to simulate the performance of the hybrid. It is using this method that the work circuit power, energy, pressure, and flow requirements are evaluated. Both of these methods and the corresponding statistics derived from each are discussed in the following sections.

Table 13: Data Collected From Data Logging

Signal	Sample Rate	Source
Engine Speed	50 Hz	Vehicle CAN Bus
Pump Speed	50 Hz	Vehicle CAN Bus
Pump Pressure (Hydraulic Arm Side)	10 Hz	0-3000psi Pressure Transducer
Vehicle Speed	10 Hz	Vehicle CAN Bus
Engine Instantaneous Fuel Rate	10 Hz	Vehicle CAN Bus
Transmission Gear Command	10 Hz	Vehicle CAN Bus
Current Transmission Gear	10 Hz	Vehicle CAN Bus
Current Transmission Gear Ratio	10 Hz	Vehicle CAN Bus
Percent Engine Torque Command	50 Hz	Vehicle CAN Bus
Percent Engine Torque Feedback	50 Hz	Vehicle CAN Bus
Accelerator Position	20 Hz	Vehicle CAN Bus
Percent Engine Load	20 Hz	Vehicle CAN Bus

Table 14: Republic Services Vehicle Specifications

Chassis	2010 Mack TerraPro LEU613 GVWR 66,000 lbf (294 kN)
Body	28 yd^3 (21.4 m^3) McNeilus M/A Side Loader
Overall Vehicle Dimensions	95.4” x 145” x 350” (W x H x L) (2.42m x 3.68m x 8.89m)
Engine	Mack MP7-325M
Transmission	Allison 4500 RDS
Torque Converter	Unknown (One of the standard models)
Rear Differential	5.02 ratio
Tires	315/80R22.5 (0.53m radius)
Telma Unit	Yes
Hydraulic Pump	Parker Tandem P350 Pump 2.25”x2.25” (94.1 cc/rev) with HOC and Pack-on-the-go flow control

Data Analysis Method 1: Overall Operation Statistics

Data from all operating conditions including vehicle warming up, driving on the highway, idling at the land fill, and stop and go driving on route are used for this analysis. This data is used to develop an engine fuel map. In addition, the overall driving characteristics of the vehicle can be examined from this data set.

Engine Fueling Map

The engine fueling map is the critical link between the work circuit hybrid design and the actual customer benefit. The hybrid acts to reduce energy used by the vehicle on-route but the payback comes from the reduction in fuel used by the engine. Therefore, the fuel burned as a function of engine speed and engine load is needed. All three elements of the map are available for logging from the CAN bus in the vehicle. The collected data is recorded as a function of time. Therefore, to generate the map, the corresponding engine speed, engine load, and engine fuel rate points can be matched up and plotted as a three dimensional scatter plot. This scatter plot of individual points is not very useful in its existing form because there are literally millions of points and there may be several different fuel rates recorded for a given speed and load. Therefore, the three dimensional scatter plot is interpolated, using average values for speed/load combinations with multiple fuel rates, to generate a three dimensional surface that is defined by a much smaller matrix of values. This map is a good representation of the engine performance and it will be validated using a dynamic model of the vehicle in the following chapter. The scatter plot and its corresponding interpolated map are shown in Figure 18. In addition, the matrix used to define this map is laid out in the Appendix. This map should be accurate for work circuit, hybrid work circuit, and stock vehicle operation because the map is a function engine speed and load only. Correctly adding the work circuit and hybrid work circuit load when calculating the engine load will lead to a fairly accurate method of predicting the resulting fuel usage. One thing to note about using this map is that the engine load is expressed as a percentage of maximum engine load. The engine torque curve is needed to determine maximum load for any given engine speed.

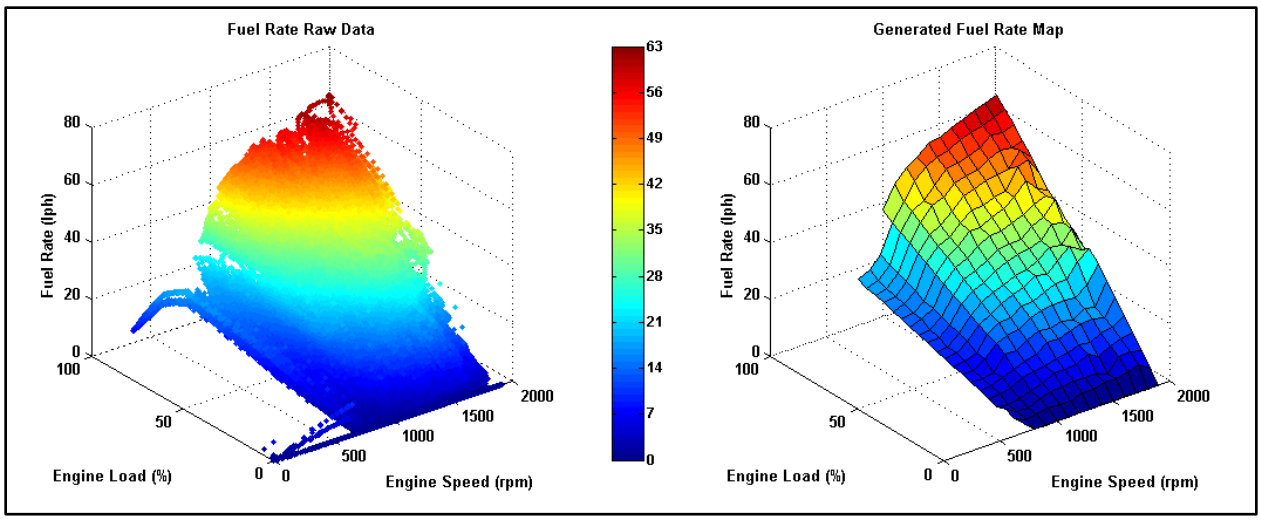

Figure 18: Fuel Rate Data and Mathematically Generated Map from a Full Day Shift on the Republic Services' Automated Side Loader Refuse Truck for a Mack MP7-325M Engine

Engine Torque and Power Curves

The torque curve for the Mack MP7-325M is not publically available; however, some specific data points for power and torque are given for certain engine speeds. From this information and by scaling torque and power curves from other similar Mack engines, a good estimation of the engine curves can be generated. The curves used for this study is shown in Figure 19 and the raw data can be found in the Appendix.

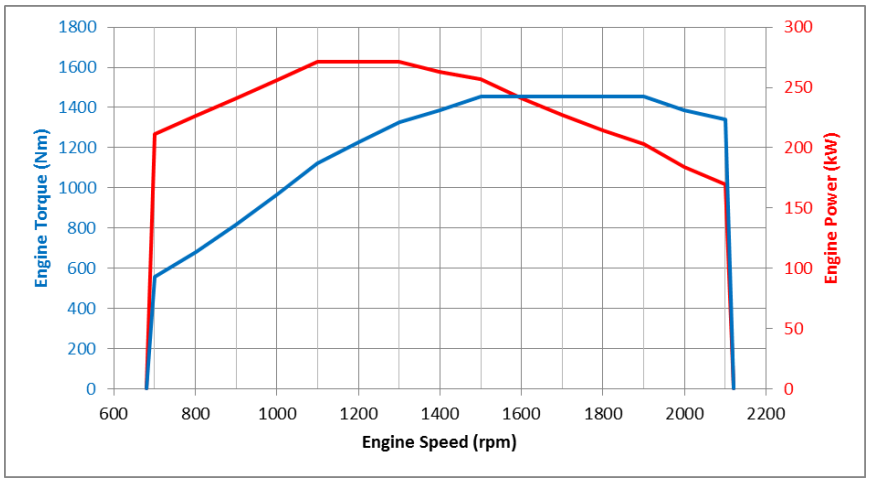

Figure 19: Estimated Mack MP7-325M Engine Torque and Power Curves

Overall Vehicle Statistics

The last piece of information that will be taken from the full data set is some statistics of how the vehicle is used overall. In particular, determining what the breakdown of time and fuel usage is between different speeds and sections of the drive cycle will be especially helpful in determining the overall benefit of adding a hybrid to the vehicle. First, the data is examined purely based on vehicle speed. Therefore, the vehicle warm up period, stops to pick up refuse, and time idling at traffic lights and at the land fill are all under the 'vehicle at idle' classification. Likewise, driving to the route and driving on-route is grouped into vehicle speed categories. The overall time and fuel spent in each of these categories is shown in Figure 20. This figure shows some astonishing results. If the vehicle's engine is running for 11 hours during a normal day of operation, the vehicle is idling almost 5.5 hours of that time. In addition to that, the vehicle spends 83.7% of the day below 30 kph. Examining the fuel usage data, the results are even more profound. 66.5% of the fuel used during a typical day is consumed when the vehicle is under 30 kph and 26.2% of that is consumed at idle. This data reinforces the fact that automated side loaders will benefit significantly from any fuel savings that can be realized at low vehicle speeds. It was also determined that the vehicle spends approximately 80% of the time driving on-route and the work circuit is in operation 13.6% of the time. 11.9% of the fuel is consumed while the work circuit is in operation although only a portion of this is used to power the work circuit.

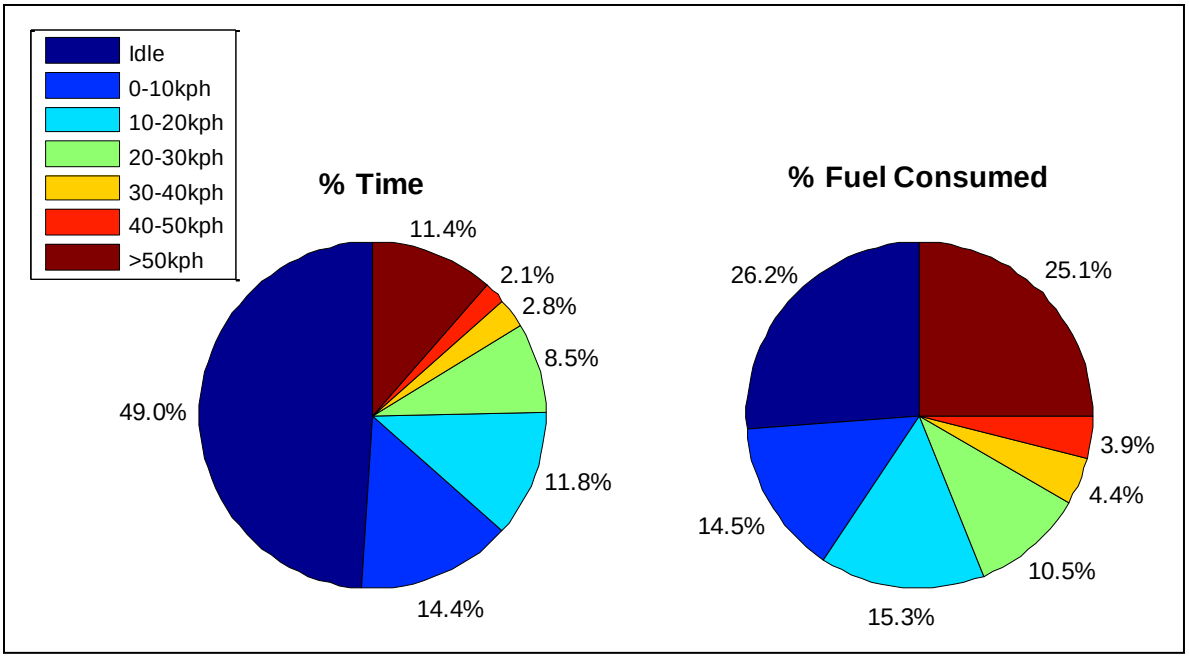

Figure 20: Time and Fuel Consumption during All Vehicle Operation

It is also helpful to check the available regenerative energy against the required hydraulic energy so that a comparison can be made with the first pass evaluation. The values for each of the data sets are shown in Table 15. The table shows that the actual energy required from the hydraulics is a smaller percentage of the available energy from regeneration than predicted originally. The first pass analysis predicted that 30-91% of the regenerative energy would be needed to operate the work circuit. There are a few conclusions to make from this information, the first being that the automated side loader may actually under-utilize the energy saving potential. It may be possible in future work to justify the application of work circuit hybrids to a more demanding hydraulic cycle. The other conclusion is that this gives a bit of head room for inefficiencies that may inherently plague this type of system. The fact that the regenerative torque must be harnessed through a rear differential, and possibly a transmission and torque converter, which are all very inefficient in the reverse direction, suggests that this may be necessary room for losses.

Table 15: Measured Energy Balance between Regeneration and Hydraulic Usage

Data Set	Measured Regenerative Energy Available (MJ)	Measured Hydraulic Energy Required (MJ)	% Utilization
2011-10-06	209	30	14.4%
2011-10-07	266	48	18.0%
2011-10-10	412	59	14.3%
2011-10-11	188	29	15.4%
2011-10-12	211	34	16.1%
2011-10-13	196	31	15.8%
2011-10-14	233	44	18.9%
2011-10-17	352	59	16.8%
AVERAGE	**258**	**42**	**16.3%**

Data Analysis Method 2: On-Route Operation Statistics

The second method of examining this data is to only look at on-route performance. By investigating the characteristics of the data on-route, a better understanding of the work circuit can be gained. In addition, characteristics about the frequency and duration of stops can be evaluated. The first conclusion derived from the data is that the drive cycle is clearly not as regular or predictable as previous studies have led us to believe. The velocity profile between stops is irregularly shaped and varies dramatically in magnitude and duration. The length of time that the vehicle is stopped and the hydraulic requirements for each stop also vary significantly. An example of the vehicle velocity and the hydraulic profiles are shown in Figure 21 and Figure 22. The peak velocity between stops varies over the route and even more dramatically between different routes. Also notice how the pump pressure is significantly higher in the first part of the profile. This may be due to the different oil viscosities from temperature variations. It seems to be a common occurrence that the pressure in the hydraulic circuit is about 1000 psi higher in the first hour and a half of operation. Never the less, the power variation over a shift varies enough

to make it difficult to predict the cycle. The hydraulic power was overlaid with the vehicle and engine speed in Figure 23 to understand where the majority of the hydraulic power is being used. This plot makes another point clear; the hydraulics often operate while the vehicle is moving. This fact was mentioned by Drozdz [3] in his research and it creates a unique situation for the work circuit hybrid. This fact means that the energy being used to operate the work circuit could be limited by the rate that the energy is being stored as these events happen simultaneously.

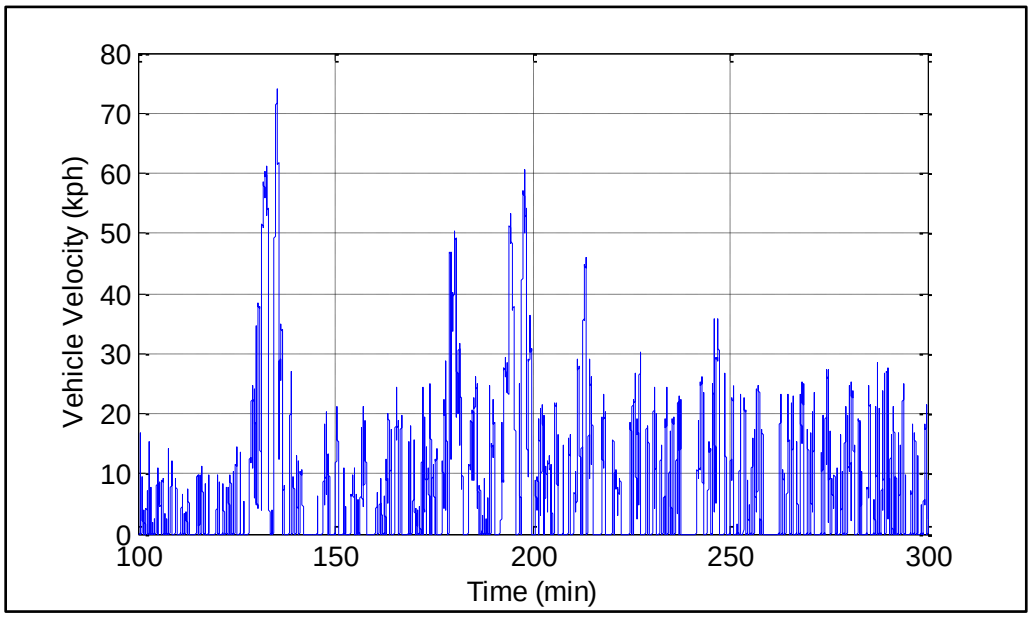

Figure 21: Republic Services' Automated Side Loader Velocity Profile for Part of a Shift

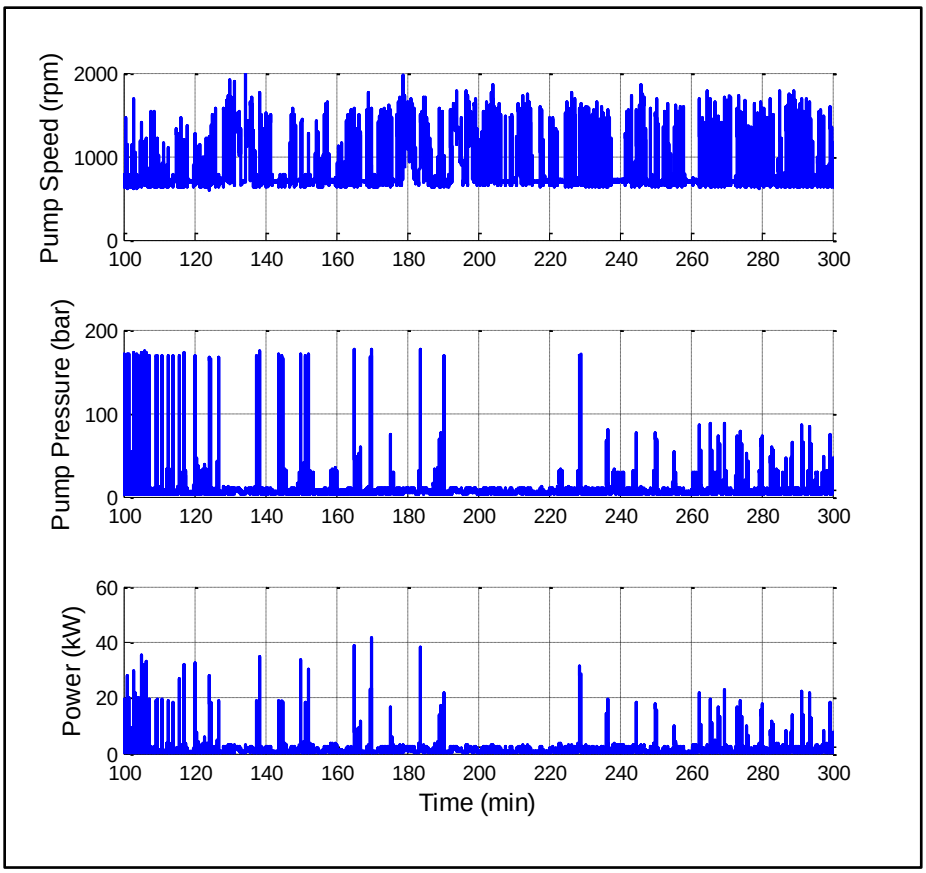

Figure 22: Republic Services' Automated Side Loader Hydraulic Profiles for Part of a Shift

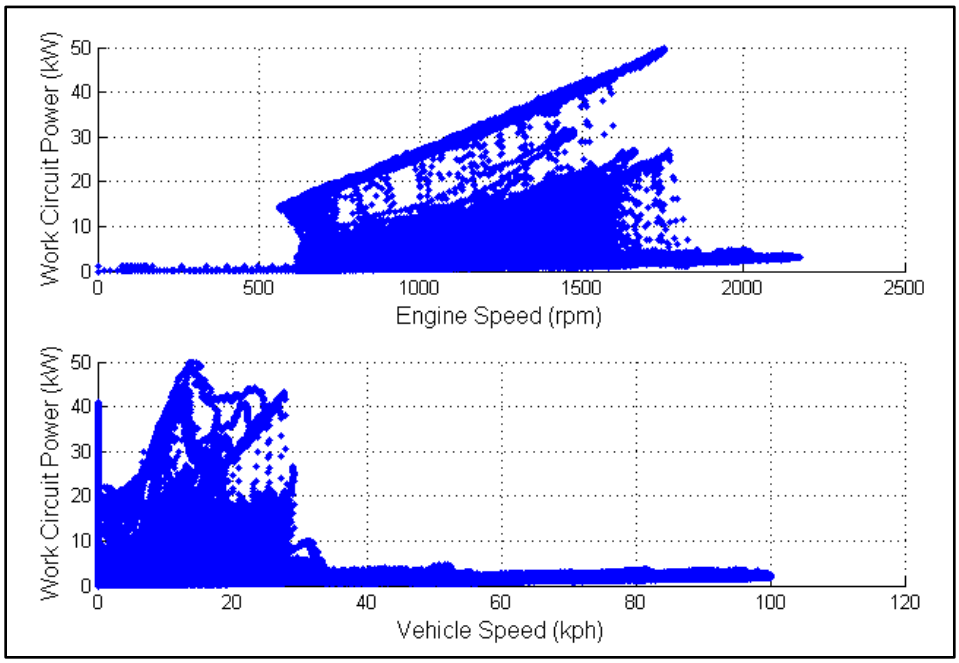

Figure 23: Republic Services' Automated Side Loader Hydraulic Power Overlaid with Engine and Vehicle Speed

Because the profiles are so irregular, it is unrealistic to generate a good representative drive cycle from this data alone. Not to mention the fact that this data is really only relevant to Denver based residential routes. In light of this fact, the best method to evaluate the performance of the work circuit hybrid with this data will be to directly feed the data into a model. This will generate more accurate results because there will be no simplifications in the data that might misrepresent the actual dynamics.

Comparison of Results to Previous Studies

As mentioned, the data collected in this study is only representative of automated side loaders on Denver residential routes. Therefore, it is useful to compare this data to other research data to understand how broadly this data can be applied. The data collected was compared to the data reported by Drozdz [3] which summarizes several different published data sets. A summary of this comparison can be seen in Table 16. The maximum speed range from this study encompasses the other data sets and the average value is close to the other reported values. The time per stop is quite a bit higher than the other studies, which is likely due to the fact that it is common in the areas surrounding Denver for items not in a collection bin to be regularly accepted. This slows down the collection process because the driver has to hand-load these items. This is also clear from the number of stops per hour. The hydraulic power required on route seems to be comparable to the St. Nicholas data set.

Table 16: Comparison of Data Collected on a Denver Refuse Vehicle to Other Published Drive Cycles

	St. Nicholas Drive Cycle [3]	**NYC Drive Cycle** [3]	**ARC Drive Cycle** [3]	**Denver Drive Cycle [This Study]**
Type of Vehicle	Automated Side Loader	Rear Loader	Automated Side Loader	Automated Side Loader
Maximum Speed (km/hr)	25	20	23	14-41 (Ave 27)
Time per Stop (s)	4-24 (Ave < 10)	16-40	16	12-55 (Ave 30-40)
Compaction Time (s)	6-8	30 (w/ 30 extra every 3rd)		
Acceleration to 20 km/hr (s)	4-5	6	5	8
Stops per Hour	144	90		57-79
Hydraulic Power per Stop (kW)	25kW for 7s (starting 2-3s prior to stop) and 42kW for 5s			10-48

The data collected from this study and presented in this chapter makes it possible to more accurately predict the performance of work circuit hybrids. To use this data for this purpose, the next step will be to build a higher fidelity model in which this data can be used to validate the model and then provide the necessary inputs to test the work circuit hybrid capabilities.

CHAPTER 3: DETAILED WORK CIRCUIT MODELING

The work circuit hybrid was analyzed at a high level in chapter one and from this first pass analysis, work circuit hybrids seem to not only be a viable option but they also offer some unique advantages. These advantages need to be more precisely measured. This chapter is meant to outline the method used to model work circuit hybrids to accomplish this goal. This model is used to flush out the details of exactly how these work circuit hybrids operate and to generate a method of measuring the benefit of this technology in the refuse hauling application. To model these systems, the dynamic equations need to be developed and implemented into modeling software. Many of the dynamic equations for work circuit hybrids have already been explored in Chapter 1 and will be utilized again in this chapter for the dynamic model. The model must be validated before it can be used to extrapolate work circuit performance measurements. To validate the model, the data collected in Chapter 2 will be used.

Stock Vehicle Model

The stock vehicle model will be the model used for the validation process. The goal of this model is to represent the vehicle dynamics with enough accuracy to predict the vehicle fuel economy within 15% of the measured values. In addition, this model must have relatively fast simulation times to allow for the evaluation of large data sets. Plus or minus 15% was chosen as an adequate validation boundary for two reasons. First, the goal of the study is to show trends of improvement between the stock vehicle and the vehicle with a work circuit hybrid. This can be accomplished without exact correlation between the measured data and the simulated data. Secondly, there is a fundamental limitation to how accurate a vehicle model represents real

operation when the model uses static engine maps. This will be discussed further in the validation section.

To decrease simulation time, the stock vehicle model is built as a reverse facing model. A reverse facing model tends to be dramatically faster than forward facing models because there are significantly fewer differential equations and most of the relationships are modeled algebraically instead. In a reverse facing model, the know outputs such as vehicle velocity and transmission gear ratio are fed into the model and the required inputs that would produce these outputs are calculated. This type of modeling is useful for situations where the goal of the model is to predict average performance instead of dynamic operation. Reverse facing models trade the ability to accurately model dynamic transients to be able to avoid modeling controllers and dynamics that are difficult to define and slow computationally. In this study we are interested in average fuel economy gains and less concerned with instantaneous fuel rates and operating conditions. The reverse facing model of the stock vehicle is shown in Figure 24 and the individual components are described below.

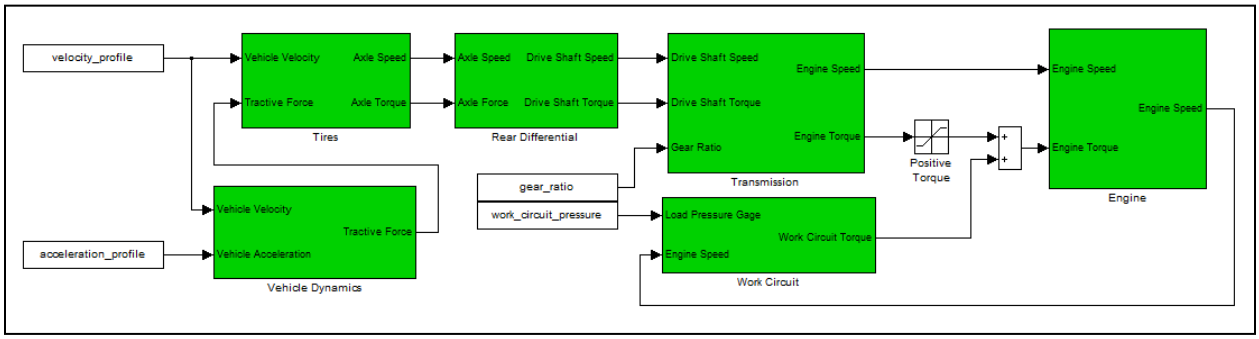

Figure 24: Reverse Facing Model of the Stock Vehicle

Vehicle

The vehicle dynamics are modeled in the same fashion as described in Chapter 1. The force balance is written as,

$$F_t - \frac{1}{2}\rho \dot{x}^2 A_f C_d - m_v g C_{rr} - m_v g sin\beta = m_{eq}\ddot{x}$$

For the reverse facing model, the vehicle acceleration and velocity profile is fed into the model and this is used to calculate the tractive torque and angular speed at the output of the transmission. The vehicle acceleration is not a measured value on the vehicle CAN bus. Therefore, it has to be calculated from the measured vehicle velocity. This can be difficult because the discrete values in the velocity vector can create sharp acceleration spikes even with a fairly smooth velocity profile. In order to avoid this issue, the velocity points within a small interval around the point of calculation are fitted into a low order polynomial. Then the polynomials are combined to create a cubic smoothing spline. This spline can be used to calculate a smoother derivative with a vector that is the same length as the original velocity vector. This is a significantly more effective method than using a high order polynomial curve fit. This is because high order curve fits tend to have poor end conditions and the equations are complicated and highly dependent on the order chosen.

Transmission and Torque Converter

The vehicle transmission is modeled as a simple gear ratio and assumes no losses. This is adequate for this model because gear losses are relatively small in comparison to other losses in the vehicle. The transmission shifting maps can be difficult to derive, even with good data sets available. Because of this fact and since transmission dynamics are of no significance to the goals of this study, the transmission gear ratio is also fed into the model as a measured value.

The torque converter of the vehicle is not modeled for this study because the dynamic equations are not easily implemented in a reverse facing model and the error caused by this component's absence in the model will be partially corrected in the engine model as a constant engine load offset. This is obviously a less than ideal assumption to make but it is made for the sake of simulation time and reduced complexity.

Engine

The engine is modeled using the torque curve and fuel map derived is Chapter 2. The engine speed is calculated from the vehicle speed and fed into the engine model. The engine load is calculated as a combination of load due to tractive effort, load due to hydraulic pump requirements, and load due to engine, transmission, and auxiliary losses. The hydraulic pump requirements modeled are only part of the overall work circuit power requirements. The pump used on the test vehicles is a tandem pump with two separately controlled sections. Both sections are gear style pumps and are connected with a common shaft. One section is used for the operation of the hydraulic arm and the other section is used for the main compaction blade and the body-lift cylinders which operate less frequently but for longer durations than the arm section. Only the hydraulic arm section of the pump was measured during testing and this section is represented as the hydraulic pump requirements in the engine load. The other section is not modeled because there is no clear way to know when this part of the pump is in operation. This will contribute to the simulation error.

Work Circuit

As discussed in the engine section, only part of the work circuit power requirements have been modeled due to lack of data on the other operations. The work circuit is modeled using the measured pressure data and the published pump displacement. The combination of the two yields

the torque required to operate the work circuit. This torque is combined with the other engine loads to calculate the overall fuel used.

Model Validation

To validate the model, the vehicle is simulated on all eight days of test data. The fuel rate calculated in the engine is integrated and the average fuel consumption is calculated at the end of each data set. Each data set represents a full day of measured data. The measured fuel rate from the vehicle CAN bus is also integrated and the actual average fuel consumption is also calculated. The results are shown in Table 17.

Table 17: Stock Vehicle Model Validation Data

Data Set	Measured Average Fuel Consumption (l/100km)	Simulated Average Fuel Consumption (l/100km)	Percent Error
2011-10-06	67.7	64.0	-5.53%
2011-10-07	69.0	64.4	-6.68%
2011-10-10	68.8	61.7	-10.20%
2011-10-11	67.3	65.8	-2.23%
2011-10-12	67.1	60.2	-10.30%
2011-10-13	61.0	59.9	-1.68%
2011-10-14	77.9	72.2	-7.36%
2011-10-17	63.9	58.3	-8.78%
AVERAGE	**67.8**	**63.3**	**-6.60%**

As discussed, there are several reasons for the error in simulated values. These sources of error include: vehicle mass variation over the cycle, inaccurate estimations of engine, transmission, and auxiliary losses, the lack of a torque converter model, and the fact that part of the work circuit power requirements are not modeled. These errors are in addition to the fact that the model fundamentally uses static engine maps to estimate a much more complex engine

controller. Just as a point of reference, the error was calculated for the case that the measured engine speed and measured engine load are fed directly into the engine fueling map bypassing the rest of the model. This is the absolute ideal case and the results are fairly shocking. As shown in Table 18, simply by using a static fuel map with measured inputs for the engine, the error in the simulation averages 2.7% and can be as large as 7.7%. This error is larger than the error calculated for some of the data sets with the whole model. This verifies the fact that plus or minus 15% is a reasonable boundary for model convergence. It also emphasizes the fact that modeling vehicle dynamics is extremely complex and a model of this fidelity is not well suited for predicting the exact fuel consumption of the vehicle but it can be used as a tool to predict the trends in fuel consumption improvement with adjustment to the drive train.

Table 18: Error from Using Derived Static Engine Map

Data Set	Measured Average Fuel Consumption (l/100km)	Simulated Average Fuel Consumption (l/100km)	Percent Error
2011-10-06	67.7	68.8	1.68%
2011-10-07	69.0	70.7	2.33%
2011-10-10	68.8	69.6	1.20%
2011-10-11	67.3	72.5	7.72%
2011-10-12	67.1	68.1	1.46%
2011-10-13	61.0	63.8	4.59%
2011-10-14	77.9	79.3	1.72%
2011-10-17	63.9	64.4	0.79%
AVERAGE	**67.8**	**69.7**	**2.69%**

Work Circuit Hybrid Model

With the data compiled in Table 17 and Table 18, the model can be considered validated and can be expected to perform adequately while predicting the benefit of the work circuit hybrid technology. With the base vehicle model validated, the next step is to develop a model of the

work circuit hybrid components and integrate them into the base vehicle model. The work circuit hybrid model will also be done in the reverse facing format. At this point, the exact control algorithms will not be developed, nor are they needed to predict the benefit of the technology. The model is shown in Figure 25 and the components are described below.

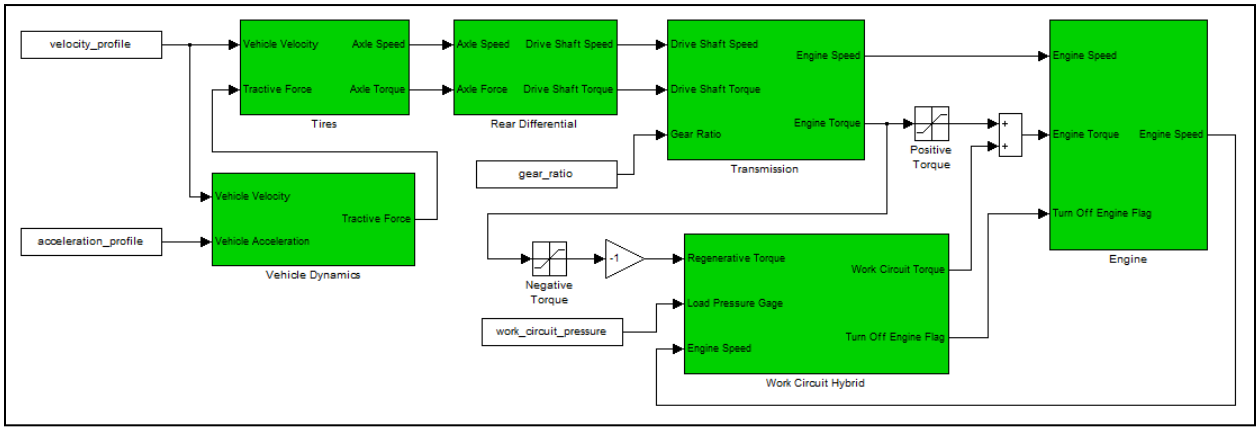

Figure 25: Reverse Facing Model of the Vehicle with a Work Circuit Hybrid Implemented

Accumulator

As discussed in Chapter 1, nitrogen charged bladder accumulators can be accurately modeled using the Benedict-Webb-Rubin (BWR) equations. These equations take into account thermal losses and deviations from an ideal gas. In the dynamic model, the option to use foam insulation and an auxiliary nitrogen bottle will be added. Recall that the BWR equations are as follows,

$$\left[1+\frac{m_f c_f}{m_g c_v}\right]\frac{dT}{dt}=\frac{T_{amb}-T}{\zeta}$$

$$-\frac{1}{c_v}\left[\frac{RT}{v}\left(1+\frac{b}{v^2}\right)+\frac{1}{v^2}\left(B_o RT+\frac{2C_o}{T^2}\right)-\frac{2c}{v^3T^2}\left(1+\frac{\gamma}{v^2}\right)e^{\frac{-\gamma}{v^2}}\right]\frac{dv}{dt}$$

$$P = \frac{RT}{v} + \frac{B_o RT - A_o - \frac{C_o}{T^2}}{v^2} + \frac{bRT - a}{v^3} + \frac{a\alpha}{v^6} + \frac{c\left(1 + \frac{\gamma}{v^2}\right)e^{-\frac{\gamma}{v^2}}}{v^3 T^2}$$

$$c_v = \left[\frac{N_1}{T^3} + \frac{N_2}{T^2} + \frac{N_3}{T} + (N_4 - 1) + N_5 T + N_6 T^2 + N_7 T^3 + N_8 \left(\frac{N_9}{T}\right)^2 \frac{e^{\frac{N_9}{T}}}{\left(e^{\frac{N_9}{T}} - 1\right)^2}\right] R$$

$$+ \frac{6}{T^3}\left(\frac{C_o}{v} - \frac{c}{\gamma}\right) + \frac{3c}{T^3}\left(\frac{2}{\gamma} + \frac{1}{v^2}\right)e^{-\frac{\gamma}{v^2}}$$

Also recall that the specific volume is defined as,

$$v = \frac{V_0 + V_{N2B} - V_{oil}}{m_{N2}}$$

The volume of the axillary nitrogen bottle must be,

$$V_{N2B} \leq V_0 \frac{\sigma^{1/n}}{n^{1/(n-1)} - \sigma^{1/n}}$$

In Chapter 1, these equations were presented but there was not a complete discussion on the difficulties associated with using the nitrogen tanks with the foam insulation. Unfortunately, there is not a method known at this time to combine the two technologies. The problem lies in the fact that the foam is forced to extrude through the gas port as the compression takes place, thus damaging the structure of the foam. The damage to the foam will destroy its functionality. Because of this issue only one of the technologies will be implemented in the model. The auxiliary nitrogen bottle only improves the system by slightly reducing the weight and while the foam greatly increases the efficiency of the energy storage process. Therefore, at the risk of adding unnecessary cost to the system, the foam will be used for the model. There will be a cost analysis at the end of the study to understand whether this technology is worth it.

The final parameter that needs to be discussed regarding the accumulator is its weight. Assuming that there is no nitrogen bottle, a relationship can be derived for the accumulator mass as a function of effective gas volume. The effective gas volume is the volume of the accumulator with no oil in it. This relationship is determined from Hydac's SB600 series bladder accumulators [78] and can be seen in Figure 26. Accumulator mass can be adequately related to effective gas volume with a linear curve fit and this curve is used to determine the weight of the accumulator based on the model inputs.

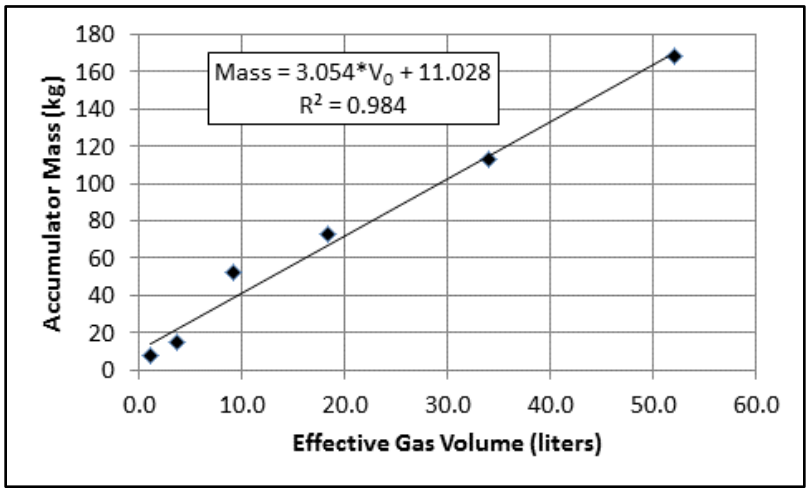

Figure 26: Accumulator Mass Linear Curve Fit Based on Hydac SB600 Series Bladder Accumulators

Pump

It was determined that an engine driven pump offers the highest potential for work circuit hybrid performance with the exception of two challenges. First, the torque converter lock up clutch must be controlled to allow the torque from vehicle momentum to be transferred through the torque converter. The second challenge is that the transmission gears affect the braking ability of the hybrid. It will be assumed that the lock up clutch can be controlled for this model. It will also be assumed that the transmission gears follow the values recorded off of the CAN bus. In reality it may be possible to improve the transmission shifting logic to produce more

braking ability but this may have adverse effects on the drivability of the vehicle. An engine driven pump will be modeled as the main case of interest despite these challenges. However, since the changing gear ratio may affect the performance negatively, the post torque converter case will be modeled for comparison.

The pump is modeled with the standard equations describing the relationship between torque and pressure and the relationship between speed and flow rate. The equations are as follows,

$$\tau_p \eta_m = P d_p$$

$$Q_p = \omega_p d_p \eta_v$$

The values for mechanical and volumetric efficiency are a function of displacement, pressure, and speed. All pumps have similar trends in efficiency with respect to these variables with an offset proportional to the size of the pump. Some commercially available pumps offer slightly higher efficiencies because of the design but the general trends hold true. In order to generalize the efficiency map to model any size pump, a map of an average sized 135 cc/rev Linde pump was normalized against maximum displacement, pressure, and speed. This allows for a scalable model that can be used in an optimization routine. Although the efficiency may vary slightly for different pump models and sizes, this assumption should hold within a few percent.

The mass of the pump can be determined using a similar method to the accumulator. Data from Linde Hydraulics on the HPV-02 Series Pumps [82] was used to generate a linear relationship between pump displacement and mass. The data and the curve fit can be seen in Figure 27. This equation will be used to determine the pump mass for a given maximum displacement chosen by the optimization routine.

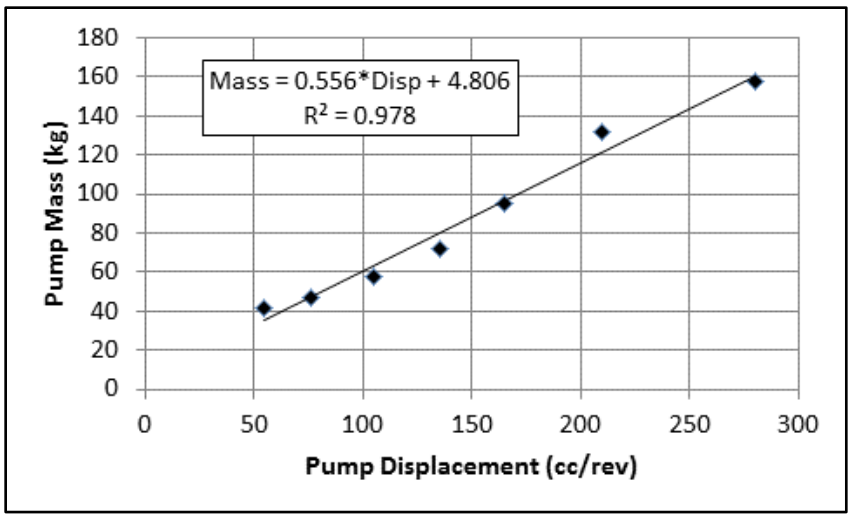

Figure 27: Pump Mass Linear Curve Fit Based on Linde HPV-02 Series Hydraulic Pumps

Flow Control Devise

It was determined that the Innas' Hydraulic Transformer was the best option for flow control based on efficiency and complexity. This method will clearly be more expensive and heavier than the variable orifice method however. The cost of this method will be discussed later. The dynamic equations for the Innas' transformer were described in Chapter 1 and are shown again below,

$$\left[P_{acc}\sin(\delta)\sin\left(\frac{\xi}{2}\right)+P_{load}\sin\left(\delta-\frac{\xi}{2}-\frac{\varsigma}{2}\right)\sin\left(\frac{\varsigma}{2}\right)+P_{res}\sin\left(\delta+\frac{\xi}{2}+\frac{\varphi}{2}\right)\sin\left(\frac{\varphi}{2}\right)\right]d = I_t\frac{d\omega}{dt}$$

$$Q_{acc}=-\omega d\sin(\delta)\sin\left(\frac{\xi}{2}\right)$$

$$Q_{load}=-\omega d\sin\left(\delta-\frac{\xi}{2}-\frac{\varsigma}{2}\right)\sin\left(\frac{\varsigma}{2}\right)$$

$$Q_{res}=-\omega d\sin\left(\delta+\frac{\xi}{2}+\frac{\varphi}{2}\right)\sin\left(\frac{\varphi}{2}\right)$$

Assuming that the pressure in the vent is zero gage and the transformer is in the equilibrium position so that no acceleration occurs,

$$P_{acc}\sin(\delta_{SS})\sin\left(\frac{\xi}{2}\right)+P_{load}\sin\left(\delta_{SS}-\frac{\xi}{2}-\frac{\varsigma}{2}\right)\sin\left(\frac{\varsigma}{2}\right)=0$$

Using the difference trigonometry identity,

$$P_{acc}\sin(\delta_{SS})\sin\left(\frac{\xi}{2}\right)+P_{load}\sin(\delta_{SS})\cos\left(\frac{\xi}{2}+\frac{\varsigma}{2}\right)\sin\left(\frac{\varsigma}{2}\right)$$
$$-P_{load}\cos(\delta_{SS})\sin\left(\frac{\xi}{2}+\frac{\varsigma}{2}\right)\sin\left(\frac{\varsigma}{2}\right)=0$$

Solving for δ_{SS},

$$\delta_{SS}=\tan^{-1}\left(\frac{P_{load}\sin\left(\frac{\xi}{2}+\frac{\varsigma}{2}\right)\sin\left(\frac{\varsigma}{2}\right)}{P_{acc}\sin\left(\frac{\xi}{2}\right)+P_{load}\cos\left(\frac{\xi}{2}+\frac{\varsigma}{2}\right)\sin\left(\frac{\varsigma}{2}\right)}\right)$$

This equation can now be used to directly solve for the steady state angular position of the port plate. Because the model is a reverse facing architecture, the steady state position is all that is needed. Then to solve for the accumulator flow, the equation for load flow is rearranged to solve for ωd,

$$\omega d=-\frac{Q_{load}}{\sin\left(\delta-\frac{\xi}{2}-\frac{\varsigma}{2}\right)\sin\left(\frac{\varsigma}{2}\right)}$$

Similar to the vehicle model, the dynamics are reduced to these algebraic equations in which the known result is fed in to calculate the required operating conditions. The load flow that was measured on the vehicle is fed in to calculate ωd and then this value is fed into the accumulator flow equation. As long as there is a combination of speeds and displacements that satisfies the

calculated value of ωd, the transformer will be used to supply the work circuit with flow. If the value exceeds the maximum that can be provided by the transformer, the original pump will be called into action to make up the difference.

In addition to these equations, an estimated efficiency map is generated. No published maps exist describing the efficiency of these units so the efficiency will be based on the standard Linde pumps. This should be a relatively close assumption because the transformer is essentially a swash plate pump with a modified port plate. Since the dynamics are calculated as a function of ωd, the efficiency map is reduced from three dimensions to two. There are several combinations of speed and displacement that can be used and the resulting efficiency will fluctuate. It will be assumed that the controller of this system will operate the transformer at the highest efficiency.

The mass of these units is also not publically available. Like the efficiency, it is expected that the relationship between transformer mass and displacement is very similar to that of a standard Linde pump. Therefore, the same linear curve fit will be used for this component as well.

If the Innas' hydraulic transformer turns out to be cost prohibitive, then the clear alternative is the adjustable orifice flow control. Modeling this option is very straight forward because this device requires that the flow to the work circuit is equal to the flow from the accumulator. Just for reference, the required effective flow area of the valve can be calculated by rearranging the orifice flow equation as follows,

$$C_d A = \sqrt{\frac{Q^2 \rho}{2(P_{acc} - P_{load})}}$$

Other Components

To round out the model, a gearbox is added to allow the post torque converter pump to be used. This gear box has no other effects on the system other than its mass and the gear ratio it provides between the pump and the driveline. Additionally, the mass associated with the plumbing, valve, and mounts are estimated. These masses, combined with the pump, accumulator, and transformer masses make up the total hybrid mass that is added to the vehicle mass.

Idle Stop Option

This hybrid system generates fuel consumption reductions by reducing the load on the engine while the hydraulic circuit is being used. This benefit alone has the potential to drive this technology forward. However, an additional and possibly an even more substantial benefit that this hybrid system offers is the ability to do idle stop. Turning off the engine when the vehicle is stopped is not possible on the current vehicles because it is the engine power that allows the work circuit to function. If this functionality is transferred to the hybrid unit then idle stop becomes a possibility. This additional fuel savings from idle stop may amount to a large percentage of the overall saving of this technology because so much of the vehicle's fuel consumption is during this idling period. It was shown in Chapter 2 that 26.2% of the overall fuel consumed in these vehicles is during idle. In light of this fact, it is of interest to add this capability to the model to understand how much additional benefit is added. To do this, the following logic is implemented. If the accumulator has charge and the engine speed is at idle, the engine will be allowed to shut off.

CHAPTER 4: WORK CIRCUIT HYBRID OPTIMIZATION

Now that the model has been built and validated, an optimization routine can be used to determine the optimal sizes of the components. For these work circuit hybrids there are two main conditions to evaluate the system for optimality. The first is to achieve the minimum fuel consumption and the second is to achieve the minimum cost over a desired length of time. An optimization algorithm chooses design inputs in a systematic method to explore the design space and locate the optimal condition.

Optimization Algorithm Selection

Optimizing a system with this complexity almost certainly guarantees that the design space will contain multiple good solutions and it can be difficult to find a global optimal solution even with a sophisticated algorithm. To provide the best possible chance of finding the global optimum solution of the system, it is recommended by Geller [83] that a heuristic, stochastic, non-gradient based, global optimizer algorithm should be used. Heuristic refers to the algorithms ability to make "educated" choices in design inputs based on previous information collected. Therefore, the longer the algorithm searches, the more the algorithm "learns". Stochastic refers to an algorithm that incorporates random search methods. This is important because it makes the algorithm more resistant to getting "stuck" in a local optimal solution. The algorithm that is recommended by Geller for these characteristics is the Simulated Annealing (SA) algorithm. This method imitates how the atoms in a hot metal move as the temperature decreases during the annealing process. To begin the search, a random set of "atoms" or design points are selected throughout the "metal" or design space. The algorithm calculates the function value of each of

these points and compares. The function values represent the performance of the system at that design point. The function values that are the lowest are remembered by the algorithm as possible optimal points. The algorithm then allows the atoms to move around in the metal but the distance of movement is constrained by the temperature of the metal which is determined by a cooling schedule. As the temperature decreases, the atoms with the best function value become more likely to be selected for further movement, thus honing in on the optimal points.

Cost Function Definition

As previously mentioned, there are two main conditions that can be used to calculate the performance of the system. Optimizing based on fuel consumption reduction is the first method. It is also important to relate the fuel consumption using the work circuit hybrid to the fuel consumption of the stock vehicle so that the actual benefit of the hybrid system can be understood. To do this, the cost function will be written as a percent reduction in fuel consumption from the stock case. It is also important to note that the Simulated Annealing algorithm is not a constraint based algorithm; therefore, any constraints that need to be implemented in the design space need to be included in the cost function. For this particular study, the only critical constraint on the component sizes is that they must be positive (real) sizes. With this constraint and the desired goal of reducing the fuel consumption, the following cost function can be written,

$$Cost = \frac{Fuel\ Consumption\ with\ Hybrid}{Fuel\ Consumption\ without\ Hybrid} * 100 + \max(0{,}5 - \%\ Component\ Size)$$

The second metric for measuring system performance will be based on a system cost over a desired period of time. The costs of components that do not vary in the study are neglected

because they have no effect on the optimization outcome. Only the cost of the fuel consumed and the hybrid components are used. It is suggested by Geller [83] that an aggregate cost function including the cost of the hybrid components as well as the present equivalent cost of the fuel can be written as follows,

$$Cost = Upfront\ Component\ Cost + Fuel\ Cost\ per\ Year * (P/A, i, t)$$

The present equivalent rate of the fuel can be described by,

$$(P/A, i, t) = \frac{(1+i)^t - 1}{i(1+i)^t}$$

Where i is the annual inflation rate and t is the time in years which are considered to be 2% and 10 years respectively in this study. Models for the cost of the hybrid components are developed based on previous experience in the field. The estimation for the accumulator cost is shown in Figure 28 and the estimations for the pump and transformer are shown in Figure 29. In addition, it was estimated that US$500 dollars of additional hardware would be requires including hoses and safety valves and an extra US$300 is needed if the variable orifice flow control is used. To calculate the cost of the fuel, it is estimated that these vehicles drive 55,000 km/yr and the average cost of diesel is US$1/liter.

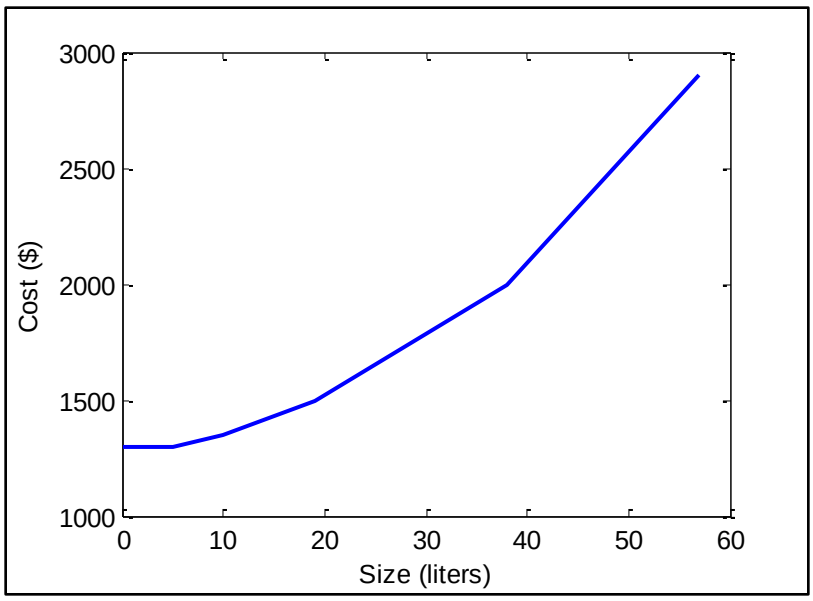

Figure 28: Estimated Accumulator Costs as a Function of Size

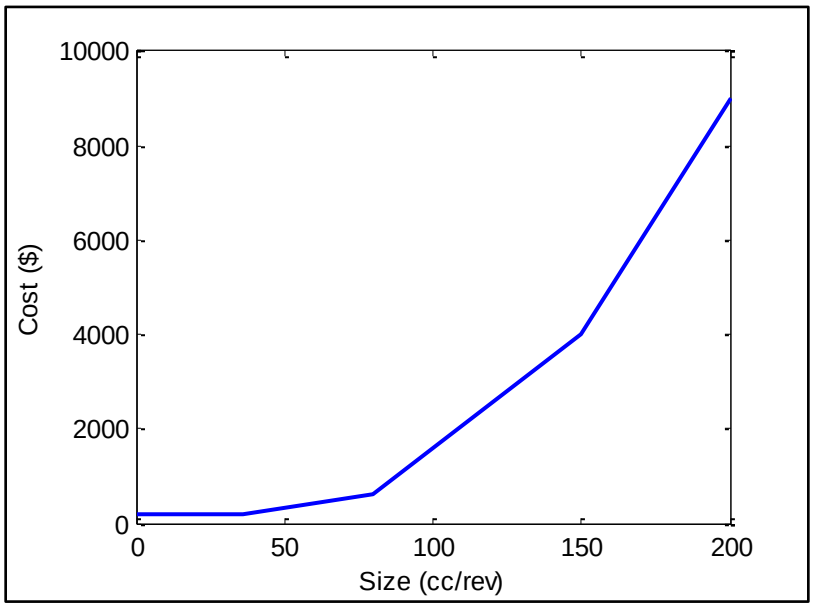

Figure 29: Estimated Pump and Transformer Costs as a Function of Size

The overall cost function for the optimization routine becomes,

$$Cost = \frac{Cost_{comp} + Cost_{fuel/yr} * (P/A, i, t)}{Cost_{fuel/yr,stock} * (P/A, i, t)} * 100 + \max(0{,}5 - \%\, Component\ Size)$$

The constraint in both cost functions causes the cost to increase if the algorithm attempts to make any component size less than 5% of the default value and thus steering the algorithm away from negative sizes. Under normal circumstances where the constraint is not invoked, the function value can be subtracted from 100% to determine the percent reduction in fuel consumption or economic cost using the work circuit hybrid.

Drive Cycle and Optimization Setup

The model is set up with the same vehicle parameters used for the validation so that a direct comparison can be made. The only change from the validation process will be the drive cycle used. Ideally, the system would be optimized using all of the drive cycle data collected to provide the most universal optimal sizes for the components. However, the computation time that is required to simulate this much data makes it difficult to complete. Therefore, it is desirable to choose a shorter drive schedule that incorporates as much of the overall characteristics as possible. In particular, the drive cycle should include each of the vehicle driving states (idling, driving on route, driving at high speeds) and secondly, it should result in similar overall fuel consumption to the average of the full data set. Because the data is all collected off of the actual vehicle, there is no concern about whether the shorter drive cycle is achievable by the vehicle as is the case for a drive cycle generated on statistical values alone. The drive cycle used here will be made up of sections of the already existing, longer drive cycle. Typically, drive cycles used for this sort of analysis are about 20-30 minutes in length. Therefore, as long as the drive cycle selected for this study is at least this long, an adequate amount of data should be represented.

To select a section of the drive cycle, one of the data sets was used to calculate a 40min moving average of fuel consumption. Figure 30 shows an overlay of the moving average fuel consumption against the velocity profile. By examining the moving average fuel consumption, it can clearly be seen that the fuel consumption varies dramatically based on whether the vehicle is idling, driving on route, or driving on the highway. This result is not surprising but in order to make the argument that a shorter section of one of the data sets represents the overall data set, each of these components needs to be included. Two sections were selected out of the middle of this data set were selected and spliced together to make a new, shorter drive cycle. This new drive cycle can be seen in Figure 31.

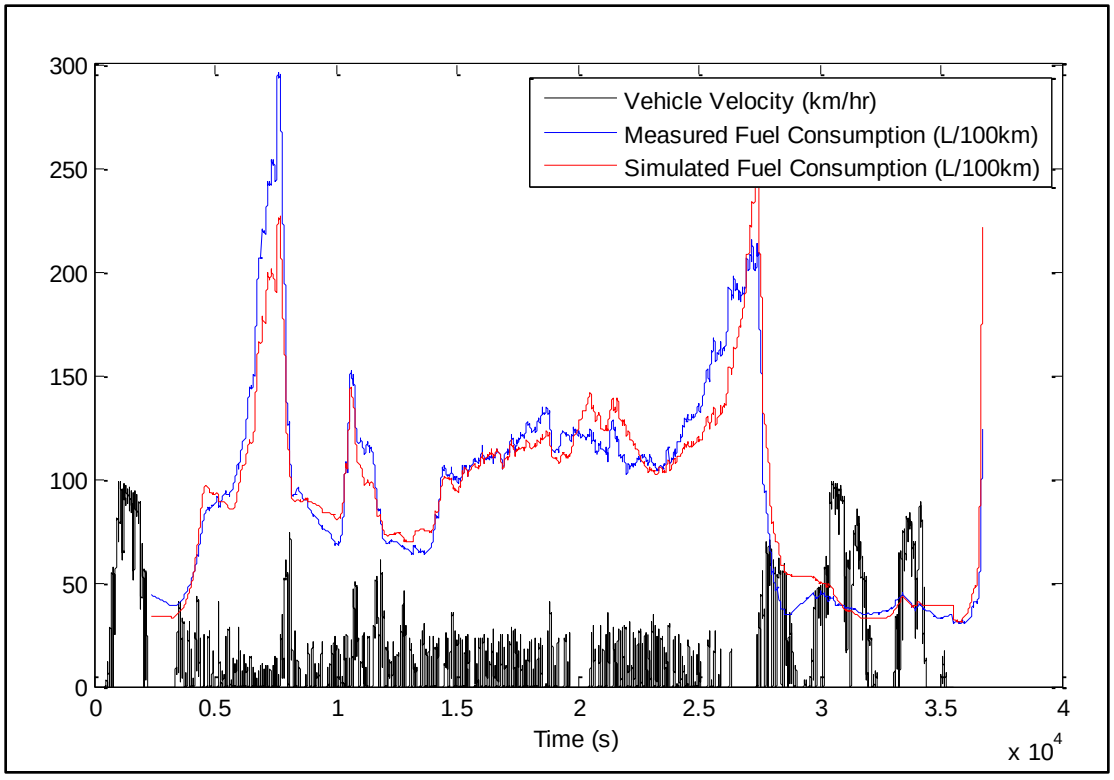

Figure 30: 2400 Second Moving Average Fuel Consumption Relation to the 2011-10-13 Velocity Profile

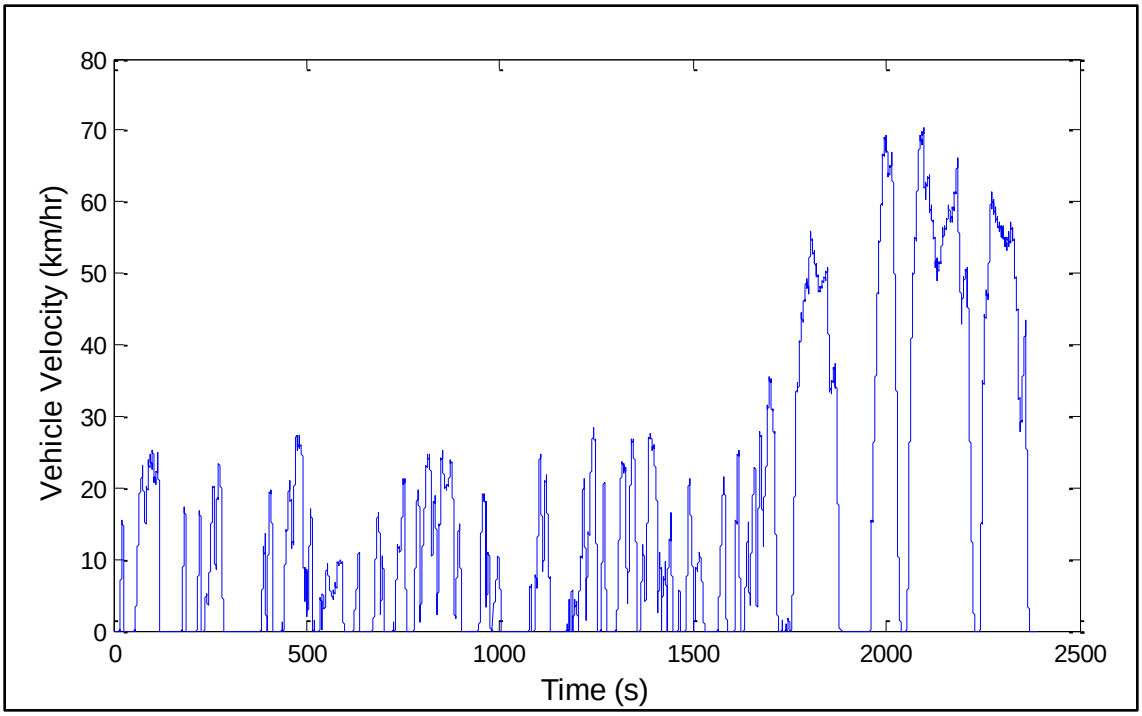

Figure 31: Selected Section of the 2011-10-13 Dataset Used for Optimization Drive Cycle

The stock vehicle was simulated on this new route which produced a measured fuel consumption of 62.5 L/100km and a simulated fuel consumption of 65.1 L/100km yielding a -4.09% average error. These values are very comparable to the averages calculated for the overall data set. The drive cycle is 2390 seconds (~40 minutes) in length and includes all three driving states as required. Using the simulated fuel consumption and present equivalent cost of the fuel, the stock vehicle will use US$41,900 of fuel per year and US$376,000 of fuel in 10 years.

Optimization Results

The optimization routine had trouble converging onto an exact solution for the method of optimizing for fuel consumption alone. This was due to the fact that many solutions were close to the best case. Essentially, as long as the components are big enough to provide all of the work

circuit energy, the only penalty for making the components larger is weight. This means the cost appears to plateau at this point, while in reality, having the smallest components that still achieve the energy needs will be the optimal solution. The important conclusion that was gained from this run was the confirmation that the hybrid can provide the required amount of energy.

The second run utilized the cost function that incorporates the present equivalent cost of the system for a ten year period. The optimization routine now has a much stronger relationship between cost and component size and the algorithm converged onto a 34 liter accumulator, an 80 cc/rev pump, and a 67 cc/rev Innas' transformer. The fuel economy gains for this system were slightly less than the solutions found in the previous case. Interestingly, the routine gave up 0.2% of the fuel consumption gains to bring down the cost of the components which shows that the cost of these components are high enough that it affects the optimal solution. This system returned a payback period of about 4 years and is summarized with the other cases in Table 19.

Table 19: Optimization Results using Aggregate Cost Function

	Variable Orifice No Idle Stop	Innas' Trans No Idle Stop	Innas' Trans Idle Stop
Optimized Accumulator Size (liters)	2	34	27
Optimized Pump Size (cc/rev)	45	80	86
Optimized Transformer Size (cc/rev)	N/A	67	64
Hybrid Estimated Cost (USD)	$2,380	$3,490	$3,540
Payback Period (yr)	>10	4.0	0.39
% Reduction of Fuel Used	0.1 %	2.3 %	21.6 %

The third run again utilized the aggregate cost function but this time incorporated a variable orifice rather than the Innas' transformer. The results for this case are very interesting. The algorithm tried to drive the accumulator size to zero. What this means is that the optimization routine found it less expensive to eliminate the hybrid than to use it. This is due to the fact that the variable orifice flow control method is extremely inefficient and cancels much of

the benefit that storing regenerative energy is aimed at. The size of the components must be increased to get the same performance which, in turn, increases the cost of the hybrid.

The last run incorporated idle stop technology with the Innas' transformer and the aggregate cost function. This substantially increases the fuel savings on the route which brings down the payback period to 6 months. The optimal sizes changed slightly to a 27 liter accumulator, an 86 cc/rev pump, and a 64 cc/rev Innas' transformer and the fuel consumption was reduced by 21.6% from the stock case. This case draws the conclusion that there is an opportunity to combine these two technologies and produce significantly more gain for hybridization.

CONCLUSION

It was known prior to this study that work circuit hybrids were a potential solution to improve the fuel economy of refuse vehicles. In fact, another study on the subject concluded that work circuit hybrids may even offer a higher fuel economy improvement than a traditional hybrid system. However, prior to this study, the design of a work circuit hybrid had not been explored in detail. It was the goal of this thesis to add to the knowledge base by answering the following questions. What are the fuel economy and cost characteristics of an optimized work circuit hybrid, and can an advanced hydraulic work circuit design justify further development towards productization?

To answer these questions the study began by exploring, at a high level, the feasibility of work circuit hybrids on refuse vehicles. Chapter 1 functionally decomposed the system into braking energy, required hydraulic energy, hybrid energy storage, hybrid energy transfer to the accumulator, and hybrid energy transfer to the work circuit. In the braking energy analysis it was determined that the typical refuse vehicle must dissipate 206-614 kJ of energy per stop depending on the weight, speed, and dimensions of the vehicle. In the required hydraulic energy analysis, side loaders required the least amount of energy and fluid volume to run the work circuit at 187 kJ and 10 liters respectively. Therefore, the side loader was determined to be the most promising candidate for hybridization. The work circuit was later shown to only use a fraction of these worst case numbers. In addition, it was determined that if the hybrid efficiency is high, there is a good likelihood that the work circuit hybrid will be able to provide all of the work circuit energy for the majority of the stops. This is important from an operational

standpoint because it is undesirable for the system to have to dynamically switch back to the traditional pumping method part way through each cycle.

The hybrid energy storage section developed a method for sizing a bladder accumulator for a mobile application and discussed the reasons why bladder accumulators are best type for this application. It was shown that for adiabatic compression of the bladder, the maximum energy storage is achieved when the precharge is 0.308σ of the maximum working pressure. Holding the pressures to this ratio, it was also determined that the oil storage capacity of the accumulator is $0.569\sigma^{0.714}$ of the initial gas volume for the ideal case. Then correction factors were developed for thermal losses and it was recommended that elastomeric foam be used to decrease these losses. Two configurations were described for transferring energy to the accumulator. The first configuration used an engine driven pump while the second used a post torque converter pump. The engine driven configuration was shown to be the better of the two because of simplicity. The last component examined was the method of transferring energy from the accumulator to the work circuit. Three methods of flow control were examined, an adjustable orifice, a traditional hydraulic transformer, and the Innas' hydraulic transformer. The Innas' transformer is clearly the best candidate for efficiency reasons; however, the technology is fairly new and not yet fully developed.

All of the sizing and energy calculations in Chapter 1 were based on a vague data set. Because there is a lack of publically available data for these vehicles, it was the goal of Chapter 2 to instrument a Denver based refuse vehicle to gain some better insight into the true operational cycles of the vehicle. Data was collected on two automated side loader, 28 cubic yard (21.4 m^3), McNeilus Street Force MA refuse vehicles that operate on residential routes throughout Denver's surrounding areas. These vehicles were made available by Republic Services which is currently

the second largest waste collection company in the US. From this data, an engine fueling map was derived and it was also determined that if the vehicle's engine is running for 11 hours during a normal day of operation, the vehicle is idling almost 5.5 hours of that time. In addition to that, the vehicle spends 83.7% of the day below 30 kph and 66.5% of the fuel used during a typical day is consumed when the vehicle is under 30 kph while 26.2% of that is consumed at idle. It was also determined that the vehicle spends approximately 80% of the time driving on-route and the work circuit is in operation 13.6% of the time. Finally, 11.9% of the fuel is consumed while the work circuit is in operation although only a portion of this is used to power the work circuit. It is also noted that the actual velocity and hydraulic cycles are highly irregular in duration and magnitude throughout all the data sets. This is contrary to what other papers have described. Yet, if the average values of the cycles are compared to the averages of the other published cycles, the statistics match relatively closely. The time per stop was the only exception which is quite a bit higher than the other studies due to the fact that it is common in the areas surrounding Denver for items not in a collection bin to be regularly accepted. This slows down the collection process because the driver has to hand-load these items.

Chapter 3 laid out a reverse facing model that can be used to simulate the performance of the work circuit hybrids. Then the data collected in Chapter 2 was used to validate the model of the stock vehicle. The model was validated within the target goal of 15% error for all data sets and had an average of 6.6% error. It is also interesting to note that the error using measured engine speed and load vectors in a static engine fuel map was as great as 7.7% which reinforces the expectation that these types of models are only accurate for comparing configurations, not predicting the exact performance of the system. By validating the model to measured vehicle data, it is then reasonable to use the hybrid model to predict the performance improvements that

these hybrids offer over the stock case. The base model was also used to calculate a few basic statistics that can be compared to the high level analysis in Chapter 1, as well as the published information in other papers. It turns out that the measured work circuit energy on these Denver based refuse vehicles only amounts to 16% of the available regenerative braking energy. This is much lower than predicted in the high level analysis. The hybrid components were built up with the methods from Chapter 1 and tested before being used with the optimization routine in Chapter 4.

Chapter 4 laid out a method of optimizing the component sizes using the Simulated Annealing algorithm. The system was optimized for both fuel consumption as well as cost. It was determined that a maximum of 2.5% reduction in fuel consumption can be achieved if all of the work circuit energy is provided by the hybrid. This is sensitive to the fuel rate at idle when the work circuit is active. This value may not be well represented in this model. This is dramatically lower than the 19% previously claimed by Drozdz [3] which is due to several reasons. First, Drozdz used a 15 stop, 360s cycle that repeated 3 times. There was no highway driving and no prolonged stopping. Significantly higher percentages can be achieved if the cycle is purely stop and go but this does not truly represent the drive cycle. Second, the benefit of this type of hybrid is fundamentally limited to the energy required by the work circuit. This means that even if additional energy is available to be stored, only the energy utilized by the work circuit will work to improve the fuel economy. With only 16% of the available braking energy being utilized in this simulation, there is potential for improvement. The last reason, as mentioned before, is that if the idle fuel rate while the work circuit is operating is misrepresented in the model, the predicted savings will be lower.

The optimized component sizes and fuel savings are summarized in Table 19 and although there is promising evidence that the work circuit hybrid alone will provide the industry with a cost effective way to reduce fuel consumption, there is even more promise when this technology is combined with idle stop technology. The ability to turn off the engine while the vehicle is idling, which is not possible with the stock system, yields 21.6% fuel consumption reduction from the stock case and a payback period of 6 months. These savings can be further increased if a more demanding drive cycle is used.

Recommendations

Upon completing this study, the questions posed at the beginning can now be answered. The fuel economy gains of an optimized work circuit hybrid are limited by the work circuit demands. This is a disadvantage from the traditional hybrid systems because it requires a good match between the drive cycle and the work circuit requirements to produce the desired benefits. In addition, if the case arises that the work circuit load is greater than the stored energy then the traditional method of operation will need to be utilized. This means that fundamentally, a work circuit hybrid must either underutilize the available energy or under preform in its desired function. Despite this fact, these hybrids are dramatically less expensive than the traditional hybrid systems and when combined with idle stop, offer comparable fuel savings. Even if the hybrid is used by itself, the payback period for the system is certainly within a reasonable range.

The second question that was posed was to understand whether advanced hydraulic work circuit design justifies further development towards productization. There are still some major challenges to overcome before this technology can truly be expected to perform as predicted. One such challenge is the fact that these hybrids require control of the torque converter lock up

clutch and the transmission shifting strategy. These issues must be addressed in future research, however, the fact that these hybrids have the potential to produce substantial improvements in fuel economy over the stock vehicle leads to the conclusion that work circuit hybrids are recommended for further development. It is clear that these hybrids offer the industry an opportunity for improving fuel economy and even though the fuel savings are lower when compared to traditional hybrids, the benefits come at a much lower cost.

WORKS CITED

[1] 2009, "Municipal Solid Waste Generation, Recycling, and Disposal in the United States: Facts and Figures for 2009," U.S. Environmental Protection Agency (EPA), EPA-530-F-010-012.

[2] Cannon J. S., 2006, "Greening Garbage Trucks: Trends in Alternative Fuel Use, 2002-2005," Inform.

[3] Drozdz P., 2005, "Hybrid Refuse Truck Feasibility Study," Prepared for the Transportation Development Centre of Transport Canada by vePower Technologies in collaboration with CEVEQ (Publication Number TP 14431E).

[4] Gaines L., Vyas A., and Anderson J. L., 2006, "Estimation of Fuel Use by Idling Commercial Trucks (Paper No. 06-2567)," Center for Transportation Research, Argonne National Laboratory.

[5] Agar B. J., Baetz B. W., and Wilson B. G., 2007, "Fuel Consumption, Emissions Estimation, and Emissions Cost Estimates using Global Positioning Data.," Journal of the Air & Waste Management Association, **57**(3), pp. 348-354.

[6] Gordon D., Burdelski J., and Cannon J. S., 2003, "Greening Garbage Trucks: New Technologies for Cleaner Air," Inform.

[7] Duffy D. P., 2009, "The Workhorses of Waste," MSW Management, Journal for Municipal Solid Waste Professionals, (October).

[8] Rozgus A., 2005, "Is Automated Collection for You? Automating a Refuse Collection Fleet has its Ups and Downs," Public Works Magazine.

[9] Everett J. W., Maratha S., Dorairaj R., and Riley P., 1998, "Curbside Collection of Recyclables I: Route Time Estimation Model," Conservation and Recycling, **22**, pp. 177-192.

[10] Everett J. W., Dorairaj R., Maratha S., and Riley P., 1998, "Curbside Collection of Recyclables II: Simulation and Economic Analysis," Conservation And Recycling, **22**, pp. 217-240.

[11] Everett J. W., and Riley P., 1997, "Curbside Collection of Recyclable Material : Simulation of Collection Activities and Estimation of Vehicle and Labor Needs," Journal of the Air & Waste Management Association, **47**(October), pp. 1061-1069.

[12] Rhoma F., Zhang Z., Luo Y., and Noche B., 2010, "Environmental & Economical Optimization for Municipal Solid Waste Collection Problems, a Modeling and algorithmic approach case study," Proceedings of the 12th WSEAS International Conference on Mathematical Methods, Computational Techniques and Intelligent Systems, World Scientific and Engineering Academy and Society (WSEAS), pp. 205–211.

[13] Wilson B. G., and Baetz B. W., 2001, "Modeling Municipal Solid Waste Collection Systems Using Derived Probability Distributions I: Model Development," Journal of Environmental Engineering, **127**(11).

[14] Wilson B. G., and Baetz B. W., 2001, "Modeling Municipal Solid Waste Collection Systems Using Derived Probability Distributions II: Extensions and Applications," Journal of Environmental Engineering, **127**(11).

[15] Nguyen T. T. T., and Wilson B. G., 2010, "Fuel Consumption Estimation for Kerbside Municipal Solid Waste (MSW) Collection Activities," Waste Management & Research: The Journal of the International Solid Wastes and Public Cleansing Association, ISWA, **28**(4), pp. 289-97.

[16] Wilson B. G., and Nguyen T. T. T., 2007, "The Use of Automated Vehicle Location Systems in Solid Waste Collection Operations," University of New Brunswick, Department of Civil Engineering.

[17] Vyas A., Saricks C., and Stodolsky F., 2002, "The Potential Effect of Future Energy-Efficiency and Emissions-Improving Technologies on Fuel Consumption of Heavy Trucks," Center for Transportation Research, Argonne National Laboratory.

[18] Siuru B., 2003, "New Study Makes Strong Case for Natural Gas Garbage Trucks: Alternative Fuels," Diesel Progress North American Edition.

[19] Gannon M. C., 2010, "Hydraulics: It's a Gas," Hydraulics & Pneumatics, (June).

[20] 2011, "Telma: Frictionless Braking Systems," http://www.telmausa.com/, 7/4/2011.

[21] 2002, "Parker Series VA20/35 and Series VG20/35: Oil Hydraulic Directional Control Valves," Parker Hannifin Corporation, Hydraulic Valve Division, Bulletin HY14-2004-B1/US.

[22] 2006, "Understanding Truck Mounted Hydraulic Systems, Sixth Edition," Muncie Power Products, Inc.

[23] 2007, "Muncie Powr-Pro and Power-Miser Parts List and Service Manual," Muncie Power Products, Inc., pp. 1-16.

[24] 2009, "Muncie Power-Miser and Powr-Pro Pump Systems," Muncie Power Products, Inc., pp. 1-8.

[25] Casey B., 2011, “Understanding Hydraulic Load Sensing Control,” Insider Secrets to Hydraulics.

[26] 2011, “Electrohydraulic Flow Matching: The Next Generation of Load-Sensing Controls,” Machine Design, http://machinedesign.com.

[27] Wendel G. R., 2002, “Hydraulic System Configurations for Improved Efficiency,” Society of Automotive Engineers International, SAE 2002-01-1433.

[28] Achten P. A. J., Fu Z., and Vael G. E. M., 1997, “Transforming Future Hydraulics: A New Design of a Hydraulic Transformer,” Proceedings of the Fifth SICFP, Linköping University, pp. 1-24.

[29] Vael G. E. M., Achten P. A. J., and Fu Z., 2000, “The Innas Hydraulic Transformer: The Key to the Hydrostatic Common Pressure Rail,” Society of Automotive Engineers International, SAE 2000-01-2561.

[30] Vael G., Achten P., and Potma J., 2003, “Cylinder Control with the Floating Cup Hydraulic Transformer,” The Eighth Scandinavian International Conference on Fluid Power, SICFP’03, May 7-9, 2003, Tampere, Finland.

[31] Achten P. A. J., 2007, “Changing the Paradigm,” The Tenth Scandinavian International Conference on Fluid Power, SICFP’07, Tampere, Finland.

[32] Achten P., Brink T. V. D., Potma J., Schellekens M., and Vael G., 2009, “A Four-Quadrant Hydraulic Transformer for Hybrid Vehicles,” The 11th Scandinavian International Conference on Fluid Power, SICFP’09, June 2-4, 2009, Linköping, Sweden.

[33] Achten P. A. J., 2011, “A Serial Hydraulic Hybrid Drive Train for Off-Road Vehicles,” 2011 IFPE Conference Proceedings.

[34] Bishop E., 2011, “Digital Hydraulic Transformer = Digital Hydraulic Muscle,” IFPE Conference Proceedings, pp. 649-656.

[35] Werndin R., and Palmberg J.-O., “Controller Design for a Hydraulic Transformer,” Department of Mechanical Engineering, Linköping University.

[36] Rydberg K.-E., 2009, “Energy Efficient Hydraulic Hybrid Drives,” The 11th Scandinavian International Conference on Fluid Power, SICFP’09, June 2-4, 2009, Linköping, Sweden, pp. 1-14.

[37] 2011, “Eaton’s Hydraulic Launch Assist Refuse Truck (HLA),” Eaton Corporation, Hybrid Power Systems Division, www.roadranger.com.

[38] Hall L. E., 2010, “Hydraulic Hybrid Developed by EPA Increases Garbage Truck Fuel Economy up to 30 Percent,” www.hybridcars.com, August 4, 2010.

[39] Hitchcox A. L., 2009, "Hydraulic Hybrid Garbage Truck Trashes Energy Waste," Hydraulics & Pneumatics, (May), pp. 12-14.

[40] Brunt J., 2011, "City Will Test Hybrid Garbage Trucks," The Spokesman-Review, July 1, 2011, www.spokesman.com.

[41] 2011, "Hydraulic Hybrids from Rexroth: Hydrostatic Regenerative Braking System (HRB)," Bosch Rexroth Corporation, Hydraulics Division, Publication Number: RA 98 310/08.08.

[42] 2010, "Parker RunWise Advanced Series Hybrid Drive," Parker Hannifin Corporation, Hydraulic Division, Bulletin HY19-1014/US.

[43] 2010, "Parker, Autocar Deliver Fuel-Efficient, Low Emissions Refuse Vehicles," Fleet Equipment.

[44] 2009, "Stored Energy Management System (SEMS)," Parker Hannifin Corporation, Chelsea Products Division.

[45] 2008, "Hydraulic Hybrids," Engineering & Technology Magazine, (Nov-Dec), pp. 40-44.

[46] 2011, "Hydraulic Hybrids from Czero," Czero, Inc., www.czero-solutions.com.

[47] 2011, "HybriDrive: The Heavy-Duty Hybrid from BAE Systems," BAE Systems.

[48] Serrao L., Hubert C. J., and Rizzoni G., 2007, "Dynamic Modeling of Heavy-Duty Hybrid Electric Vehicles," ASME International Mechanical Engineering Congress and Exposition, Proceedings, pp. 121-128.

[49] Baseley S., Ehret C., Greif E., and Kliffken M., 2007, "Hydraulic Hybrid Systems for Commercial Vehicles," Society of Automotive Engineers International, SAE 2007-01-4150.

[50] Cheong K. L., Li P. Y., Sedler S., and Chase T. R., 2011, "Comparison between Input Coupled and Output Coupled Power-split Configurations in Hybrid Vehicles," IFPE Conference Proceedings, pp. 243-252.

[51] Hui S., Ji-hai J., and Xin W., 2009, "Torque Control Strategy for a Parallel Hydraulic Hybrid Vehicle," Journal of Terramechanics, **46**(6), pp. 259-265.

[52] Hui S., and Junqing J., 2010, "Research on the System Configuration and Energy Control Strategy for Parallel Hydraulic Hybrid Loader," Automation in Construction, **19**(2), pp. 213-220.

[53] Montazeri-Gh M., and Asadi M., 2011, "Intelligent Approach for Parallel HEV Control Strategy Based on Driving Cycles," International Journal of Systems Science, **42**(2), pp. 287-302.

[54] Wu B., Lin C.-C., Filipi Z., Peng H., and Assanis D., 2004, "Optimal Power Management for a Hydraulic Hybrid Delivery Truck," Vehicle System Dynamics, **42**, pp. 23-40.

[55] Yan Y., Liu G., Chen J., and Na T., 2009, "NLPQL of Control Rules for Improving Fuel Economy of a Parallel Hydraulic Hybrid Bus," International Journal of Modeling, Identification and Control, **7**(4), pp. 315–320.

[56] Mensing F., and Li P. Y., 2011, "Sizing and Optimal Operation of a Power Split Hydraulic Hybrid Drive Train," 52nd National Conference on Fluid Power (IFPE), pp. 253-262.

[57] Hui S., 2010, "Multi-Objective Optimization for Hydraulic Hybrid Vehicle Based on Adaptive Simulated Annealing Genetic Algorithm," Engineering Applications of Artificial Intelligence, **23**, pp. 27-33.

[58] Prater Jr. G., Shahhosseini A. M., Osborne G. M., and Zhang S., 2010, "Simulation Studies for Determining the Response Characteristics of a Hydraulic Hybrid Powertrain Subframe," International Journal of Heavy Vehicle Systems, **17**(2), pp. 99–118.

[59] Matheson P., and Stecki J., 2003, "Development and Simulation of a Hydraulic Hybrid Powertrain for Use in Commercial Heavy Vehicles," Society of Automotive Engineers International, SAE 2003-01-3370.

[60] Sonesson U., 2000, "Modeling of Waste Collection: A General Approach to Calculate Fuel Consumption and Time," Waste Management & Research, **18**(2), pp. 115-123.

[61] Elahinia M. H., Nguyen T., Olson W. W., and Fountain P., 2006, "Noise and Vibration Control in Hydraulic Hybrid Vehicles," Society of Automotive Engineers International, SAE 2006-01-1970.

[62] Dembski N., Rizzoni G., Soliman A., Fravert J., and Kelly K., 2005, "Development of Refuse Vehicle Driving and Duty Cycles," Society of Automotive Engineers International, SAE 2005-01-1165.

[63] 2007, "SmartWay Fuel Efficiency Test Protocol for Medium and Heavy Duty Vehicles," U.S. Environmental Protection Agency (EPA), EPA420-P-07-003.

[64] Ivani Ž., 2007, "Data Collection and Development of New York City Refuse Truck Duty Cycle," Society of Automotive Engineers International, SAE 2007-01-4118.

[65] O'Keefe M. P., Simpson A., Kelly K. J., and Pederson D. S., 2007, "Duty Cycle Characterization and Evaluation towards Heavy Hybrid Vehicle Applications," Society of Automotive Engineers International, SAE 2007-01-0302.

[66] 2010, "EZ Pack Refuse Truck Bodies," EZ Pack Manufacturing, LLC, www.ezpacktrucks.com.

[67] 2010, "McNeilus Garbage Trucks," McNeilus Truck and Manufacturing, Oshkosh Corporation, www.mcneilusgarbagetrucks.com.

[68] 2010, "New Way Refuse Trucks," New Way Trucks, Scranton Manufacturing Company, Inc., refusetrucks.scrantonmfg.com.

[69] 2010, "Labrie Group Refuse Vehicles," Labrie Enviroquip Group, www.labriegroup.com/en/.

[70] 2011, "Hydraulic Accumulators," Damen Technical Agencies (DTA), www.dta.eu.

[71] Rabie M. G., 2009, "Fluid Power Engineering," McGraw Hill, New York.

[72] Otis D. R., and Pourmovahed A., 1985, "An Algorithm for Computing Nonflow Gas Processes in Gas Springs and Hydropneumatic Accumulators," Journal of Dynamic Systems, Measurement, and Control, **107**, pp. 93-96.

[73] Pourmovahed A., Beachley N. H., and Fronczak F. J., 1992, "Modeling of a Hydraulic Energy Regeneration System: Part I: Analytical Treatment," Journal of Dynamic Systems, Measurement, and Control, **114**(1), pp. 155-159.

[74] Pourmovahed A., Baum S. A., Beachley N. H., and Fronczak F. J., 1988, "Experimental Evaluation of Hydraulic Accumulator Efficiency with and without Elastomeric Foam," Journal of Propulsion and Power, **4**(2), pp. 185-192.

[75] Pourmovahed A., and Otis D. R., 1990, "An Experimental Thermal Time-Constant Correlation for Hydraulic Accumulators," Journal of Dynamic Systems, Measurement, and Control, **112**(1), pp. 116-122.

[76] Roston G. P., Witte M., and O'Brien II J. A., 2011, "Optimal Accumulator Sizing for Mobile Applications," 52nd National Conference on Fluid Power (IFPE), pp. 355-362.

[77] Pourmovahed A., 1990, "Durability Testing of an Elastomeric Foam for Use in Hydraulic Accumulators," Journal of Solar Energy Engineering, **112**(3), pp. 223-229.

[78] 2008, "Hydac Accumulators," Hydac Corporation, Accumulator Division, Accumulator Brochure #02068195.

[79] Achten P. A. J., 2005, "Volumetric Losses of a Multi Piston Floating Cup Pump," NFPE/IFPE 2005, Las Vegas, March 16-18.

[80] 1997, "J1939/71 Vehicle Application Layer," Society of Automotive Engineers (SAE) Handbook, Warrendale, p. 23.644.

[81] 1997, "J1939/21 Data Link Layer," Society of Automotive Engineers (SAE) Handbook, Warrendale, p. 23.627.

[82] 2005, "Linde Hydraulic Drives Product Catalog," Linde Hydraulics Division.

[83] Geller B. M., 2010, "Increased Understanding of Hybrid Vehicle Design through Modeling, Simulation, and Optimization," Thesis, Colorado State University, Fort Collins, CO.

APPENDIX I: ENGINE DATA

Table 20: Estimated Mack MP7-325M Engine Fuel Map - Section #1 of 3 (lps)

		Engine Speed (rpm)				
		700	**800**	**900**	**1000**	**1100**
Engine Load (%)	**0**	8.063E-04	2.078E-05	3.936E-06	6.037E-07	1.222E-06
	5	8.793E-04	3.850E-04	4.242E-04	7.724E-04	7.965E-04
	10	9.880E-04	5.988E-04	7.119E-04	1.108E-03	1.356E-03
	15	1.021E-03	1.232E-03	1.156E-03	1.767E-03	1.751E-03
	20	1.250E-03	1.422E-03	1.505E-03	2.072E-03	2.374E-03
	25	1.707E-03	1.553E-03	2.031E-03	2.531E-03	3.053E-03
	30	1.977E-03	1.899E-03	2.397E-03	3.213E-03	3.664E-03
	35	2.144E-03	2.302E-03	2.903E-03	3.929E-03	4.392E-03
	40	2.387E-03	2.612E-03	2.969E-03	4.450E-03	4.966E-03
	45	2.621E-03	2.824E-03	3.513E-03	4.859E-03	5.528E-03
	50	2.869E-03	2.896E-03	3.829E-03	5.222E-03	6.058E-03
	55	3.147E-03	3.328E-03	4.164E-03	5.803E-03	6.708E-03
	60	3.394E-03	3.618E-03	4.496E-03	6.174E-03	7.376E-03
	65	3.670E-03	4.035E-03	4.760E-03	6.776E-03	7.990E-03
	70	3.974E-03	4.314E-03	5.050E-03	7.310E-03	8.422E-03
	75	4.250E-03	4.469E-03	5.368E-03	7.759E-03	8.868E-03
	80	4.506E-03	4.821E-03	5.710E-03	8.275E-03	9.564E-03
	85	4.748E-03	5.125E-03	6.102E-03	8.901E-03	9.983E-03
	90	4.998E-03	5.366E-03	6.313E-03	9.122E-03	1.067E-02
	95	5.279E-03	5.608E-03	6.845E-03	9.778E-03	1.133E-02
	100	5.579E-03	5.908E-03	7.155E-03	8.889E-03	1.213E-02

Table 21: Estimated Mack MP7-325M Engine Fuel Map - Section #2 of 3 (lps)

		Engine Speed (rpm)				
		1200	**1300**	**1400**	**1500**	**1600**
Engine Load (%)	**0**	1.060E-05	6.615E-06	8.332E-06	3.872E-05	2.064E-05
	5	8.623E-04	1.188E-03	1.213E-03	1.600E-03	1.374E-03
	10	1.937E-03	1.881E-03	1.833E-03	1.805E-03	2.132E-03
	15	2.000E-03	2.846E-03	2.613E-03	2.963E-03	2.554E-03
	20	2.645E-03	2.953E-03	3.274E-03	3.515E-03	4.413E-03
	25	3.110E-03	3.760E-03	3.848E-03	4.187E-03	4.022E-03
	30	4.208E-03	4.663E-03	5.169E-03	4.623E-03	5.295E-03
	35	4.556E-03	5.152E-03	5.665E-03	6.007E-03	5.402E-03
	40	5.420E-03	5.792E-03	7.069E-03	6.343E-03	7.040E-03
	45	5.888E-03	6.486E-03	6.907E-03	7.860E-03	7.711E-03
	50	6.532E-03	6.958E-03	7.578E-03	7.701E-03	8.162E-03
	55	7.525E-03	7.749E-03	8.392E-03	8.512E-03	8.622E-03
	60	7.761E-03	8.303E-03	8.970E-03	9.171E-03	9.355E-03
	65	8.544E-03	9.459E-03	9.530E-03	9.932E-03	1.047E-02
	70	9.279E-03	1.013E-02	1.008E-02	1.072E-02	1.126E-02
	75	9.701E-03	1.054E-02	1.111E-02	1.130E-02	1.162E-02
	80	1.023E-02	1.137E-02	1.248E-02	1.250E-02	1.267E-02
	85	1.155E-02	1.186E-02	1.282E-02	1.416E-02	1.354E-02
	90	1.164E-02	1.263E-02	1.376E-02	1.409E-02	1.416E-02
	95	1.267E-02	1.328E-02	1.443E-02	1.488E-02	1.542E-02
	100	1.353E-02	1.466E-02	1.543E-02	1.579E-02	1.599E-02

Table 22: Estimated Mack MP7-325M Engine Fuel Map - Section #3 of 3 (lps)

		Engine Speed (rpm)				
		1700	**1800**	**1900**	**2000**	**2100**
Engine Load (%)	**0**	5.937E-05	0.000E+00	0.000E+00	0.000E+00	0.000E+00
	5	1.311E-03	1.920E-03	2.020E-03	9.841E-04	0.000E+00
	10	2.967E-03	2.189E-03	1.881E-03	1.954E-03	0.000E+00
	15	3.128E-03	2.778E-03	3.604E-03	2.492E-03	0.000E+00
	20	3.748E-03	3.464E-03	3.625E-03	3.295E-03	0.000E+00
	25	4.697E-03	5.411E-03	4.026E-03	4.099E-03	0.000E+00
	30	5.154E-03	4.618E-03	5.843E-03	4.919E-03	0.000E+00
	35	5.898E-03	6.308E-03	6.496E-03	5.673E-03	0.000E+00
	40	6.642E-03	7.081E-03	7.491E-03	6.355E-03	0.000E+00
	45	8.340E-03	8.566E-03	8.394E-03	7.255E-03	0.000E+00
	50	8.187E-03	9.185E-03	8.246E-03	8.453E-03	0.000E+00
	55	9.156E-03	9.310E-03	9.505E-03	9.231E-03	0.000E+00
	60	9.615E-03	1.069E-02	1.033E-02	1.180E-02	0.000E+00
	65	1.075E-02	1.167E-02	1.166E-02	1.042E-02	0.000E+00
	70	1.186E-02	1.279E-02	1.297E-02	1.139E-02	0.000E+00
	75	1.204E-02	1.378E-02	1.437E-02	1.227E-02	0.000E+00
	80	1.282E-02	1.414E-02	1.410E-02	1.359E-02	0.000E+00
	85	1.408E-02	1.461E-02	1.436E-02	1.451E-02	0.000E+00
	90	1.546E-02	1.502E-02	1.544E-02	1.537E-02	0.000E+00
	95	1.564E-02	1.594E-02	1.608E-02	1.632E-02	0.000E+00
	100	1.661E-02	1.690E-02	1.720E-02	1.757E-02	0.000E+00

Table 23: Estimated Mack MP7-325M Engine Torque and Power Curves

Engine Speed (rpm)	Engine Torque Max (Nm)	Engine Power Max (kW)
600	0	0
700	1268	93
800	1357	114
900	1447	136
1000	1537	161
1100	1627	187
1200	1627	204
1300	1627	221
1400	1577	231
1500	1543	242
1600	1446	242
1700	1361	242
1800	1286	242
1900	1218	242
2000	1104	231
2100	1017	224
2200	0	0

APPENDIX II: PUMP AND TRANSFORMER TORQUE DERIVATION

This derivation works for both swash plate and bent axis design. Start with the force from the pressure in one cylinder as shown in Figure 32.

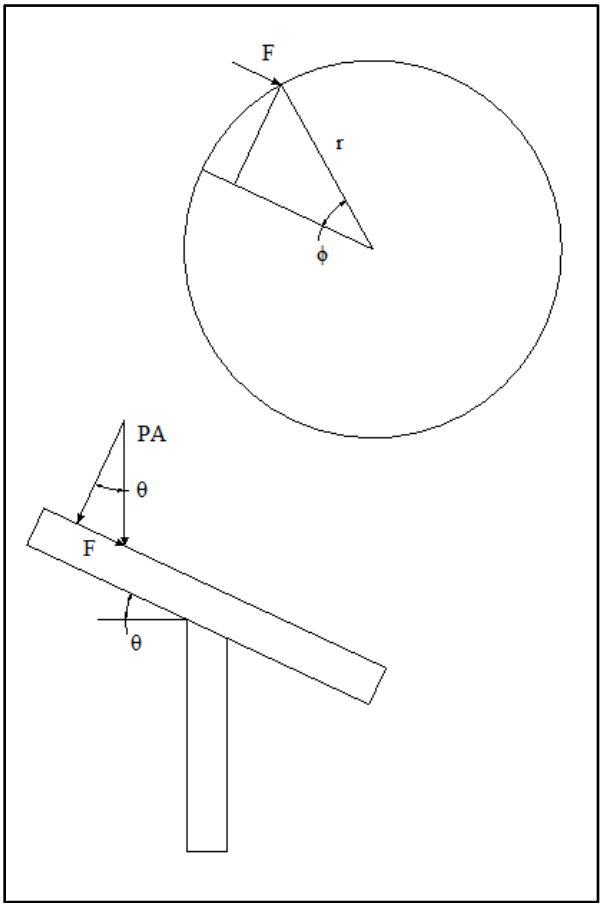

Figure 32: Pump and Transformer Torque Derivation Diagram

$$F = PA \sin\theta$$

Relate the force to the torque on the pivot point.

$$\tau = Fr \sin\phi = PA \sin\theta \, r \sin\phi$$

We define the displacement of that cylinder as,

$$d = A2r\sin\theta$$

$$Ar\sin\theta = \frac{d}{2}$$

Substituting back into the torque equation,

$$\tau = \frac{Pd}{2}\sin\phi$$

It is assumed that there are enough pistons to make it look like continuous torque through the whole angle ϕ. We can check the standard equation for a regular pump by integrating the torque from 0 to π.

$$\tau_{total} = \int_0^{\pi} \frac{Pd}{2}\sin\phi \; d\phi = Pd$$

For the case of the transformer, if $\phi \neq 180°$ as shown in Figure 33,

$$\tau_{total} = \int_{\delta - {}^{\alpha}/_{2}}^{\delta + {}^{\alpha}/_{2}} \frac{Pd}{2}\sin\phi \; d\phi$$

$$\tau_{total} = \frac{Pd}{2}\left[-\cos\left(\delta + \frac{\alpha}{2}\right) + \cos\left(\delta - \frac{\alpha}{2}\right)\right]$$

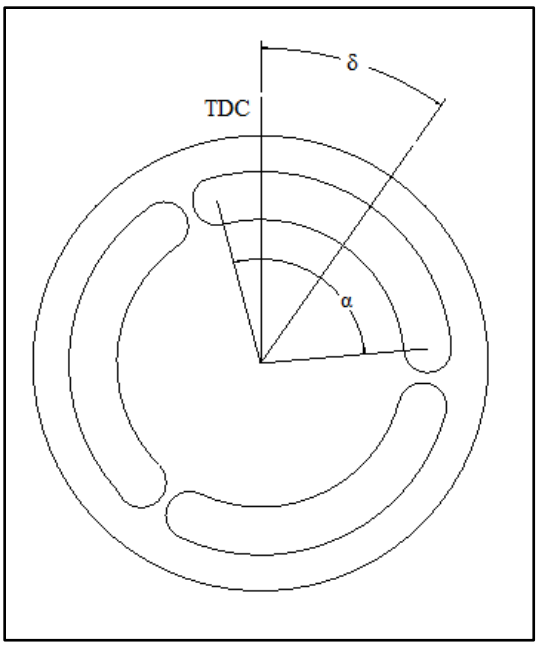

Figure 33: Transformer Torque Derivation Diagram

Use the trigonometry identity, $\cos\left(\delta \pm \frac{\alpha}{2}\right) = \cos\delta\cos\left(\frac{\alpha}{2}\right) \mp \sin\delta\sin\left(\frac{\alpha}{2}\right)$

$$\tau_{total} = Pd\sin\delta\sin\left(\frac{\alpha}{2}\right)$$

This equation is for one port. Now to calculate the flow rate we start with Figure 34. Note the fact that the piston height moves in an elliptical profile as the barrel rotates. The equation for an ellipse is,

$$\left(\frac{x}{a}\right)^2 + \left(\frac{y}{b}\right)^2 = 1$$

In this case we set $y = h$ and we know that when $h = 0$, then $x = r$ and when $x = 0$, then $h = r\sin\theta$. Therefore, we can solve for a and b yielding,

$$\left(\frac{x}{r}\right)^2 + \left(\frac{h}{r\sin\theta}\right)^2 = 1$$

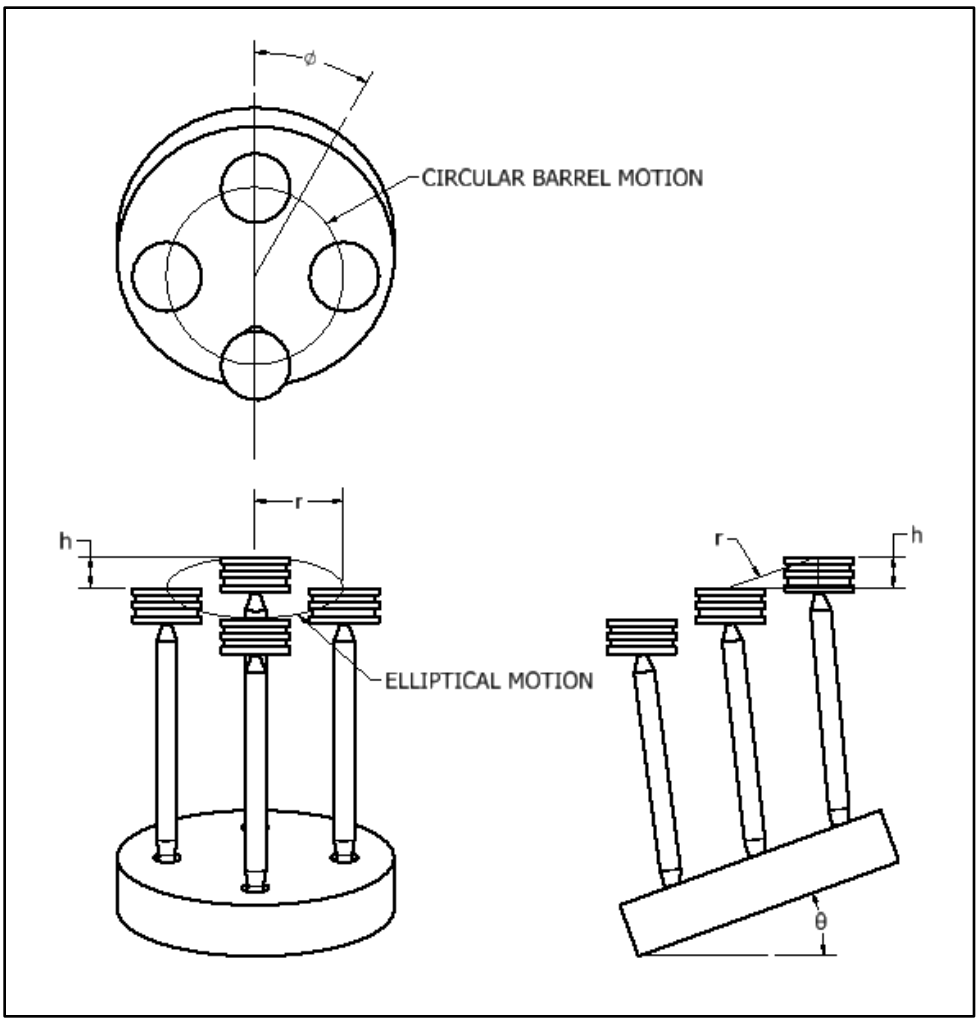

Figure 34: Transformer Flow Derivation Diagram

Therefore,

$$h = r \sin\theta \sqrt{1 - \left(\frac{x}{r}\right)^2}$$

Now it is desirable to relate x to $\emptyset$. This can be done as follows,

$$x = r \sin\phi$$

Substituting,

$$h = r \sin\theta \sqrt{1 - (\sin\phi)^2} = r \sin\theta \cos\phi$$

The value for θ remains constant in time, therefore if we integrate with respect to ∅,

$$\dot{h} = r\omega \sin\theta \sin\phi$$

By definition,

$$Q = A\dot{h} = Ar\omega \sin\phi \sin\theta$$

Substituting in the definition of pump displacement,

$$Q = \omega d \frac{\sin\phi}{2}$$

This equation represents the elemental flow rate of any point around the port plate. To calculate how much flow comes from one half of a revolution (the normal flow from a swash plate pump), the flow must be integrated over the angle,

$$Q_{total} = \int_0^{\pi} \omega d \frac{\sin\phi}{2} d\phi = \omega d$$

The equation results in the standard pump flow rate equation. In the case of a transformer,

$$Q_{total} = \int_{\phi_o}^{\phi_f} \omega d \frac{\sin\phi}{2} d\phi$$

$$Q_{total} = \frac{\omega d}{2} \left(\cos\phi_o - \cos\phi_f\right)$$

Recall the trigonometry identity,

$$\cos\phi_o - \cos\phi_f = -2 \sin\left(\frac{\phi_o + \phi_f}{2}\right) \sin\left(\frac{\phi_o - \phi_f}{2}\right)$$

And defining the Innas' variables, α and δ as,

$$\alpha = \phi_o - \phi_f$$

$$\delta = \frac{\phi_o + \phi_f}{2}$$

The final result is,

$$Q_{total} = -\omega d \sin\delta \sin\left(\frac{\alpha}{2}\right)$$

This equation represents the flow out of one of the ports in the Innas' Transformer.

APPENDIX III: PAYBACK PERIOD DERIVATION

The condition that defines the payback period is when the hybrid component cost plus the present equivalent cost of the fuel used by the hybrid vehicle is equal to the present equivalent cost of the fuel used by the stock vehicle in the same time period. This can be shown mathematically as,

$$Cost_{fuel/yr,stock} * \frac{(1+i)^t - 1}{i(1+i)^t} = Cost_{comp} + Cost_{fuel/yr} * \frac{(1+i)^t - 1}{i(1+i)^t}$$

Rearranging,

$$\frac{(1+i)^t - 1}{i(1+i)^t} = \frac{Cost_{comp}}{Cost_{fuel/yr,stock} - Cost_{fuel/yr}}$$

The left side of the equation is then separated,

$$\frac{1}{i} - \frac{1}{i(1+i)^t} = \frac{Cost_{comp}}{Cost_{fuel/yr,stock} - Cost_{fuel/yr}}$$

Multiplying both sides by i and rearranging,

$$\frac{1}{(1+i)^t} = 1 - \frac{iCost_{comp}}{Cost_{fuel/yr,stock} - Cost_{fuel/yr}}$$

Inverting both sides,

$$(1+i)^t = \frac{1}{1 - \frac{iCost_{comp}}{Cost_{fuel/yr,stock} - Cost_{fuel/yr}}}$$

Simplifying again,

$$(1+i)^t = \frac{Cost_{fuel/yr,stock} - Cost_{fuel/yr}}{Cost_{fuel/yr,stock} - Cost_{fuel/yr} - iCost_{comp}}$$

Using the definition of a logarithm, $x = a^y \leftrightarrow y = \log_a x$

$$t = \log_{(1+i)}\left[\frac{Cost_{fuel/yr,stock} - Cost_{fuel/yr}}{Cost_{fuel/yr,stock} - Cost_{fuel/yr} - iCost_{comp}}\right]$$

This can be more easily calculated by using the change of base formula yielding,

$$t = \frac{\ln\left[\frac{Cost_{fuel/yr,stock} - Cost_{fuel/yr}}{Cost_{fuel/yr,stock} - Cost_{fuel/yr} - iCost_{comp}}\right]}{\ln(1+i)}$$

This equation can be used directly to calculate the payback period for the hybrid system.